DOWNEY PLANT

RESEARCH AND ENGINEERING DIVISION

FINAL REPORT

BLAST AND FIREBALL COMPARISON OF CRYOGENIC AND HYPERGOLIC PROPELLANTS

Contract No. NAS 9-2055

Report No. 0822-01(01)FP /June 1964 / COPY 61

AEROJET GENERAL TIRE GENERAL

AEROJET-GENERAL CORPORATION

AEROJET-GENERAL CORPORATION
Research and Engineering Division
11711 Woodruff Avenue
Downey, California

BLAST AND FIREBALL COMPARISON OF CRYOGENIC AND HYPERGOLIC PROPELLANTS

FINAL REPORT

0822-01(01)FP

Contract No. NAS 9-2055

Prepared for

Gemini Program Office
National Aeronautics and Space Administration
Manned Spacecraft Center
Houston, Texas

Prepared by: R. E. Pesante
M. Nishibayashi
D. G. Frutchey
R. D. Erickson
W. J. Helm

Date: 26 June 1964

Reviewed by: M. Nishibayashi
for D. V. Paulson, Head
Propellant Physics Deparment
Research Division

No. of Pages: 146

Approved by: H. L. Rogers for
H. J. Fisher, Manager
Research Division

Classification: UNCLASSIFIED

NOTICE

THIS DOCUMENT HAS BEEN REPRODUCED FROM THE BEST COPY FURNISHED US BY THE SPONSORING AGENCY. ALTHOUGH IT IS RECOGNIZED THAT CERTAIN PORTIONS ARE ILLEGIBLE, IT IS BEING RELEASED IN THE INTEREST OF MAKING AVAILABLE AS MUCH INFORMATION AS POSSIBLE.

ACKNOWLEDGEMENTS

The experimental studies on this program were directed by Mr. R. F. Fletcher, Project Manager, Gemini Fireball Program, NASA, Manned Spacecraft Center (MSC), Houston, Texas.

Special acknowledgement is given to the Explosion Kinetics Branch, Ballistics Research Laboratory, Aberdeen Proving Grounds, Maryland, for assistance in supplying pressure gages and technical support at no expense to this program. The effort of J. Meszaros, R. Reisler, and E. O'Leary, who were involved in supporting this task, is greatly appreciated.

The contributions of the following personnel is also gratefully acknowledged: C. Creech and A. Olsen of MSC, Instrumentation and Electronic Systems Division, for instrumentation evaluation. R. Brown of MSC, Structures and Mechanics Division, for guidance in presenting the spectral radiation analysis in this report. J. Hammack of MSC, Gemini Program Office, for his full cooperation and support.

CONTENTS

ILLUSTRATIONS

ILLUSTRATIONS (Cont)

ILLUSTRATIONS (Cont)

ILLUSTRATIONS (Cont)

TABLES

1. INTRODUCTION

The use of storable, hypergolic liquid propellants in large space-vehicle booster systems requires a realistic assessment of potential explosion, fire, and radiation hazards. This is particulary true for man-rated booster systems. Accurate assessment of these hazards is essential to provide design criteria for assuring the safety of the astronauts in the event of any malfunction of the propulsion system requiring an abort condition. Information concerning the explosive hazards of cryogenic propellants [e. g., liquid oxygen (LOX)/RP-1] is available through observation of actual malfunctions occuring in full-scale missile test flights. Such information is not available for hypergolic propellants. The purpose of this study was to obtain accurate estimates of the hazards to personnel and equipment resulting from the nitrogen tetroxide (N_2O_4) and a 50/50 mixture of hydrazine and unsymmetrical dimethyl hydrazine (UDMH) propellant. [Referred to as Aerozene -50 (A-50).]

It should be emphasized that it was not the intent of this program to obtain data for the purpose of extrapolating to larger quantities of propellants, nor was it intended for the experimental data to be construed as the complete answer to the full-scale evaluation of the explosive characteristics of a launch vehicle containing either hypergolic or cryogenic propellants.

2. OBJECTIVE

The objective of this program was to compare the basic blast properties of hypergolic propellants with cryogenic propellants. Specific parameters to be considered in establishing a comparison between the two types of propellants were peak overpressure, shockwave velocity, positive pressure impulse and duration, and radiant heat flux, as well as fireball size, duration, and temperature.

3. SUMMARY

A total of twenty-three tests was conducted with hypergolic (N_2O_4/ Aerozine-50) and cryogenic (LOX/RP-1) propellants from 9 September 1963 to 13 April 1964 to evaluate the explosive and fireball characteristics of the two materials with controlled contact area and mixture ratio conditions. The propellants were combined using a mixing technique that permitted variation from test to test of the oxidizer/fuel mixture

ratio and contact area for a 300-lb sample quantity of propellant. Oxidizer/fuel mixing was accomplished by placing oxidizer-filled glass dewars in a fuel-filled pan and dropping the dewar pan assembly on a steel plate.

A computer program was devised to determine the proper size and number of dewars and pan geometry. The pertinent test design parameters were programed into an IBM 1620 computer for analysis to provide a geometrical and economical solution to the problem.

The cryogenic impact tests with glass dewars reacted spontaneously on striking the steel plate, which prevented the determination of an optimum mixing time before initiation. Therefore, all cryogenic dewar tests were conducted without an initiation delay after mixing.

A dewar/pan assembly was impacted with a 30 caliber bullet which initiated a violent explosion reaction after a 30-sec delay. If a similar projectile or fragment should strike a fueled launch vehicle it could be catastrophic.

An N_2O_4 vapor and A-50 liquid initiation was observed during the test program. A stopper was thus required in each dewar to prevent the varporized oxidizer from escaping into the fuel pan.

The test results indicated the contact area had a definite effect on the explosive yield, fireball size and duration, and thermal radiation. A maximum equivalent blast yield* of 0.34 to less than 0.02 lb of TNT per lb of propellant was indicated for the hypergolic propellant tests. The cryogenic propellant tests indicated TNT equivalences* of 0.36 to 0.04 lb of TNT per lb of propellant. An ultimate mix test with a LOX/RP-1 sample yielded an equivalence of 1.2 lb of TNT per lb of propellant.

A comparison of the hypergolic propellant test results with TNT impulse data indicated equivalences of 0.42 to 0.02 lb of TNT per lb of propellant. The cryogenic propellant tests indicated TNT equivalences based on impulse data of 0.49 to 0.08 lb of TNT per lb of propellant.

Propellant sample maximum fireball temperatures were recorded of approximately 3070°F for N_2O_4/A-50, and 3380°F for LOX/RP-1. Maximum total thermal radiation yields of 2.4×10^8 joules were observed for the N_2O_4/A-50, and of 6.1×10^8 joules were observed for LOX/RP-1.

---

*Based on peak overpressure data.

4. TECHNICAL DISCUSSION

4.1 APPROACH

Although several test programs to determine the explosion hazards of hypergolic propellants have been conducted by various agencies (References 1 through 7), none have measured completely: (1) the thermal energy emitted, (2) the effects of surface area between the oxidizer and the fuel, or (3) the effects of the blast. The objectives of this program were approached with the concept of eliminating test variables, such as contact area and oxidizer/fuel ratios, that had been experienced in previous tests.

4.2 TEST CONFIGURATION DESIGN

Contact interface area control was accomplished by using cylindrical glass dewar flasks to contain the oxidizers, and aluminum pans to contain both the flasks and the fuels. Oxidizer/fuel mixing was accomplished by impacting the pans on a steel plate, which shattered the dewars, thus providing simultaneous initial contact of the oxidizer and fuel surfaces. Variation of the contact area between the oxidizer and the fuel was accomplished by using dewars of different sizes. The contact area between the oxidizer and the fuel was computed on the mean radius of the double-wall glass dewars. To determine the effect of the oxidizer/fuel ratio on the various blast parameters, a test plan was devised that evaluated three different oxidizer/fuel mixture ratios at three different contact area ratios, or a total of nine tests for each propellant system. The mixture ratios and initial contact interface ratios are presented in Table 1. The total weight of the propellant sample in each test was limited to 300 lb.

Determination of the proper number and size of dewars and of the proper pan size to provide the required contact interface areas and mixture ratios was accomplished with a computer program. A computed solution to the problem was necessary because of the large number of volume and area variables involved. A program was developed (Appendix A) and the pertinent test design parameters were fed into an IBM 1620 computer for analysis. This program provides a geometrical and economical solution to the problem, based on available standard dewar sizes and prices, for the conditions indicated in Table 1.

Table 1. Propellant Test Plan.

Oxidizer/Fuel Weight Ratios*	Relative Oxidizer/Fuel Area Ratios*
N_2O_4/A-50	
3:1 (Fuel-Lean)	1, 2, 4
2:1 (Stoichiometric)	1, 2, 4
1:1 (Fuel-Rich)	1, 2, 4
LOX/RP-1	
3.5:1 (Fuel-Lean)	1, 2, 4
2.5:1 (Stoichiometric)	1, 2, 4
1.5:1 (Fuel-Rich)	1, 2, 4

*One test for each condition.
18 tests total.
Total propellant weight for each test was 300 lb.

The pans to contain the dewars and fuels were fabricated from aluminum sheet material to the sizes indicated by the computer program. The sides of the pans were 1/8-in. -thick sheet welded to a 3/16-in. -thick aluminum bottom sheet. All joints of the pans were welded and reinforced with 1/8-in. -thick aluminum angle.

The pans were designed to remain intact after impact on a steel plate from a drop height of 20 ft when filled with propellant and dewars. This provided dynamic mixing of the fuel and oxidizer on impact of the pan.

4.3 TEST OPERATION

The cylindrical, round-bottom dewars were supported vertically by a thin-wire grid secured to the pan walls both to prevent spillage of the oxidizer into the pan and to compensate for buoyant forces on the dewars from the fuel in the pan. The bare bottom tip of the dewar was allowed to rest on the bottom of the pan. A typical pan assembly, containing seventy-three 1.0-liter dewars and three 4.3-liter dewars is shown in Figure 1. An aluminum-foil-covered plywood lid was placed on top of the dewars to prevent propellant splashing at impact. The plywood lid was secured to the sides of the pan with rigid fasteners.

The pan and dewar assembly was raised to the desired impact height on a 25-ft-high droptower with a hand-operated winch. To provide stability to the pan during raising operations and ensure its proper attitude during the subsequent fall, guide cables were secured at each of the four corners of each pan with eyebolts. The pan assembly was released at a desired time by an exploding-bolt release mechanism. The test fixture is shown in Figure 2, with a pan assembly ready for raising to the drop position.

To provide for personnel safety, the fuel was added (at a rate of $\approx$ 1 gal/min) to the pan assembly in the elevated drop position by remote control. The loading operation was accomplished from a reinforced concrete instrumentation and personnel building approximately 125 ft from the test fixture (Figure 3).

An air-driven fuel pump and a reservoir were located in a pit adjacent to the test fixture. The desired quantity of fuel, which had been carefully measured previously in a separate vessel, was added to the fuel reservoir adjacent to the fuel pump. The tank was pumped dry to obtain the desired amount of fuel in the dewar pan assembly. Prior to

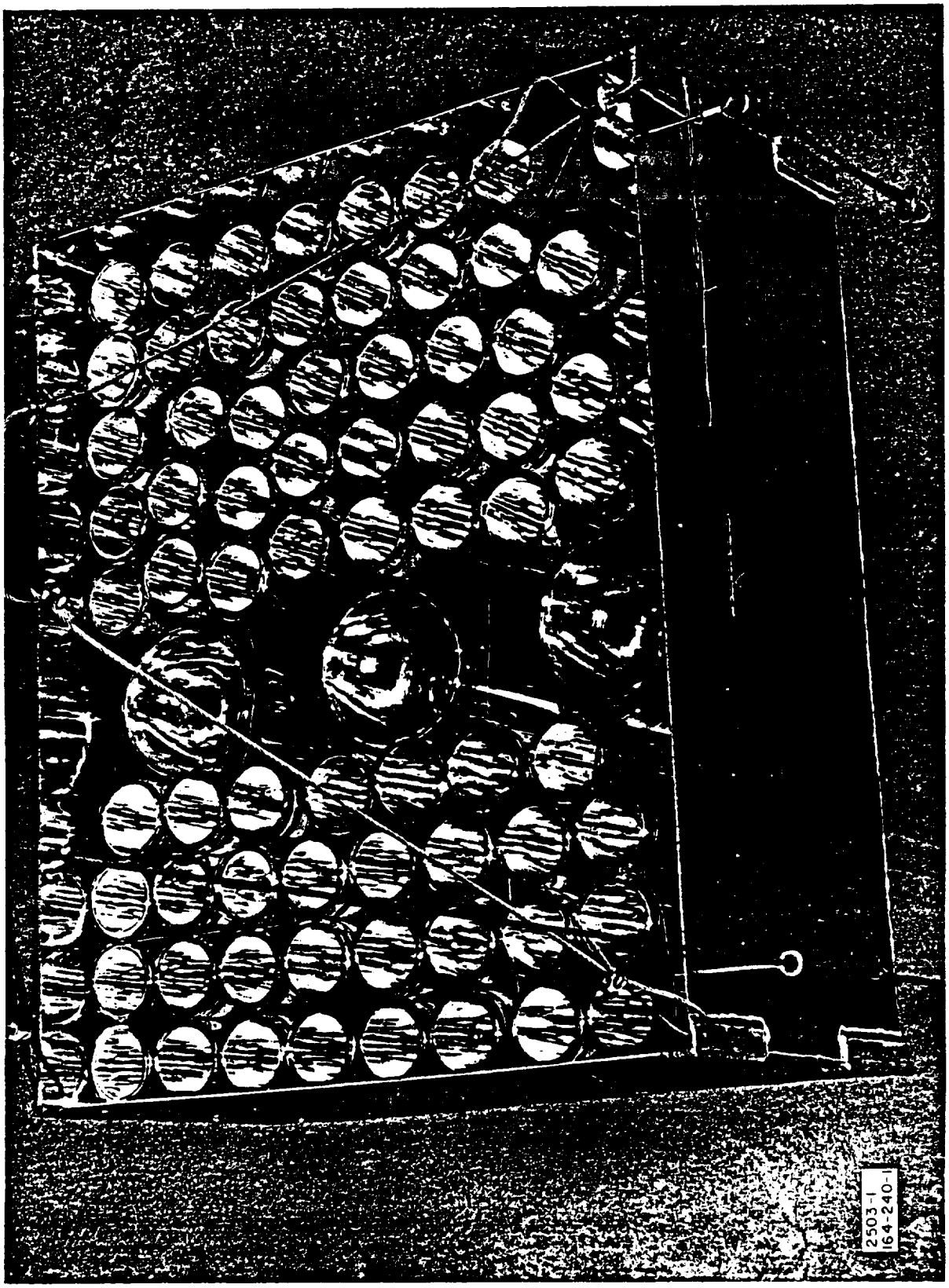

Figure 1. Typical Dewar Pan Assembly.

Figure 2. Propellant Test Area.

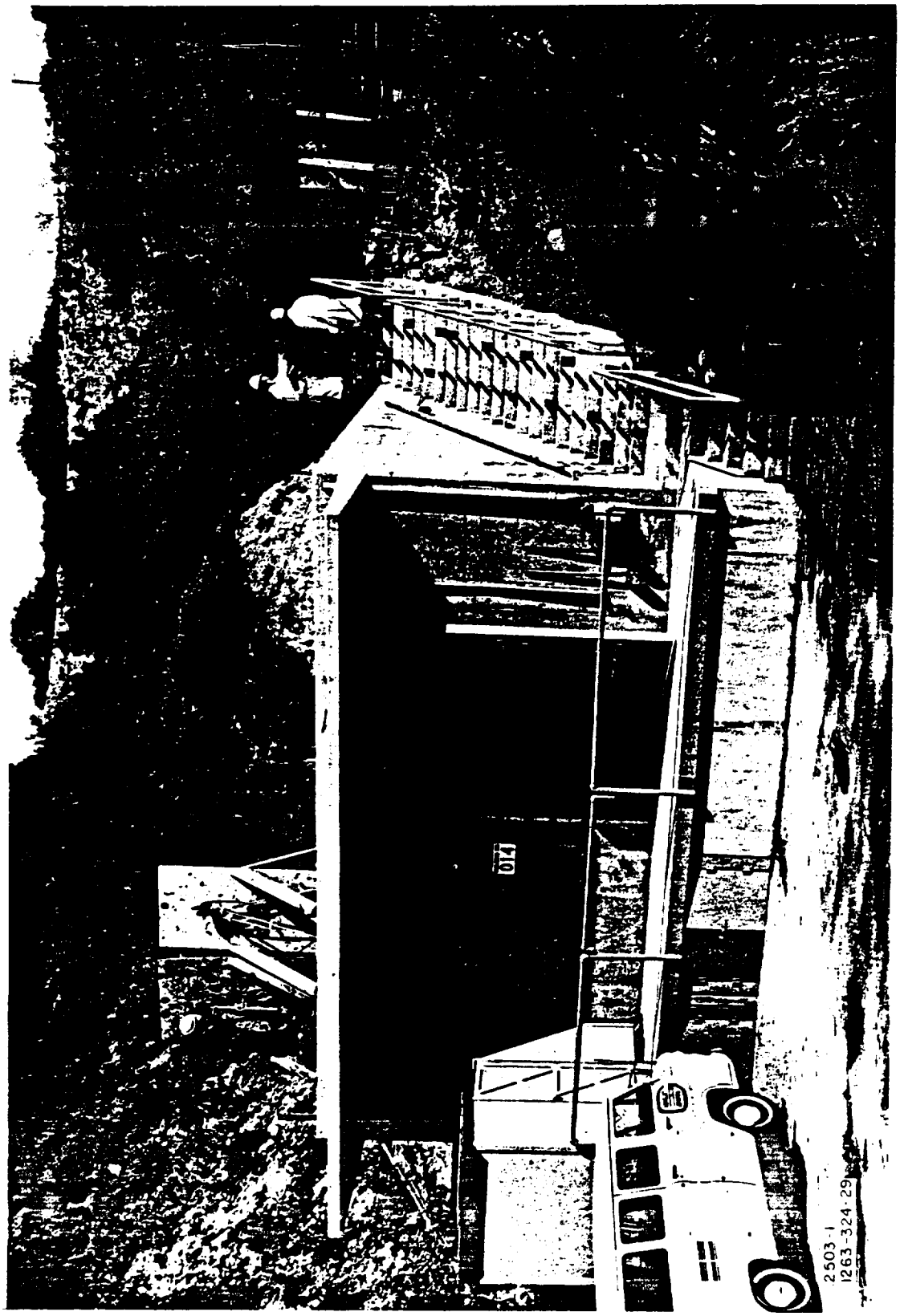

Figure 3. Instrumentation and Personnel Building.

each test, a small quantity of fuel was placed in the fuel reservoir tank and the tank was then pumped dry to fill the pump and transfer lines. The pumping time required for each test varied, depending on the mixture ratio of the propellants. The pump was operated during the test after the fuel in the pump reservoir was exhausted to prevent siphoning of the fuel from the pan back into the reservoir.

The size of the pans was varied to correspond with the number and size of the dewars and the volume of the propellants.

A typical test was conducted in the following manner:

> The desired number of dewars of proper size were secured in the pan, and were filled with the oxidizer to a height that was predetermined to provide the desired contact surface with the surrounding fuel. The plywood cover was positioned in the pan. The pan assembly was then raised by the winch system to a desired height, which was 15 ft for the low-contact-area tests and 10 ft for all other tests. The fuel was then pumped into the pan around the dewars to a height equal to that of the oxidizer in the dewars. At a predetermined time the pan assembly was released and the various blast and thermal radiation parameters were measured.

4.4 PRELIMINARY SHATTER TEST

A series of preliminary shatter tests was conducted to determine the efficiency of the dewar shattering technique, and especially the optimum drop height. The tests were conducted with a dewar/pan assembly that had a Plexiglas window in one side and no cover lid (Figure 4). A solution of RP-1/water-insoluble red dye (Methylamines anthraquinone) was placed in the dewars and water was used in the pan to simulate the fuel. The water-insoluble dye was employed to follow the mixing reaction of the RP-1 and water without discoloring the water by chemical reaction. Two Fastax high-speed cameras at a rate of 2000 frames/sec were used to record the test both from the side and top.

The results of the film coverage indicated the mix time was less than 10 msec from impact. The film records indicated that the dewars were shattered in relatively small pieces (Figure 5) if the drop height was greater than 6 ft. A height of 10 ft was selected for ensuring total breakage of all dewars in the pan. However, all low-contact-area-ratios tests were conducted from a height of 15 ft to compensate for the larger and heavier glass dewars employed in the test fixture.

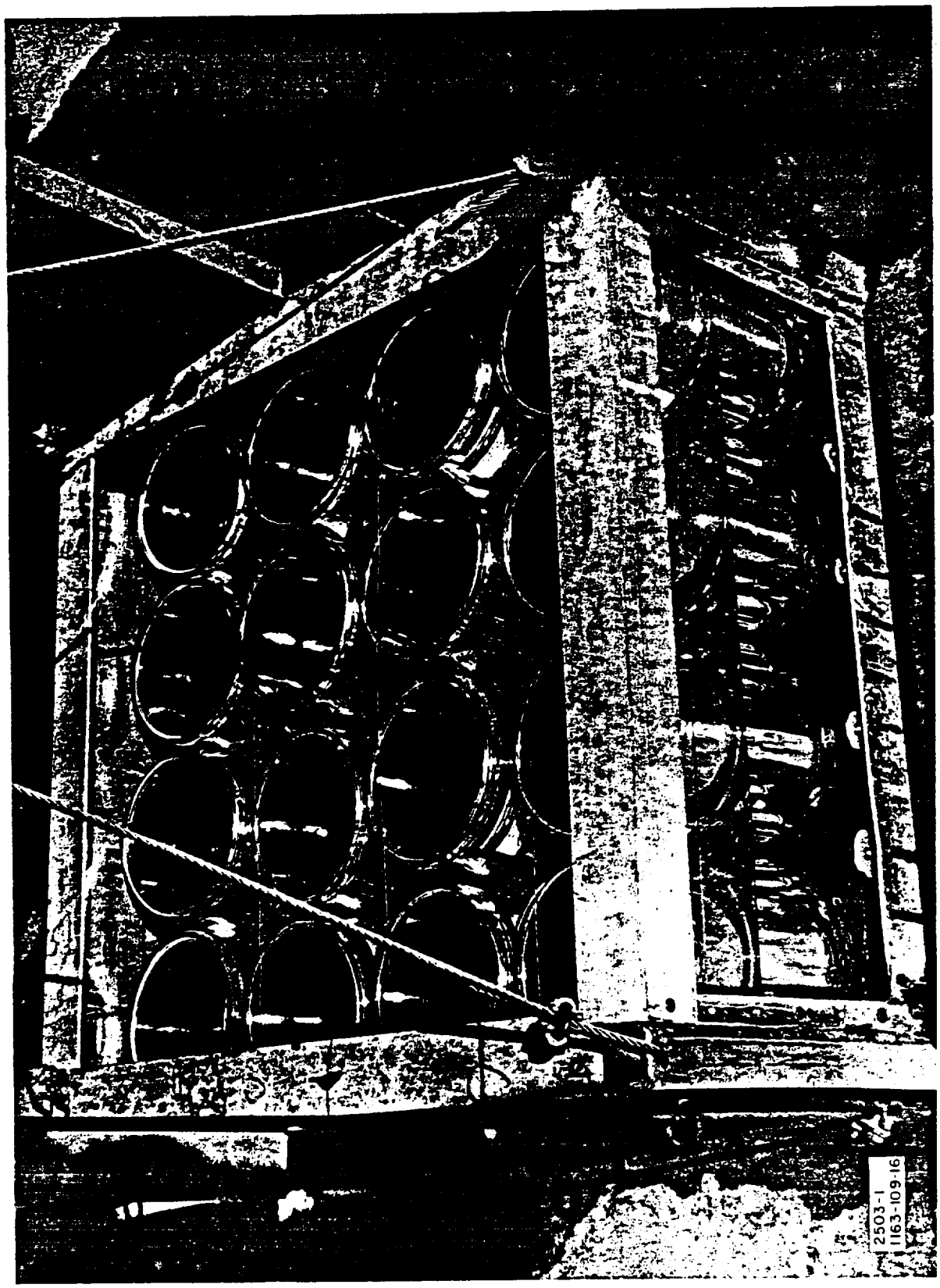

Figure 4. Shatter Test Fixture.

Figure 5. Test Remains of a Dewar Shatter Test with Test Liquid Removed.

4.5 INSTRUMENTATION

4.5.1 Layout

Three instrumentation stations were established in each of the four quadrants surrounding the test fixture at distances of 10, 25, and 40 ft from the center of the test area. Overpressure, temperature, and heat flux measurements were made at each station. A layout of the various instrumentation stations is shown in Figure 6, and a photograph of the test area is presented in Figure 7. All instrumentation cables were placed approximately 6 in. below the ground surface to prevent any damage from blast overpressures and pan fragments.

The thermal radiation instrumentation was located 400 ft from the test fixture at a site elevated approximately 150 ft above the level of the test area. A camera was located adjacent to the radiation instruments to record fireball size. The top of the control building, approximately 120 ft horizontal from the center of the test site served as a second camera site (Figure 6).

The data-recording equipment was located in a concrete control building (Figure 3), which is below the level of the test site and is capable of withstanding the blast of 100 lb of high explosive at a 10-ft standoff. This building was occupied by test personnel during all propellant fuel loading operations and tests. Visual observation of the fuel loading and pan assembly release was permitted through a periscope system in the top of the building. The instrumentation control panel is shown in Figure 8. The radiation recording equipment and its operating personnel were housed in a protected mobile instrumentation van at the radiation sensor position. An intercommunication system and firing signal pulse were provided between the van and the control building.

4.5.2 Air-Blast Measurements.

The air-blast overpressures from the various test mixtures were measured with two types of pressure-measuring instruments: Atlantic Research Corp. (ARC) Model LC-33 pencil piezoelectric transducers, and Ballistic Research Laboratory self-recording pressure gages.

The ARC pencil gages were placed 2 ft above the ground in rigid pipe stands (Figure 9). Peak pressure, shockwave velocity, positive impulse, and positive overpressure duration were determined from the

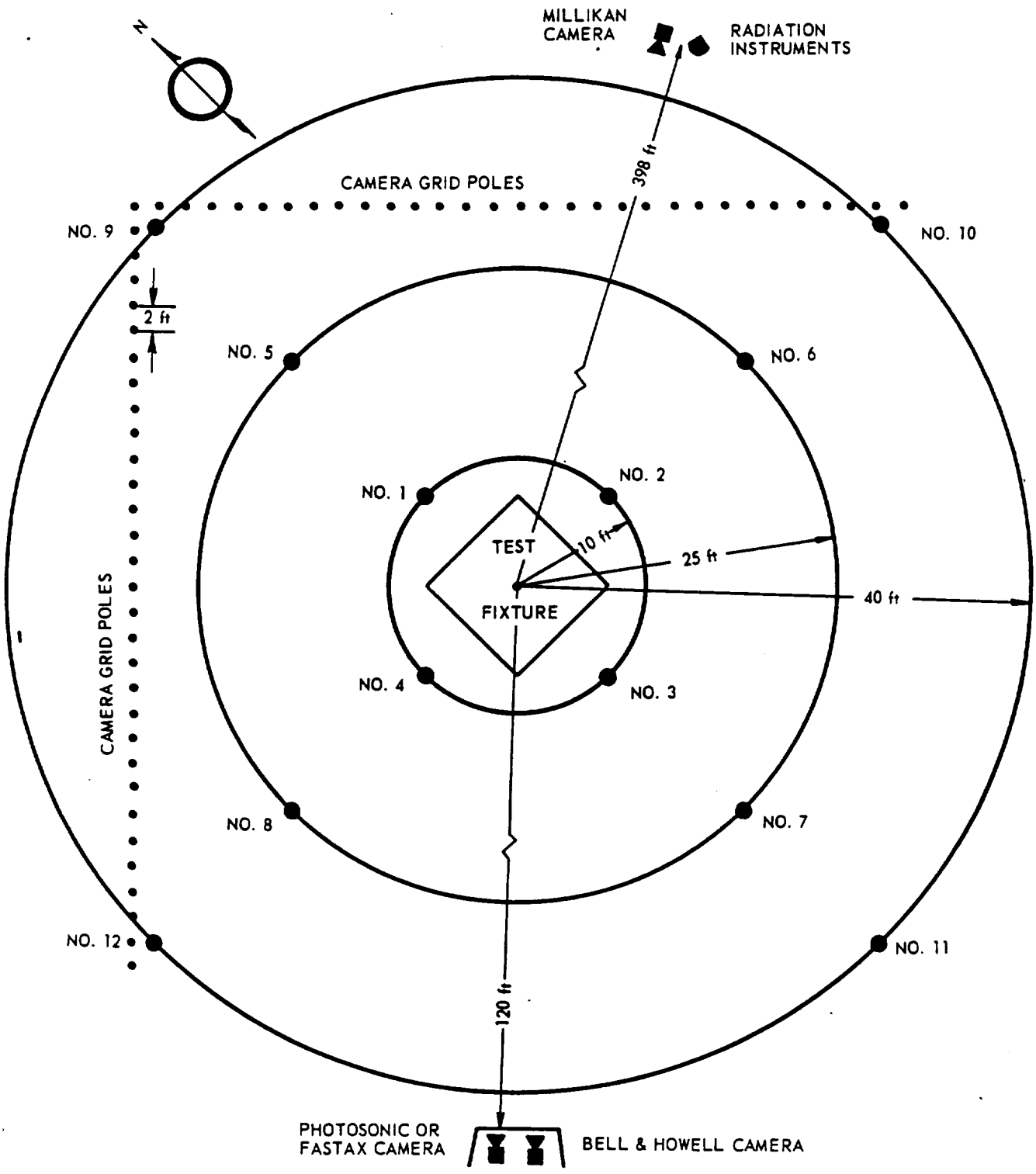

Figure 6. Instrumentation Layout.

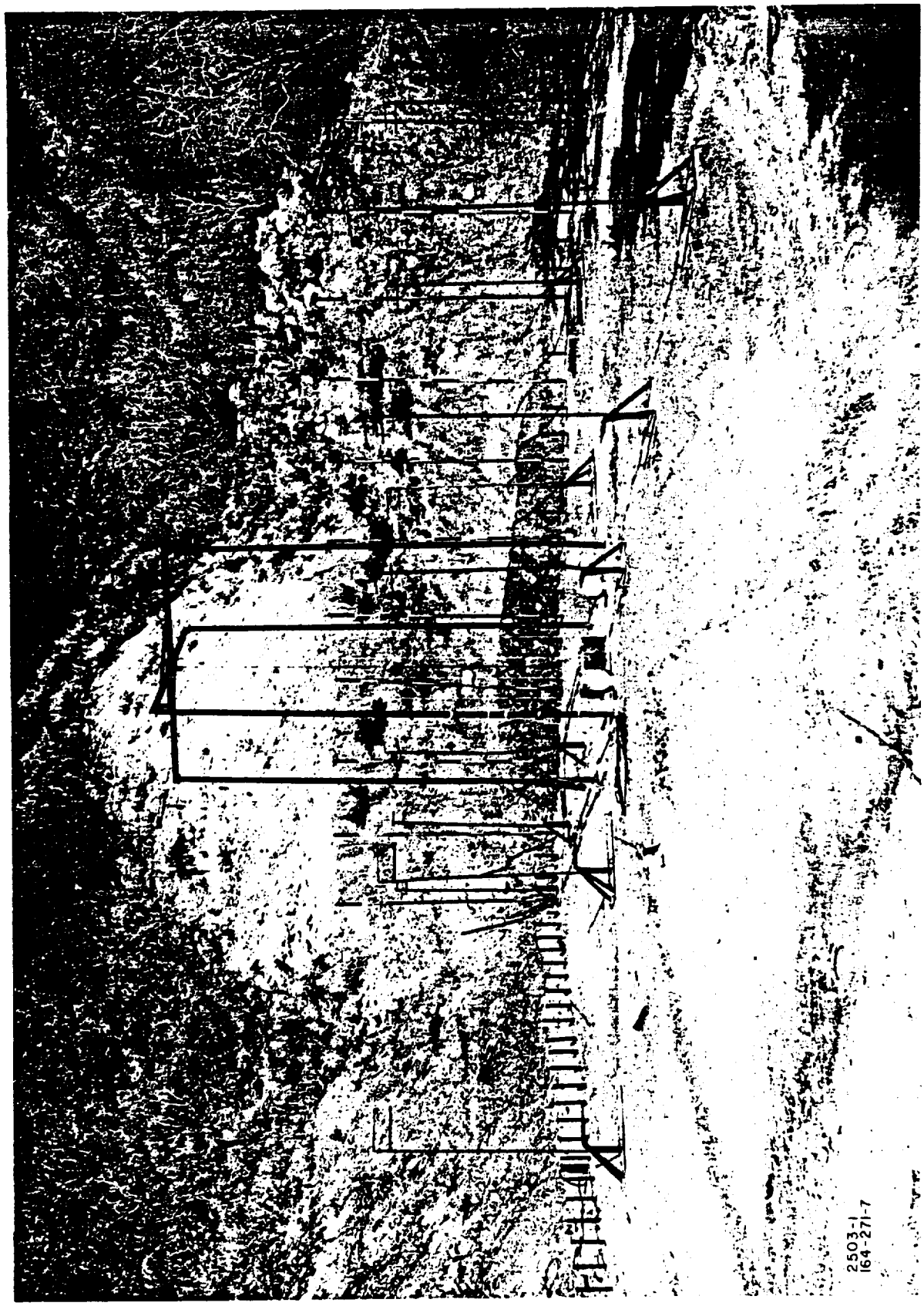

Figure 7. Propellant Test Fixture and Instrumentation Stations.

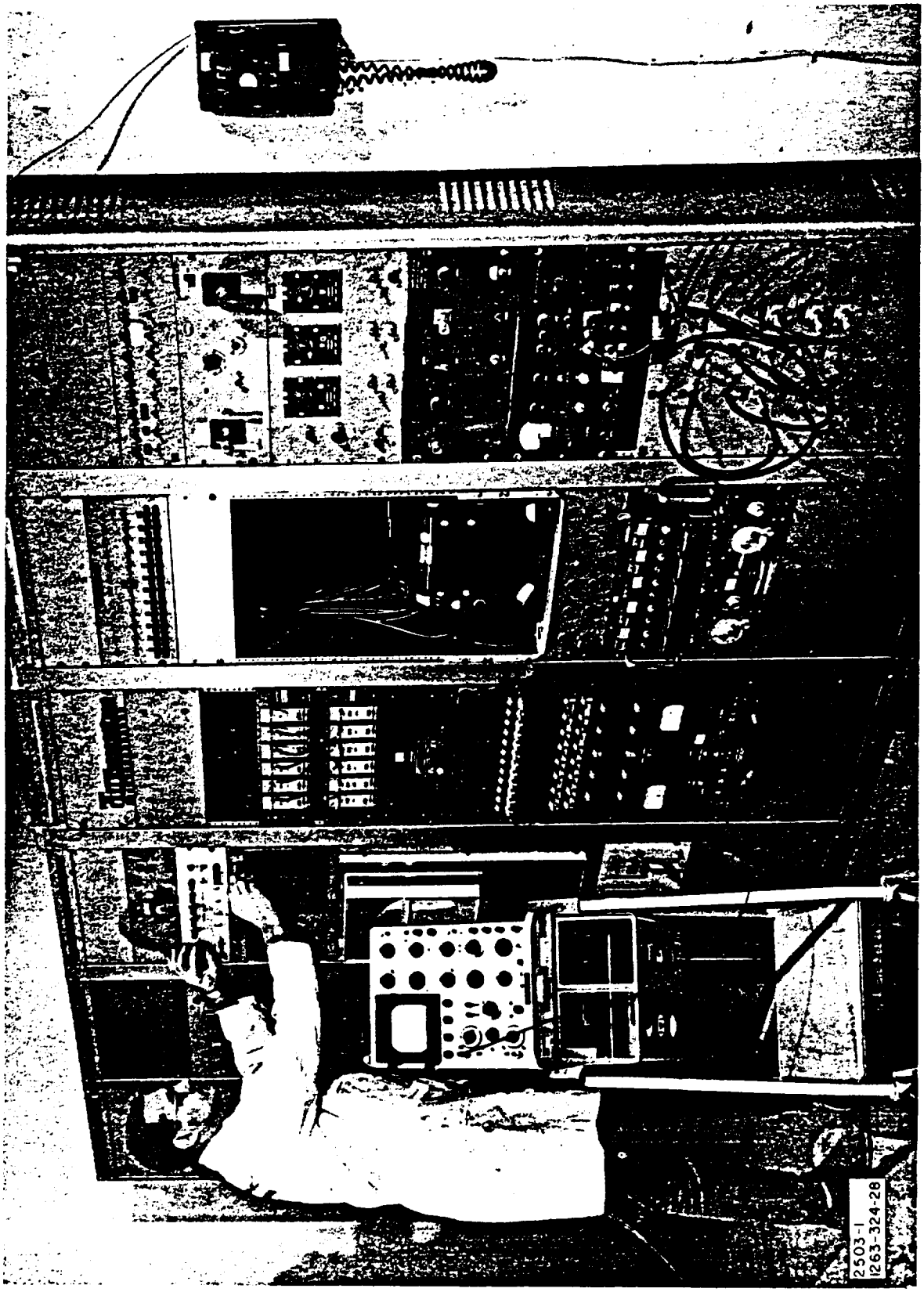

Figure 8. Instrumentation Control Panel.

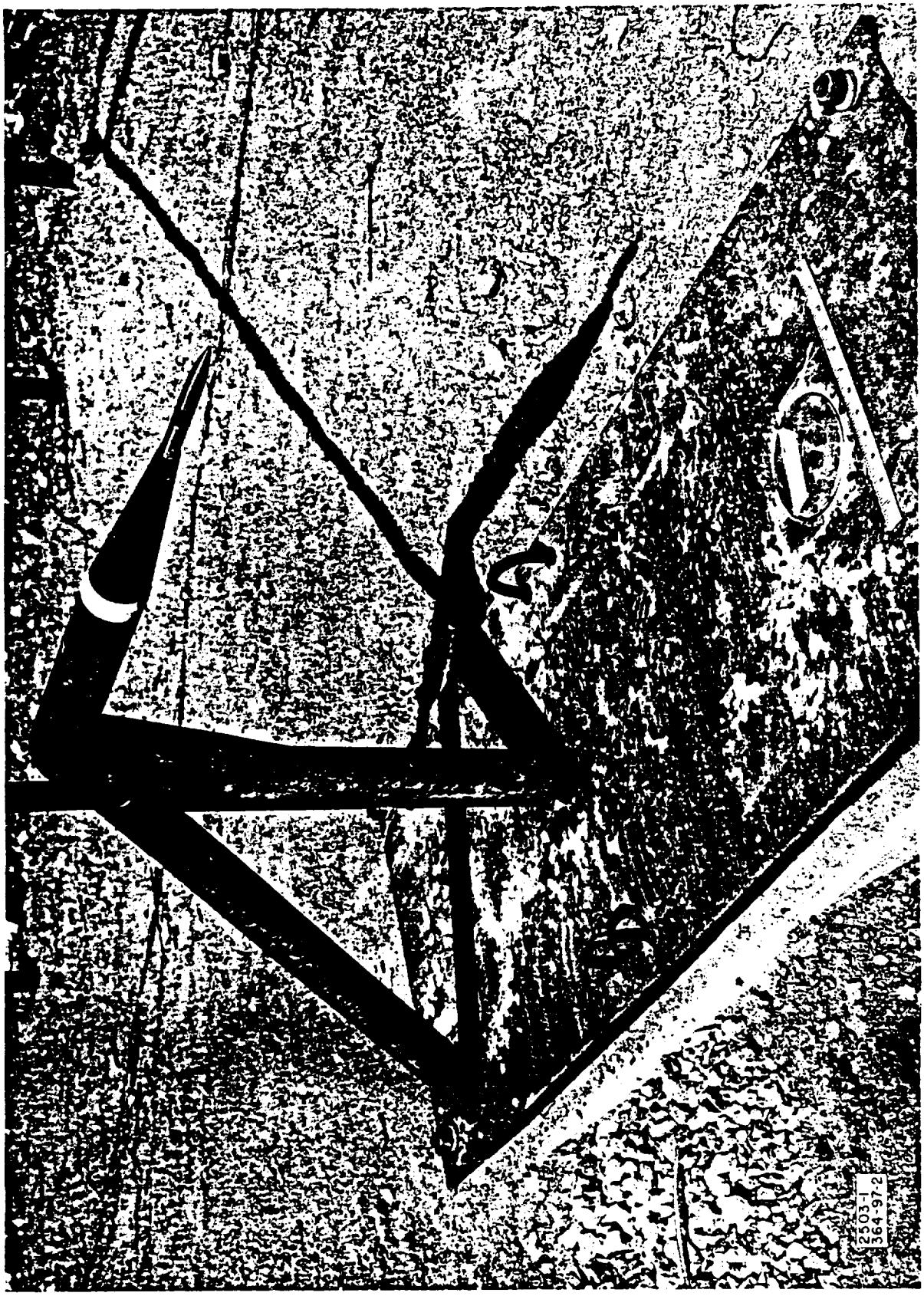

Figure 9. Pencil Gage, Holder and BRL Gage Position.

data recorded with these gages. The gage output was fed through ARC 908-25 low-noise cable into a calibration unit and then into ARC Model 104A low-impedance amplifiers. The amplifier output was recorded on a magnetic tape recorder (Precision Instruments Model 214), which was operated at a speed of 60 in./sec. To obtain readable records for data reduction, it was necessary to play the tape record back at low speed (15 ips) into a recording oscillograph (CEC Model 5-114) operating at 57.6 in./sec. CEC Type 7-362 oscillograph galvanometers were used for the record playback. The graph records represented a four to one time expansion playback advantage for data reduction purposes.

Prior to a test, a calibration was recorded on the tape system for subsequent data reduction control. The calibration was obtained by applying a square-wave pulse of known voltage through a known value capacitor to each pressure-gage channel. The recorder output represented, in pico-coulombs, the expected charge output of the gage on that channel. Data reduction was accomplished by determining what part of the calibration the event represented and then dividing this amount by the gage sensitivity (pico-coulomb/psi) to obtain the pressure (psi). Thus it was possible, by varying the calibration voltage (10 to 100 v) and the calibration capacitance (240 to 9000 μμf), to obtain records for the wide range of overpressures experienced with only small differences in wave amplitude for any of the tests.

A Tektronic Type RM181 time mark generator was used to provide 10-msec timing marks on each tape record for time history purposes. It provided the time base required in determining impulse rise rate, shockwave velocity and duration.

A description of the Ballistic Research Laboratory gages is included in Appendix B.

Prior to starting the actual experimental studies, a series of calibration tests were conducted with explosive charges having known blast characteristics. These preliminary tests were conducted both to check out the instrumentation system and to evaluate the utilization of BRL overpressure data (Reference 8) for TNT equivalence reference curves.

The TNT equivalence of the propellant is defined as the weight of TNT, that will give the same peak overpressure (or impulse) at the same distance as that obtained from the material under test. The TNT equivalences in this report are expressed as the ratio of pounds of TNT equivalent to a pound of propellant.

Calibration tests were conducted with cylindrical, 5-lb TNT and Composition C-4 charges and 25-lb TNT charges, which were positioned near the ground level of the test area on a plywood base to protect the dewar/pan assembly impact surface.

A comparison of the calibration test results with the BRL data (Reference 8) indicated only a negligible variation at the three gage distances. The pencil gages located close to the calibration charge were damaged during the 25-lb TNT tests; therefore, it was decided to omit further large-scale calibration tests and rely on the BRL overpressure data for charges weighing more than 25 lb.

4.5.3 Temperature Measurements

The temperature profile of the propellant fireball was determined with No. 30 AWS platinum/platinum-13% rhodium thermocouples at each of the twelve gage positions. The fine wire size was selected to obtain a high response with commensurate strength. The response time of the thermocouples was approximately 10 msec. The thermocouple output was fed through platinum/platinum-rhodium thermocouple extension wire and a Pace platinum/platinum-rhodium thermocouple reference junction compensator to a calibration unit. A reference temperature of 150°F was maintained in the reference junction unit. The calibration unit output was fed into a galvanometer oscillograph (CEC Model 5-114) using a 100-msec timing grid and operating at 9.6 in./sec. CEC Type 7-325 galvanometers were used to record the calibration unit output.

Prior to each test, a known voltage was applied to each galvanometer through an adjustable resistance in the calibration unit. Thus, it was possible to control the deflection on the graph by adjusting the galvanometer deflection. The deflection was recorded on the graph to provide a reference for subsequent data reduction. Prior to each test the known voltage was removed from the calibration unit.

The thermocouples were positioned in the end of a 1/2-in.-dia pipe that was located 12 ft above the test area level. The thermocouple junction protruded approximately 1 in. beyond the end of the pipe. The gage stand used to hold the thermocouples is shown in Figure 10. The thermocouple wires were separated from the pipe walls with Epon 828 resin.

4.5.4 Heat Flux Measurements

The radiant heat flux was measured at each of the twelve gage positions with an asymptotic thermocouple calorimeter. The calorimeters were positioned adjacent to the thermocouple junctions in the end of a 1-in.-dia pipe (Figure 10) 11.5 ft above the level of the test area level. This kind of calorimeter was selected for its fast response characteristics

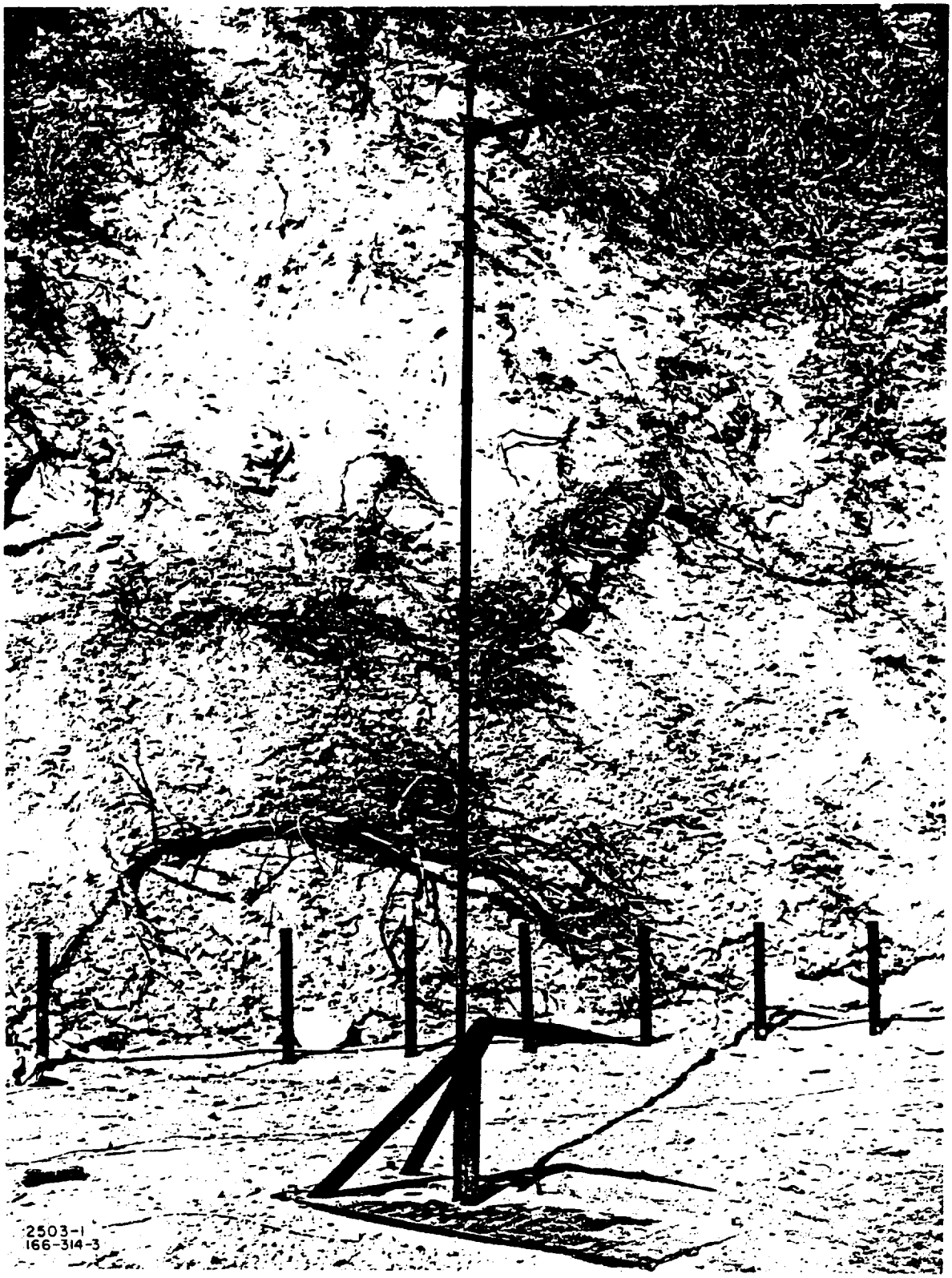

Figure 10. Instrumentation Station with Thermocouple and Heat-Flux Gage Stand.

which give it the ability to measure transient heating rates. Hy-Cal Engineering Type 1300 gages with capacities of 300, 120, 60, and 30 BTU/ft^2-sec were employed at the various stations, depending on the distance from the test fixture and the corresponding radiation yield. These gages have response times of $\leq$ 150 msec, depending on the gage capacity.

The gage consists of a constantan-foil sensing disc that is metallurgically bonded to a water-cooled copper heat sink, which also serves as the calorimeter body. A schematic drawing of the gage is presented in Figure 11. A 0.002-in.-dia copper wire is welded to the center of the constantan foil, providing a thermocouple junction of copper to constantan. This results in a differential thermocouple that indicates the temperature of the sensor without regard for the temperature of the heat sink of the calorimeter body. The heating rate in BTU/ft^2-sec is expressed by:

$$Q = 4SK/R^2 \Delta T \quad (1)$$

where

S = Sensor thickness

K = Sensor thermal conductivity

R = Sensor radius

ΔT = Temperature differential

The direct effect of ΔT on the heating rate is nonlinear, but is offset by the K change with temperature in the opposite direction. Over a broad range, a linear relationship of gage output can be used and the heating rate can be expressed as the product of C x E, where C is a gage constant based on the sensor design and E is the sensor output in mv. The constant, C, is verified for each calorimeter during pretest calibration by the manufacturer.

The gage output voltage was fed into an 18-channel galvanometer oscillograph (CEC Model 5-114) operating at a rate of 9.6 in./sec. CEC Type 7-351 galvanometers were used to record the gage signals. A known calibration voltage controlled by an adjustable resistance was fed into the galvanometers prior to each test. Thus, it was possible to adjust the galvanometer deflection to a desired width on the graph, commensurate with gage output. The deflection was recorded on the graph to provide a reference for data reduction. Prior to each test, the reference voltage was removed from the calibration unit.

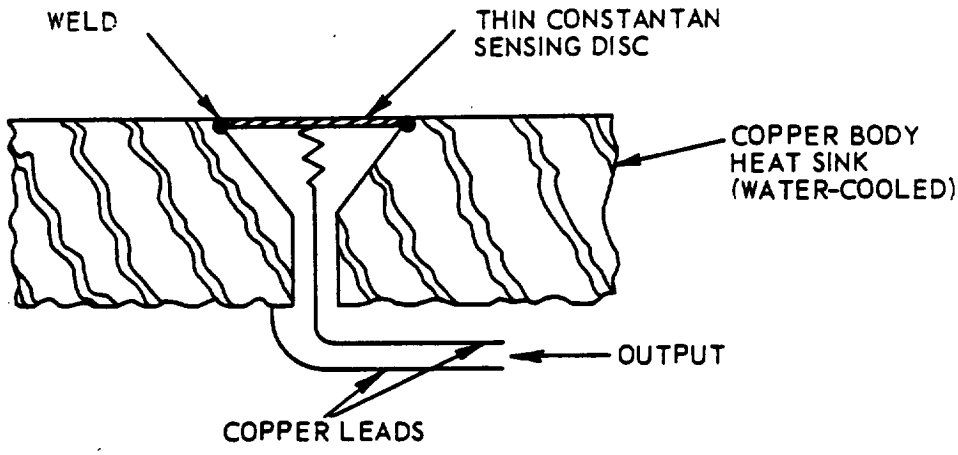

Figure 11. Asymptotic Calorimeter Schematic.

4.5.5 Overpressure Based Upon the Rankine-Hugonoit Equation

The theoretical basis for determining peak overpressure in the 5- to 90-psi range from shockwave and sonicwave velocity measurements is given by Kalovski (Reference 9). With this approach, it is possible to establish a relation between shockwave velocity and the peak pressure from the Rankine-Hugoniot equations and the properties of the medium. With the assumptions that the ratio of the specific heat at constant pressure and volume is a constant across the shock boundary, it is possible to derive the following equation, which is based on the ideal gas law:

$$\frac{P_s}{P_o} = \frac{2\gamma}{\gamma+1} \left(\frac{U^2}{C_o^2} - 1 \right) \tag{2}$$

where

P_s = Peak pressure in the shock front above atmospheric pressure

P_o = Atmospheric pressure

U = Shockwave propagation velocity

C_o = Velocity of sound in undisturbed air

γ = Ratio of specific heat at constant pressure to specific heat at constant volume

The velocity of sound was determined from the formula

$$C = C_o \left(1 + \frac{t}{273}\right)^{1/2} \tag{3}$$

where

C = Velocity of sound in dry air at temperature, t

C_o = Velocity of sound in dry air at $0^{\circ}C$

t = Temperature of air in degrees centigrade

Since humidity has a negligible effect only on γ and not on U, C_o, or P_o (since they are measured quantities at the test humidity), it is possible to eliminate consideration of humidity with only a small overall error of less than 0.1% in the calculated pressure.

The shockwave velocities utilized in Equation 2 were determined from time-of-arrival data at the pencil gages. The velocities were computed by dividing the gage-to-gage elapsed time by the gage-to-gage distance. The velocities calculated are higher than the measured shockwave velocity because the calculated velocities are average velocities over a known distance and the shockwave velocity does not attenuate at a linear rate, but rather at some exponential function depending on the explosive material and the distance from the event. The results of the velocity measurements and the calculated overpressures are presented in Tables 2 and 3.

4.5.6 Radiation Measurements

A measurement of total radiation intensity was deemed insufficient to meet situations where the absorptance of receiving surfaces varies with wavelength; this required knowledge of the spectral distribution. A scanning spectrometer would be inadequate because of the rapid change in fireball intensity. For this reason, a 5-channel radiometer, simultaneously measuring total radiation, as well as radiation, in each of four spectral bands in the 0.4- to 5.0-micron wave-length region was chosen.

The 5-channel radiometer used for these tests is shown in Figure 12. Each channel was provided with a detector, a suitable filter for the four narrow band regions, apertures to define the $\approx 30^{\circ}$ field of view, and a preamplifier. A common chopper blade was used for the unit. Some of these details are visible in Figure 13, which shows the interior of the radiometer.

Total radiation measurements were made with a thermistor bolometer equipped with a KRS-5 window. The window material is transparent over the approximate wavelength interval between 0.5 and 35 microns. This region encompasses virtually all of the radiation emitted by the fireball. The detector filter combinations used to define the narrow-band region were: (1) a brown color-glass filter and a silicon photodiode for the visible region, (2) an infrared-transmitting glass filter and a silicon photodiode for the near infrared region, (3) a germanium filter and a lead sulfide (PbS) detector for the 0.8- to 2.7-micron region, and (4) a long-wavelength pass interference filter and an uncooled lead selenide (PbSe) detector for the 3- to 5-micron region.

Table 2. Shockwave Velocities and Rankine-Hugoniot Pressures (N_2O_4/A-50).

Oxidizer/Fuel Ratio	Contact Area (ft^2)	Position (Gage No. to Gage No.)		Average* Velocity (ft/sec)	Calculated Shock Overpressure (psi)
3:1	51.01	1	5	2273	51.4
		2	6	2174	45.7
		3	7	2206	47.5
		4	8	2143	43.9
		5	9	1579	16.2
		6	10	1515	13.7
		7	11	1485	12.5
		8	12	1546	14.8
	25.44	1	5	1514	13.1
		2	6	1516	13.2
		3	7	1456	10.9
		5	9	1370	7.80
		6	10	1374	7.96
		7	11	1376	8.06
		8	12	1415	9.45
	12.64	1	5	1056	-
		3	7	1111	-
		4	8	1087	-
		5	9	1095	-
		6	10	1103	-
		7	11	1079	-
		8	12	1103	-
2:1	45.53	1	5	2381	57.2
		2	6	2380	57.2
		3	7	2344	54.9
		4	8	2340	54.6
		5	9	1685	20.5
		6	10	1744	23.2
		7	11	1765	25.1
		8	12	1724	22.3
	22.90	1	5	1604	17.4
		2	6	1613	17.9
		3	7	1579	16.4
		5	9	1402	9.45
		6	10	1389	9.00
		7	11	1376	8.52
		8	12	1382	8.70

*Shockwave velocities computed from piezoelectric gage data by dividing gage-to-gage distance by gage-to-gage elapsed time.

Table 2. (Continued).

Oxidizer/Fuel Ratio	Contact Area (ft^2)	Position (Gage No. to Gage No.)		Average* Velocity (ft/sec)	Calculated Shock Overpressure (psi)
2:1	11.39	1	5	1027	-
		2	6	1136	-
		3	7	1145	-
		4	8	1136	-
		5	9	1103	-
		6	10	1087	-
		7	11	1091	-
		8	12	1103	-
1:1	35.90	1	5	2083	40.8
		2	6	2206	47.8
		3	7	2143	45.2
		4	8	2273	51.8
		5	9	1648	19.4
		6	10	1705	21.9
		7	11	1648	19.3
		8	12	1667	20.2
	17.96	1	5	1376	8.61
		2	6	1389	9.17
		3	7	1402	9.62
		4	8	1351	7.80
		5	9	1351	7.80
		6	10	1339	7.33
		7	11	1339	7.33
		8	12	1364	8.25
	8.88	1	5	974	-
		2	6	1172	-
		3	7	1145	-
		4	8	1111	-
		5	9	1128	-
		6	10	1119	-
		7	11	1111	-
		8	12	1172	-

*Shockwave velocities computed from piezoelectric gage data by dividing gage-to-gage distance by gage-to-gage elapsed time.

Table 3. Shockwave Velocities and Rankine-Hugoniot Pressures (LOX/RP-1).

Oxidizer/Fuel Ratio	Contact Area (ft^2)	Position (Gage No. to Gage No.)		Average* Velocity (ft/sec)	Calculated Shock Overpressure (psi)
3.5:1	57.85	1	5	2143	45.4
		2	6	2344	56.4
		3	7	2381	58.7
		4	8	2272	52.0
		5	9	1685	21.1
		6	10	1630	18.6
		7	11	1648	19.4
		8	12	1667	20.2
	32.06	1	5	1807	25.9
		2	6	1765	24.9
		3	7	1648	18.7
		4	8	1744	22.9
		5	9	1339	6.7
		6	10	1339	6.7
		7	11	1376	8.1
		8	12	1415	9.4
	16.02	1	5	1500	12.7
		2	6	1485	12.1
		3	7	1500	12.7
		4	8	1471	11.5
		5	9	1250	--
		6	10	1210	--
		7	11	1220	--
		8	12	1316	--
2.5:1	59.38	1	5	2420	62.3
		4	8	2380	59.7
		5	9	1649	20.1
		6	10	1630	19.2
		7	11	1649	20.1
		8	12	1668	20.9

*Shockwave velocities computed from piezoelectric gage data by dividing gage-to-gage distance by gage-to-gage elapsed time.

Table 3. (Continued).

Oxidizer/Fuel Ratio	Contact Area (ft^2)	Position (Gage No. to Gage No.)		Average* Velocity (ft/sec)	Calculated Shock Overpressure (psi)
2.5:1	29.65	1	5	1730	22.0
		2	6	1710	21.1
		3	7	1730	22.0
		4	8	1685	20.0
		5	9	1420	9.4
		6	10	1420	9.4
		7	11	1420	9.4
		8	12	1420	9.4
	14.83	1	5	1630	19.1
		2	6	1668	20.7
		3	7	1668	20.7
		4	8	1649	19.9
		5	9	1340	7.51
		6	10	1316	6.68
		7	11	1293	5.87
		8	12	1303	6.23
1.5:1	50.67	1	5	2345	56.7
		2	6	2345	56.7
		5	9	1705	22.2
		6	10	1648	19.6
		7	11	1725	23.1
		8	12	1630	18.9
	25.35	1	5	1704	22.4
		2	6	1704	22.4
		3	7	1667	20.6
		4	8	1724	23.3
		5	9	1415	10.1
		6	10	1389	9.25
		7	11	1415	10.1
		8	12	1442	11.3
	12.67	1	5	1830	26.5
		2	6	1900	29.8
		3	7	1830	26.5
		4	8	1875	28.6
		5	9	1409	8.98
		6	10	1375	7.79
		7	11	1415	9.17
		8	12	1415	9.17

*Shockwave velocities computed from piezoelectric gage data by dividing gage-to-gage distance by gage-to-gage elasped time.

Figure 12. Five-Channel Radiometer.

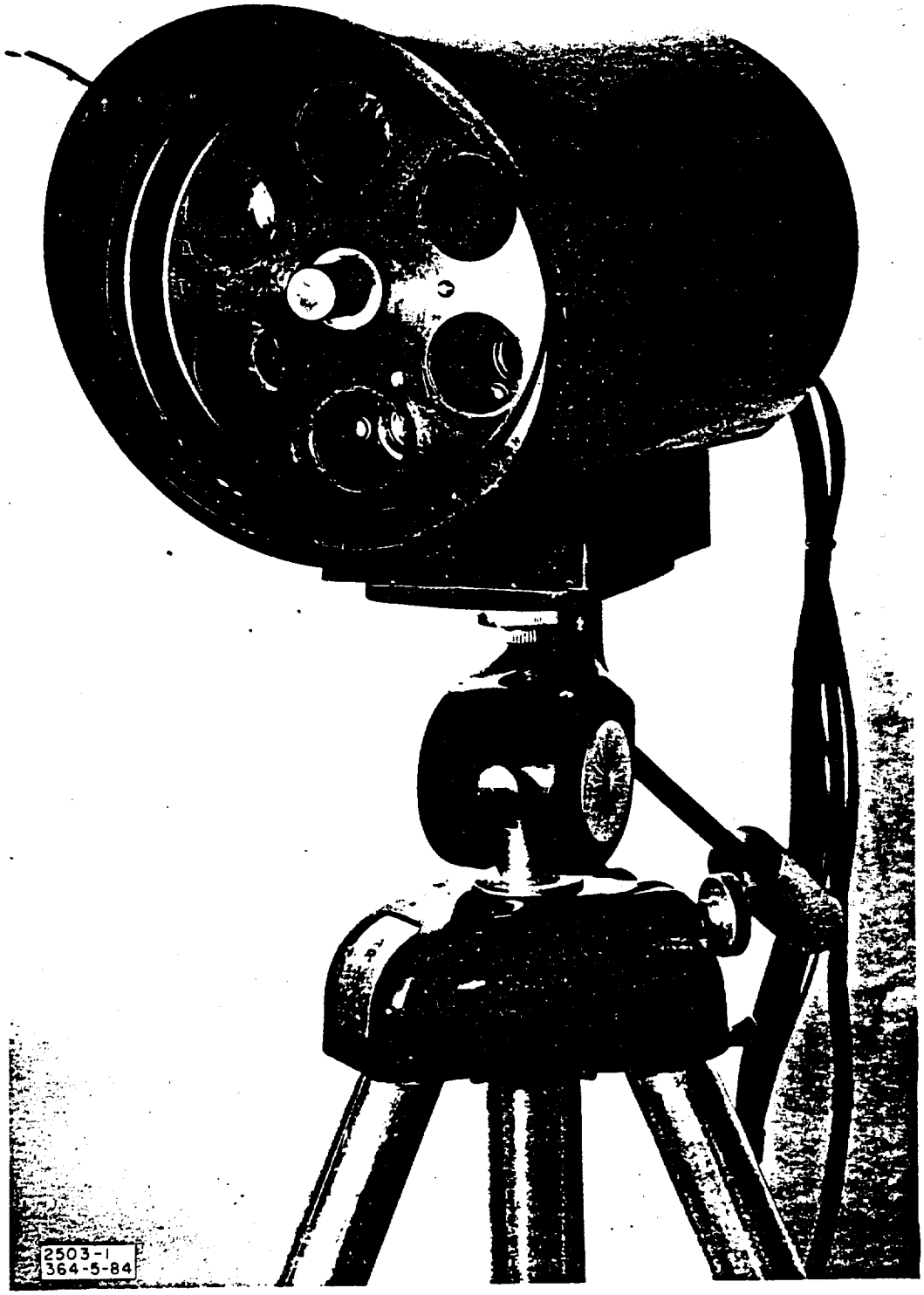

Figure 13. Radiometer Enclosure.

The relative spectral responses of each detector/filter combination were measured by comparison with a thermocouple, using a Perkin-Elmer spectrometer. The results are shown in Figures 14, 15, 16, and 17.

The radiometer was calibrated in terms of effective power for each spectral region; i. e., for the incident spectrum weighted by the spectral response of each detector. Mathematically, this is expressed by:

$$P\ (\text{effective}) = \int_0^\infty P(\lambda)\ R(\lambda)\ d\lambda \qquad (4)$$

where $P(\lambda)$ is the spectrum of the incident radiation, and $R(\lambda)$ is the normalized spectral response of a given channel. The effective irradiance during calibration was calculated by graphical evaluation of this integral. An 800°C blackbody was used for the calibration of PbS and PbSe detectors, and a tungsten strip filament lamp, spectrally calibrated by NBS, was used for the two silicon detectors. During individual calibrations for each test, another tungsten filament lamp, which had been compared with the NBS lamp, was used as a working standard; the 800°C blackbody was used with the other three channels.

Test measurements were made from the top of a ravine overlooking the test site. The radiometer and a tripod-mounted boresighted camera, were located approximately 400 ft from the test site, looking down at an angle of approximately 30° from horizontal. Output signals from the radiometer preamplifiers were further amplified and recorded on a CEC Model PR 2300 tape recorder.

The tape recorder and supporting equipment were located in a mobile instrumentation van positioned out of direct line-of-sight with the test area. Calibration of the radiometer was performed shortly before or after each test, with the calibration signals also being recorded on the tape system.

The recorded signals were subsequently played back on an oscillograph. Oscillograph deflections were measured, and the effective irradiance vs time was calculated by comparison with the calibrations. These values were then converted to apparent fireball intensity through multiplication by range squared. The term "apparent" is used because no corrections were made for atmospheric absorption in the 400-ft path.

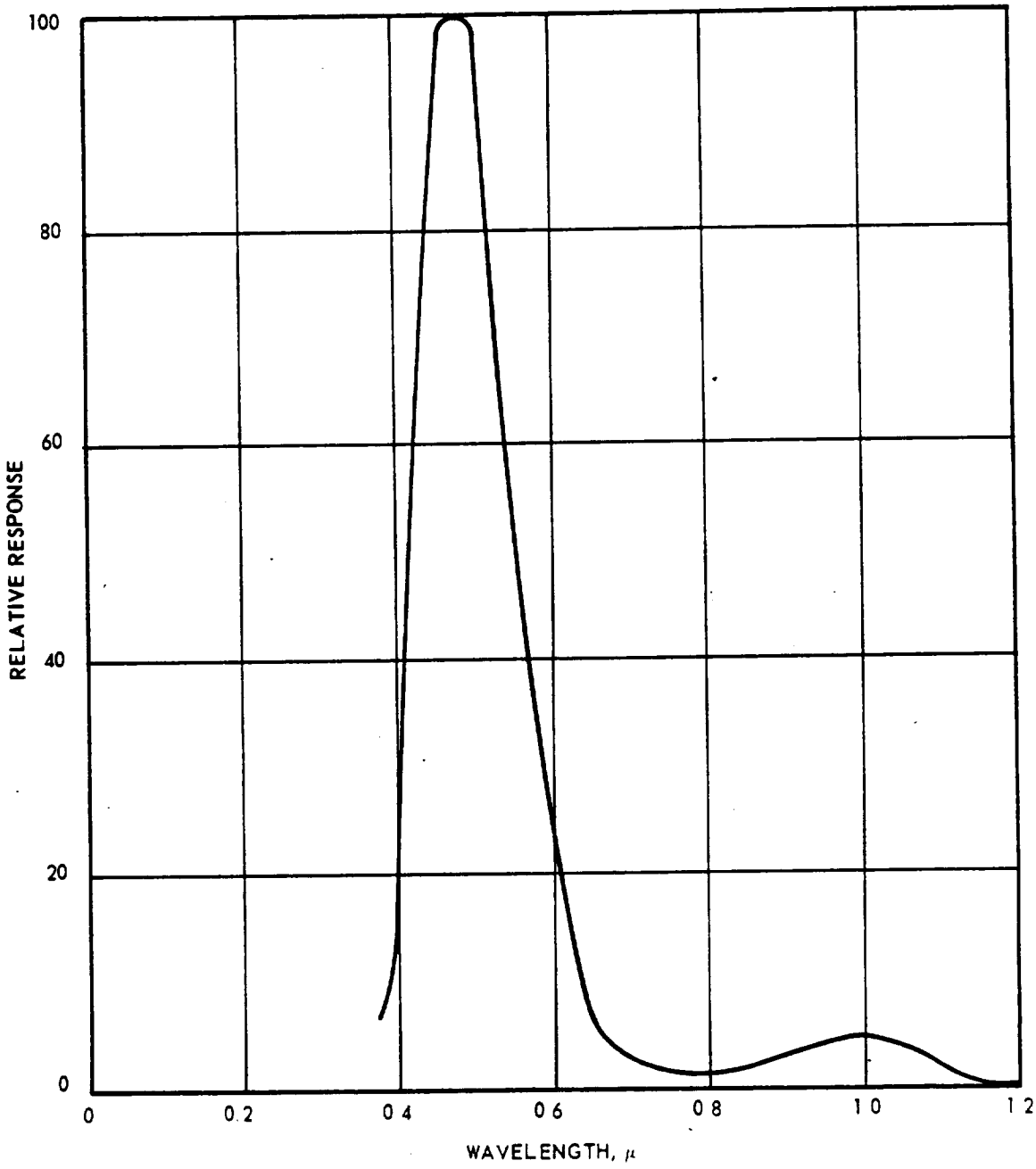

Figure 14. Relative Spectral Response - Short Wavelength Silicon Detector.

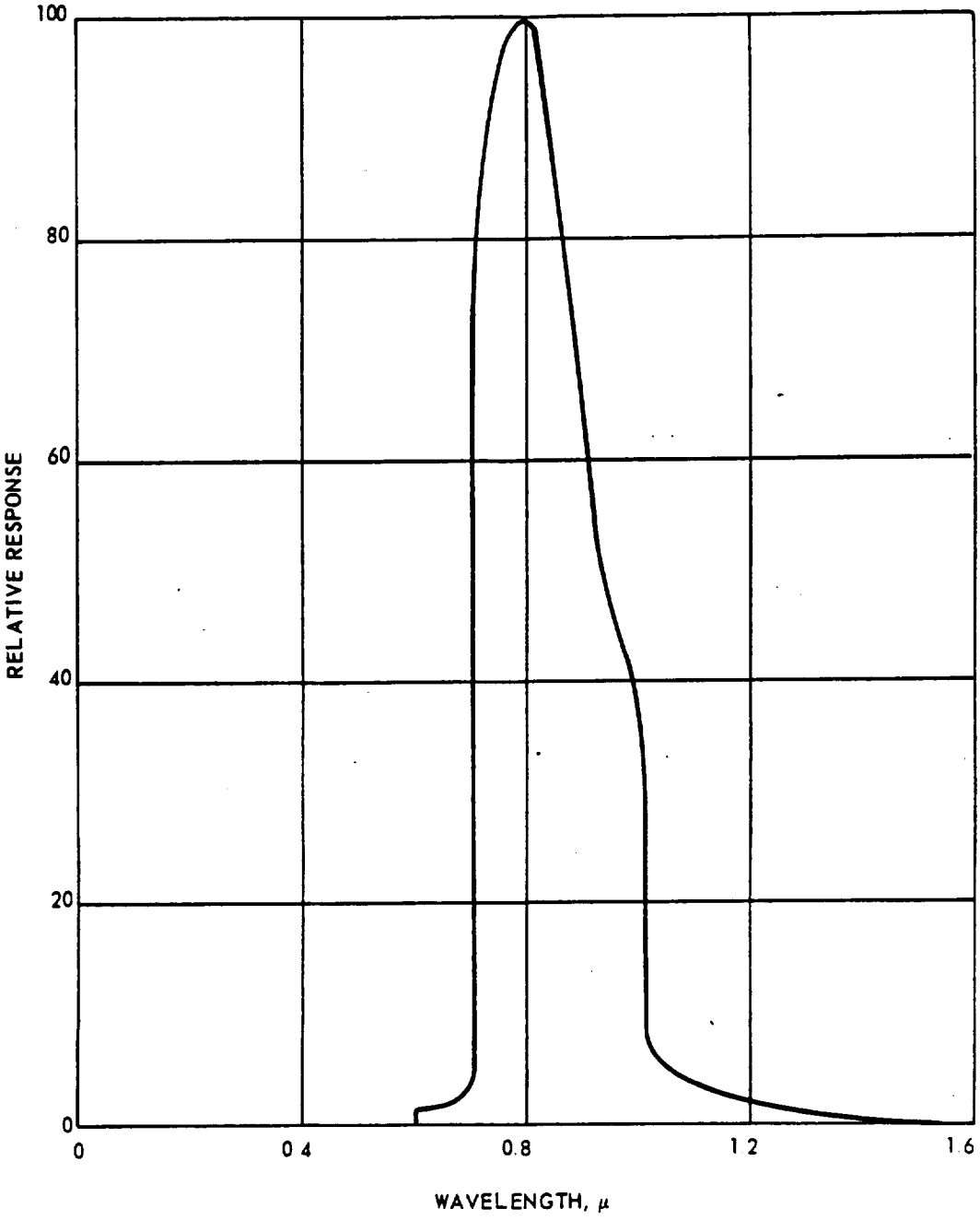

Figure 15. Relative Spectral Response - Long Wavelength Silicon Detector.

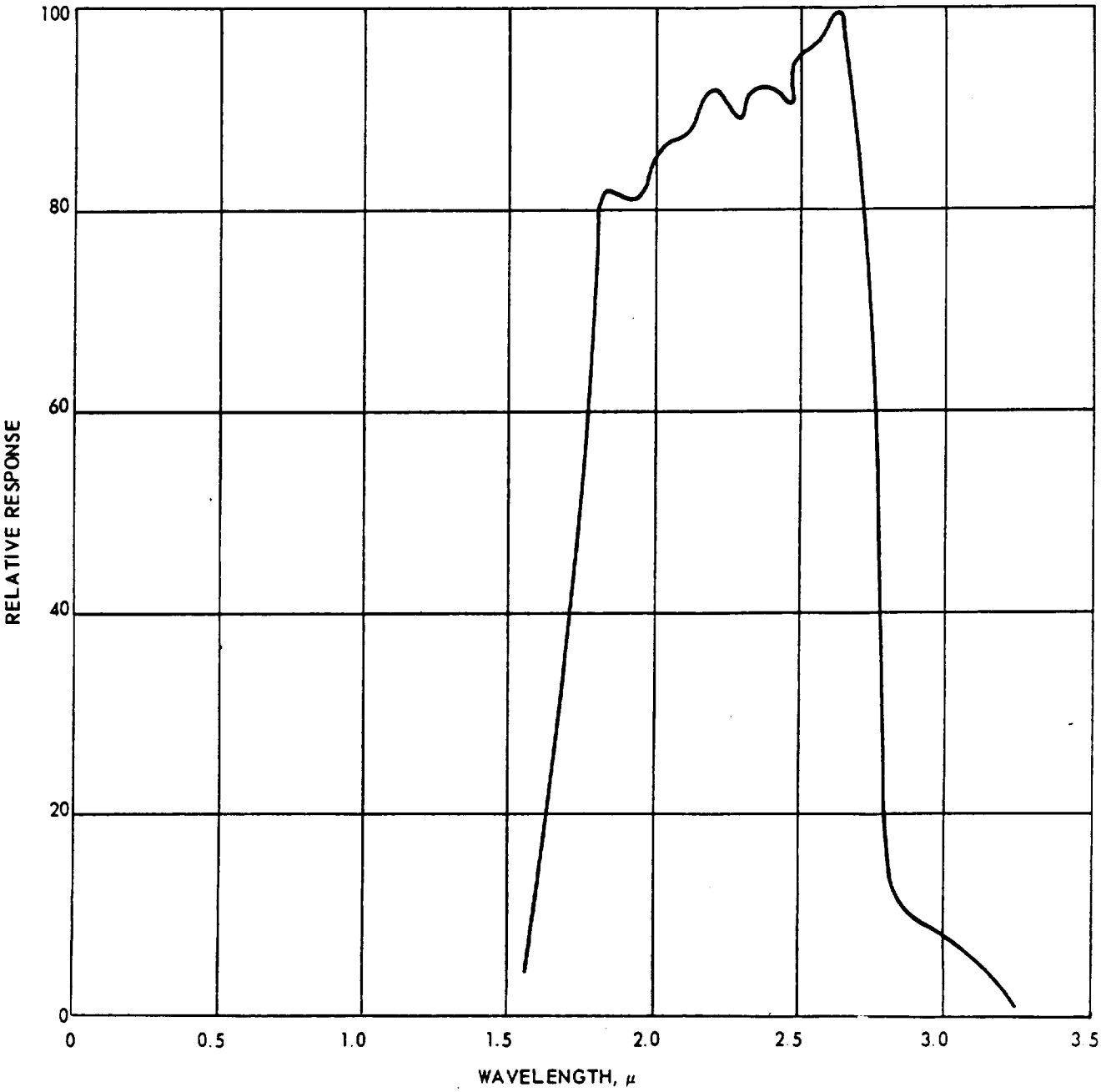

Figure 16. Relative Spectral Response - PbS Detector.

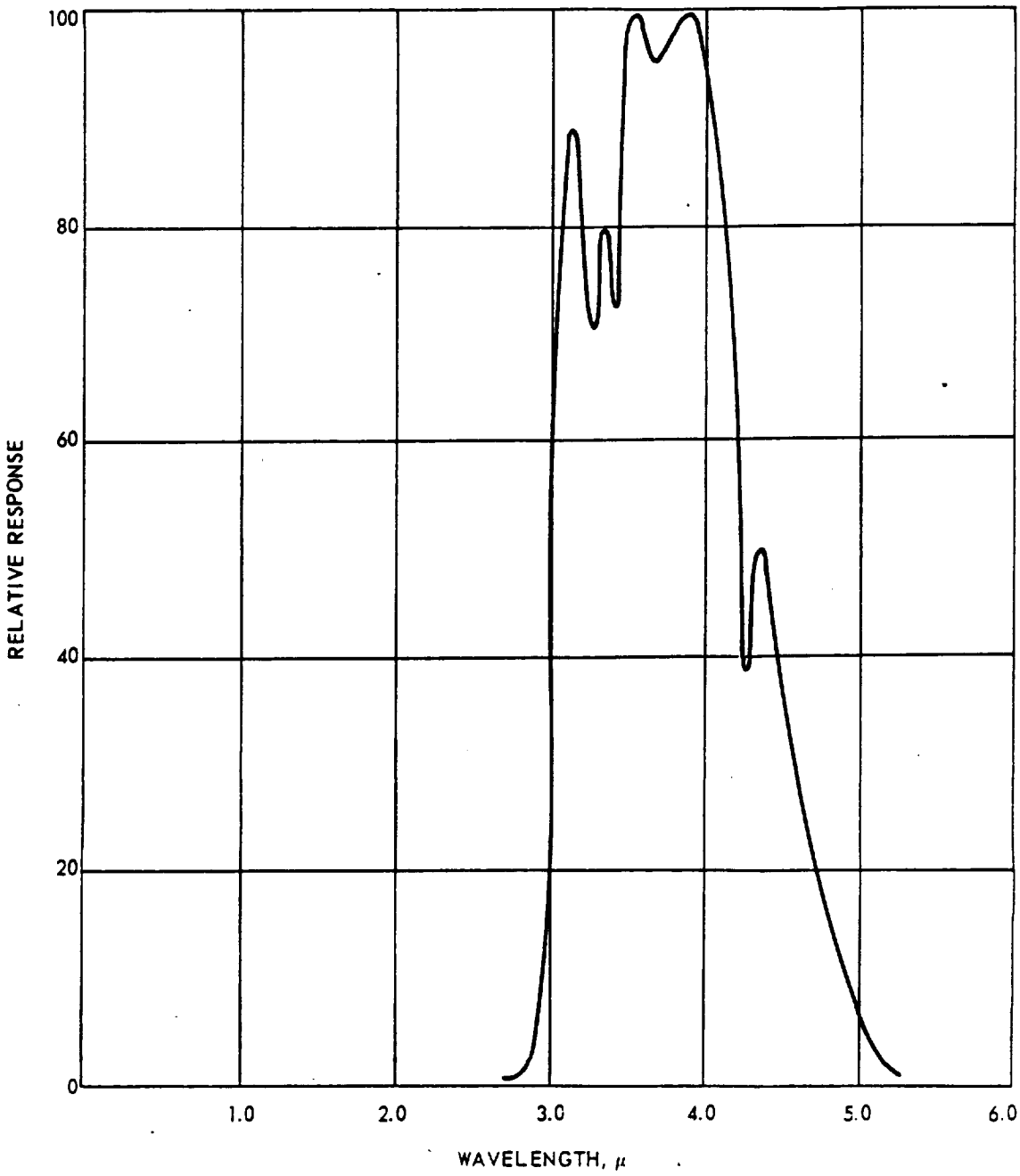

Figure 17. Relative Spectral Response - PbSe Detector.

Fireball temperatures were calculated from the wideband radiation measurements to provide a rough cross-check on temperatures measured with the thermocouple arrays.

In obtaining temperature values, which were calculated arbitrarily at the time of maximum radiation, the following assumptions were made:

a. The fireball shape was taken to be ellipsoidal with major and minor axes each given by the measured diameter and height at the time of maximum radiation (during the first 0.6 sec).

b. Obscuration of the fireball by smoke and dust was ignored.

c. Uniform temperature across the fireball and unit emissivity were assumed.

A more precise measurement of fireball area than that given by assuming the ellipsoidal shape was deemed unwarranted in view of the uncertainties introduced by the other factors.

The time of peak radiation was chosen arbitrarily, but with the allowance that obscuration would tend to be minimal at this point. Any obscuration was ignored, because there is no means of accounting for this effect.

Assumption of a uniform temperature is necessary because no attempt was made to determine the temperature profile. This results in average temperature values in the fourth-power sense.

The calculated temperatures can be corrected for emissivity values other than unity through division by $\epsilon^{1/4}$. For example, the calculated temperatures would be multiplied by 1.19 if $\epsilon = 0.5$ were assumed.

The fireball temperature is given by

$$T^4 = \frac{\pi J}{\sigma A}$$

where

T = temperature in ^{o}K

J = peak fireball intensity in w/steradian

A = fireball area in ft^2 at time of peak radiation

σ = Steffan-Boltzmann constant, 5.27×10^{-9} $w/cm^2 deg^4$

4.5.7 Fireball Size Measurements

The fireball size and history profiles were recorded with three cameras located at two viewing sites (Figure 6). The dimensions of the fireball were determined with a Millikan camera located approximately 400 ft from the test fixture. The Millikan camera was operated at the rate of 500 frames/sec to provide a time resolution that was commensurate with the operating duration of the camera. A Fastax or Photosonic camera was used to record the fireball on a horizontal plane with the test site. This camera served as a backup to the Millikan camera coverage.

The dimensions of the fireball were measured with a Gerber variable scale from a projected image of the film record. The scale was calibrated against the drop tower height (25 ft) and the measurements were made directly from the projected image.

A backup method of determining the dimensions of the fireball was utilized during the initial part of the program. This method consisted of a system of grid poles positioned on two sides of the test area (Figure 2). The aluminum poles were positioned 2 ft apart and were marked at 2-ft intervals with black paint (Figure 18). A comparison of the fireball dimensions from the two methods indicated no discrepancies, and therefore the backup method was eliminated.

The fireball duration was judged by the time at which the flame was no longer visible. The end of the propellant reactions was characterized by one or more localized fireballs, which were partially obscured by the combustion by-products. The termination point was difficult to determine in some tests due to this cloud of by-products.

4.5.8 Meteorological Measurements

Readings of humidity, temperature, atmospheric pressure, and wind velocity were recorded for each test. The humidity and temperature were determined with a Brown-chart-type recorder. The atmospheric pressure was measured with a mercury barometer. Due to the wind conditions at the test site, wind velocity was determined with an anemometer held next to the test fixture before and after each test.

Figure 18. A Typical Dewar/Pan Assembly Immediately After Impact on a Steel Pan (Note Propellant Reaction as Evidenced by Light Reflecting from the Top of the Tower).

4.5.9 Supporting Measurements

The supporting measurements consisted of small-scale Bikini-foil gage measurements and a cursory survey of the pan fragment dispersion. The foil gages were intended to serve as a dual purpose means of measurement. They were intended both to provide a rapid means of obtaining an estimate of the blast yield and to serve as backup instrumentation for the piezoelectric and BRL pressure gages. The gage results were inconsistent and no analysis will be made in this report.

The fragment survey was carried out with only limited success, because of the topography of the test site. The difficulty in obtaining most of the fragments after a test, especially in the high-yield studies, prevented a complete analysis. Only in the hypergolic low-contact-area tests did parts of the pan remain intact. In these tests the propellant reaction was insufficient to overcome the strength of the aluminum pan and the sides separated only at the welded corners.

In most tests, little of the pan assembly was found, and even if they were found, an accurate evaluation of the fragment horizontal flight distance could not be made because of the hill confinement on three sides of the test area.

4.6 TEST RESULTS

The test results from the experimental studies conducted on this program are presented in Tables 2 through 18.

4.6.1 TNT Equivalence

Results of the calibration tests are presented in Figures 19 through 33 by superimposing the pertinent TNT equivalence percentage curves over the results of the overpressure measurements for the various contact areas and mixture ratios. The calibration curves (Figures 19 and 24) permit a direct evaluation of the TNT equivalences for each test mixture and contact area. To permit a direct comparison of the test results for comparable mixture ratios and contact areas of the hypergolic and cryogenic propellants, the peak overpressure results were replotted in Figures 25 through 33 with the pertinent TNT data for equivalence determination.

Table 4. Test Results - N_2O_4/A-50; 3:1.

Contact Area (ft^2)	Distance from Event (ft)	Gage No.	Peak Overpressure (psi)	Positive Impulse (psi-msec)	Positive Pulse Duration (msec)	Maximum Radiant Heat Flux (BTU/ft^2-sec)	Maximum Temperature (^oF)
51.01	10	1	97.6	*	*	47.0	830
		2	85.0	186.0	7.4	46.0	1045
		3	103.0	*	*	43.0	> 235*
		4	103.1	147.0	4.8	51.0	1456
		mean	97.2	166.5	6.1		
	25	5	30.3	80.1	8.0	40.0	2016
		6	36.0	89.9	8.2	14.0	416
		7	20.4	55.2	6.0	12.0	240
		8	26.3	72.2	8.4	19.0	205
		mean	28.3	74.4	7.7		
	40	9	14.5	58.4	14.6	**	1109
		10	10.8	43.7	13.2	3.4	212
		11	12.3	43.2	11.8	**	240
		12	15.0	51.6	9.5	2.8	169
		mean	13.2	49.2	12.3		
25.44	10	1	21.7	95.2	13.7	57.0	3069
		2	16.3	85.5	14.3	46.0	2233
		3	19.5	84.3	9.6	45.0	1620
		4	**	**	**	**	**
		mean	19.2	88.3	12.5		
	25	5	10.3	39.5	10.4	25.5	482
		6	13.2	52.5	12.6	25.0	960.
		7	10.3	29.7	6.1	26.0	868
		8	11.0	34.5	9.5	15.5	320
		mean	11.2	39.1	9.2		
	40	9	5.4	29.5	12.3	**	198
		10	4.9	23.1	12.0	9.7	309
		11	5.5	24.7	15.9	**	1086
		12	6.7	25.5	10.0	4.9	218
		mean	5.5	25.7	12.5		
12.64	10	1	4.4	26.8	11.7	36.0	2695
		2	*	*	*	29.0	2341
		3	5.2	28.8	8.3	36.0	2040
		4	5.0	26.9	10.4	27.0	2326
		mean	4.9	27.5	10.1		
	25	5	2.3	12.0	11.2	45.0	2613
		6	2.5	12.0	8.8	40.0	1258
		7	2.3	10.5	7.3	12.5	Amb
		8	2.5	14.0	9.8	23.0	1589
		mean	2.4	12.1	9.3		
	40	9	1.3	8.6	11.1	**	Amb
		10	1.4	7.3	9.4	4.0	Amb
		11	1.5	7.5	8.6	**	Amb
		12	1.8	7.5	7.2	4.8	Amb
		mean	1.5	7.7	9.1		

*Gage damaged by fragments
**No gage

Table 5. Test Results - N_2O_4/A-50; 2:1.

Contact Area (ft^2)	Distance from Event (ft)	Gage No.	Peak Overpressure (psi)	Positive Impulse (psi-msec)	Positive Pulse Duration (msec)	Maximum Radiant Heat Flux (BTU/ft^2-sec)	Maximum Temperature (°F)
45.53	10	1	52.6	163.0	19.8	60.0	*
		2	52.9	104.0	3.7	51.0	*
		3	81.3	133.0	4.1	62.0	1765
		4	70.7	*	*	66.0	270
		mean	64.4	133.3	9.3		
	25	5	24.9	77.9	11.1	15.0	1362
		6	35.7	106.0	11.8	46.5	2025
		7	19.1	55.8	5.4	20.0	187
		8	23.9	*	*	*	150
		mean	25.9	79.7	9.4		
	40	9	10.7	54.4	14.1	**	Amb
		10	10.0	49.4	11.8	5.0	898
		11	11.1	50.3	11.1	**	197
		12	14.5	47.6	6.2	6.1	179
		mean	11.6	50.4	10.8		
22.90	10	1	22.9	103.1	12.9	61.0	2347
		2	20.2	92.5	13.7	50.0	2891
		3	19.4	80.6	9.2	73.0	3125
		4	*	*	*	*	*
		mean	20.8	92.1	11.9		
	25	5	10.5	45.8	12.0	60.5	3002
		6	13.7	58.1	13.1	39.0	2129
		7	9.8	41.8	12.1	36.2	1178
		8	10.1	40.6	10.0	23.0	325
		mean	11.0	46.6	11.8		
	40	9	5.8	33.2	13.3	*	290
		10	5.4	26.2	11.9	10.0	225
		11	5.7	28.1	13.4	*	185
		12	6.7	29.7	10.3	7.2	205
		mean	5.9	29.3	12.2		
11.39	10	1	2.4	21.5	13.4	36.0	2515
		2	3.2	29.3	11.6	33.0	2865
		3	4.0	25.4	9.9	49.0	1994
		4	3.2	26.1	10.3	35.0	2368
		mean	3.3	25.6	11.3		
	25	5	1.7	12.7	15.1	30.0	2004
		6	2.2	16.6	16.0	36.0	2539
		7	1.9	12.3	15.9	16.0	212
		8	2.0	12.2	9.8	23.0	1897
		mean	2.0	13.5	14.2		
	40	9	1.2	8.7	12.6	**	Amb
		10	1.0	6.6	10.5	9.5	336
		11	1.1	7.3	10.4	**	186
		12	1.4	8.4	10.4	9.0	212
		mean	1.2	7.8	11.0		

*Gage damaged by fragments
**No gage

Table 6. Test Results - N_2O_4/A-50; 1:1.

Contact Area (ft^2)	Distance from Event (ft)	Gage No.	Peak Overpressure (psi)	Positive Impulse (psi-msec)	Positive Pulse Duration (msec)	Maximum Radiant Heat Flux (BTU/ft^2-sec)	Maximum Temperature (^oF)
35.90	10	1	52.8	144.0	8.5	62.0	2952
		2	75.8	172.0	7.1	57.0	2226
		3	56.5	131.0	5.4	66.0	*
		4	75.0	147.0	6.8	64.0	2356
		mean	65.0	148.3	7.0		
	25	5	24.9	73.9	10.3	57.5	3013
		6	34.2	81.5	8.8	36.0	*
		7	22.2	62.9	9.5	69.0	2163
		8	28.5	82.4	9.1	54.0	> 2739*
		mean	27.5	75.2	9.4		
	40	9	11.5	55.4	13.9	**	2152
		10	10.9	39.8	12.1	16.4	299
		11	11.4	43.6	11.7	**	263
		12	13.7	52.1	8.7	15.4	330
		mean	11.9	47.7	11.6		
17.96	10	1	11.9	67.3	14.6	62.0	> 568*
		2	13.5	91.5	12.0	51.0	2193
		3	12.2	62.3	8.9	80.0	> 269*
		4	11.5	69.7	14.0	75.0	>1613*
		mean	12.3	72.7	12.4		
	25	5	8.0	43.2	15.2	47.0	1979
		6	6.7	32.4	12.8	35.0	1197
		7	7.1	37.3	12.0	43.5	265
		8	8.9	44.7	11.5	40.0	994
		mean	7.7	39.4	12.9		
	40	9	4.6	27.3	13.2	**	249
		10	3.1	17.3	16.5	16.3	334
		11	4.6	22.1	9.3	**	223
		12	4.3	19.3	12.1	11.7	216
		mean	4.2	21.5	12.8		
8.88	10	1	4.2	25.6	14.3	45.0	2998
		2	3.3	23.0	13.2	43.0	2931
		3	3.6	20.7	11.4	55.0	2061
		4	5.0	33.6	12.8	40.0	2337
		mean	4.0	25.7	12.9		
	25	5	2.1	12.3	12.4	38.0	2338
		6	2.5	17.4	16.0	23.0	840
		7	2.2	12.3	16.9	19.0	202
		8	3.0	13.9	11.9	19.5	Amb
		mean	2.5	14.0	14.3		
	40	9	1.5	10.5	16.2	**	Amb
		10	1.1	8.0	14.1	12.0	265
		11	1.6	9.7	16.2	**	Amb
		12	2.1	9.3	11.9	7.3	Amb
		mean	1.6	9.4	12.1		

*Gage damaged by fragments
**No gage

Table 7. Test Results - LOX/RP-1; 3. :1.

Contact Area (ft^2)	Distance from Event (ft)	Gage No.	Peak Overpressure (psi)	Positive Impulse (psi-msec)	Positive Pulse Duration (msec)	Maximum Radiant Heat Flux (BTU/ft^2-sec)	Maximum Temperature (°F)
57.85	10	1	76.4	120.4	3.3	90.0	2219
		2	79.5	164.1	6.2	80.0	*
		3	98.3	196.7	5.7	90.0	1750
		4	76.8	147.4	3.4	115.0	*
		mean	82.8	157.1	4.7		
	25	5	27.7	61.1	5.5	42.0	1007
		6	25.4	55.9	5.7	28.0	1064
		7	26.7	61.9	5.7	37.0	1607
		8	30.3	63.6	6.1	72.0	*
		mean	27.5	60.6	5.6		
	40	9	13.0	42.5	6.8	>12.2*	*
		10	12.4	46.0	8.9	12.5	1371
		11	10.9	47.4	12.5	**	Amb
		12	12.2	34.6	7.8	13.0	Amb
		mean	12.1	42.6	9.0		
32.06	10	1	39.2	107.6	5.8	62.0	2735
		2	43.9	101.8	7.1	>43.0	>1252*
		3	32.7	107.2	6.8	**	2586
		4	44.2	139.0	7.7	87.0	2848
		mean	40.0	113.9	6.4		
	25	5	16.1	48.0	6.9	38.0	2168
		6	15.1	50.4	9.1	25.0	*
		7	15.1	49.2	7.6	48.5	889
		8	19.4	51.6	7.0	37.0	276
		mean	16.4	49.8	7.7		
	40	9	8.0	42.2	15.5	9.5	Amb
		10	6.6	31.8	13.0	12.1	253
		11	7.1	36.0	13.6	**	305
		12	7.6	28.6	8.2	9.2	Amb
		mean	7.3	34.7	12.6		
16.02	10	1	33.7	59.5	4.8	76.0	2276
		2	37.0	71.7	5.9	71.0	2464
		3	43.0	65.4	6.4	87.0	2581
		4	47.8	64.8	5.4	78.0	2253
		mean	40.4	65.4	5.6		
	25	5	11.0	43.3	12.5	20.0	1145
		6	13.2	43.8	7.4	56.0	1866
		7	10.3	27.4	7.3	53.0	1909
		8	12.9	43.1	7.7	44.0	1979
		mean	11.9	39.4	8.7		
	40	9	4.0	18.5	12.0	**	2239
		10	3.6	16.4	10.3	16.4	1647
		11	3.7	18.6	15.5	**	1639
		12	4.1	20.7	10.5	17.0	1317
		mean	3.9	18.6	12.1		

*Gage damaged by fragments
**No gage

Table 8. Test Results - LOX/RP-1; 2.5:1.

Contact Area (ft^2)	Distance from Event (ft)	Gage No.	Peak Overpressure (psi)	Positive Impulse (psi-msec)	Positive Pulse Duration (msec)	Maximum Radiant Heat Flux (BTU/ft^2-sec)	Maximum Temperature (^oF)
59.38	10	1	96.4	259.6	8.1	263.0	*
		2	*	*	*	80.0	*
		3	*	*	*	110.0	*
		4	110.4	312.4	8.6	35.0	*
		mean	103.4	286.0	8.4		
	25	5	30.6	68.8	6.5	*	*
		6	29.0	95.0	11.2	12.0	2239
		7	29.8	57.8	4.9	52.0	2241
		8	35.2	75.8	6.6	63.0	1435
		mean	31.3	74.4	7.3		
	40	9	14.2	69.4	14.9	20.0	303
		10	12.6	52.0	13.4	18.0	231
		11	13.2	43.6	8.3	**	2515
		12	13.4	48.8	7.9	14.3	243
		mean	13.3	53.5	11.1		
29.65	10	1	32.7	125.5	12.2	167.0	*
		2	23.0	110.5	11.8	145.0	3240
		3	30.4	110.0	9.6	171.0	3362
		4	36.0	95.7	10.5	135.0	> 936*
		mean	30.3	110.4	11.0		
	25	5	11.5	46.2	8.3	125.0	3208
		6	13.4	58.2	11.8	109.0	3198
		7	13.1	52.1	13.5	125.0	3076
		8	12.4	39.8	9.2	*	*
		mean	12.6	49.8	10.7		
	40	9	6.9	34.4	10.5	31.0	384
		10	6.7	33.3	15.9	28.0	Amb
		11	6.2	30.7	14.8	**	Amb
		12	6.3	30.7	15.2	23.5	721
		mean	6.5	32.3	14.1		
14.83	10	1	39.1	59.0	4.6	*	2650
		2	30.7	52.1	3.8	100.0	3007
		3	34.4	54.1	3.1	98.0	2426
		4	32.7	53.4	3.5	42.0	2718
		mean	34.2	54.7	3.8		
	25	5	10.0	30.1	10.7	45.0	> 1548***
		6	10.9	33.3	7.0	64.0	2530
		7	9.3	28.5	9.3	41.8	*
		8	9.7	29.8	8.2	100.0	3307
		mean	10.0	30.4	8.8		
	40	9	4.8	19.8	8.7	46.3	2465
		10	4.8	17.2	8.0	39.7	>2189***
		11	4.5	19.8	12.4	**	> 811***
		12	4.9	15.9	6.2	26.5	> 989***
		mean	4.8	18.2	8.8		

*Gage damaged by fragments
**No gage
***Loss of electrical power terminated record before completion

Table 9. Test Results - LOX/RP-1; 1.5:1.

Contact Area (ft^2)	Distance from Event (ft)	Gage No.	Peak Overpressure (psi)	Positive Impulse (psi-msec)	Positive Pulse Duration (msec)	Maximum Radiant Heat Flux (BTU/ft^2-sec)	Maximum Temperature (^oF)
50.67	10	1	88.0	*	*	133.0	> 590**
		2	75.3	*	*	> 100.0**	> 430**
		3	*	*	*	> 100.0**	*
		4	*	*	*	> 50.0**	2365
		mean	81.6				
	25	5	25.7	81.9	10.3	97.0	3220
		6	25.8	72.2	6.3	> 39.0**	**
		7	29.6	83.7	10.4	> 11.0**	**
		8	33.0	81.5	6.8	53.0	631
		mean	28.5	79.8	8.5		
	40	9	11.4	68.1	14.7	36.5	2418
		10	10.6	52.5	13.0	> 5.0**	**
		11	9.6	62.4	21.3	***	**
		12	13.4	55.8	7.9	19.4	**
		mean	11.3	59.7	14.2		
25.35	10	1	33.8	102.4	12.6	127.0	3172
		2	30.5	95.1	9.4	*	*
		3	*	*	*	165.0	3380
		4	31.4	62.7	5.1	152.0	1805
		mean	31.9	86.7	9.0		
	25	5	10.8	39.2	9.6	107.0	2675
		6	10.8	38.9	9.2	76.5	2306
		7	10.5	34.7	8.2	118.8	3220
		8	12.3	39.8	8.5	101.5	2368
		mean	11.1	38.2	8.9		
	40	9	6.3	33.3	14.5	27.2	269
		10	5.3	27.8	15.7	28.8	376
		11	5.6	27.1	12.5	***	338
		12	6.2	27.5	12.2	25.5	312
		mean	5.9	28.9	13.7		
12.67	10	1	40.9	95.2	7.0	78.0	2670
		2	50.9	83.5	5.0	65.0	2900
		3	46.7	67.5	5.3	74.0	*
		4	57.3	78.1	5.2	81.0	3000
		mean	49.0	81.1	5.6		
	25	5	12.0	47.8	8.5	69.0	2980
		6	12.2	32.0	6.5	74.0	2530
		7	11.9	41.3	5.2	56.9	2120
		8	12.7	32.6	6.2	87.0	2860
		mean	12.2	38.4	6.6		
	40	9	6.8	32.2	10.6	29.4	885
		10	4.7	21.3	7.8	44.0	2360
		11	3.9	17.5	11.1	***	203
		12	4.6	16.7	6.5	37.9	1003
		mean	5.0	21.9	9.0		

*Gage damaged by fragments
**Fragment severed instrumentation cable before record completed
***No gage

Table 10. Fireball Size and Duration Data

Oxidizer/Fuel Ratio	Contact Area (ft^2)	Maximum Size Height (ft)	Maximum Size Diameter (ft)	Duration (sec)
		LOX/RP-1		
3.5:1	57.85	48	79	1.90
	32.06	55	97	1.99
	16.02	47	108	2.55
2.5:1	59.38	60	80	1.70
	29.65	51	66	2.25
	14.83	30	103	1.99
1.5:1	50.67	71	85	2.50
	25.35	83	81	2.49
	12.67	36	102	2.07
		N_2O_4/A-50		
3:1	51.01	44	59	0.5
	25.44	31	62	1.2
	12.64	33	66	1.8
2:1	45.53	41	67	0.8
	22.90	52	58	1.97
	11.39	31	62	2.2
1:1	35.90	47	80	2.2
	17.96	44	71	2.0
	8.88	59	70	2.9

Table 11. Fireball Spectral Distribution and Intensity - N_2O_4/A-50.

Oxidizer/Fuel Ratio	Contact Area (ft^2)	Time (sec)	Intensity (w/steradian) Channel 1[a] (0.4 to 0.7μ)	Channel 2[b] (0.7 to 1.1μ)	Channel 3[c] (1.8 to 2.7μ)	Channel 4[d] (3 to 5μ)	Channel 5[e] (0.5 to 35μ)
3:1	51.01	0.07	-	-	1.14×10^6	8.10×10^5	-
		0.1	2.60×10^4	1.30×10^5	1.02×10^6	7.80×10^5	5.00×10^6
		0.2	1.15×10^4	5.70×10^4	5.00×10^5	4.40×10^5	2.50×10^6
		0.3	9.60×10^3	5.70×10^4	3.70×10^5	2.50×10^5	1.35×10^6
		0.4	1.25×10^4	3.60×10^4	1.36×10^5	1.42×10^5	9.70×10^5
		0.6	-	-	7.00×10^4	6.50×10^4	6.30×10^5
		0.8	-	-	3.80×10^4	5.30×10^4	5.00×10^5
		1.0	-	-	4.20×10^4	1.85×10^4	3.40×10^5
		1.2	-	-	-	-	3.20×10^5
		Note: The first two channels were barely above signal due to sunlit terrain.					
	25.44	0.1	4.80×10^4	1.56×10^5	1.75×10^6	1.32×10^6	1.09×10^7
		0.13	-	-	1.82×10^6	1.38×10^6	-
		0.2	4.80×10^4	1.26×10^5	1.77×10^6	1.39×10^6	1.11×10^7
		0.3	3.30×10^4	7.90×10^4	1.50×10^6	1.22×10^6	9.30×10^6
		0.4	2.60×10^4	5.50×10^4	1.23×10^6	9.70×10^5	6.80×10^6
		0.5	-	-	1.00×10^6	8.10×10^5	6.00×10^6
		0.6	1.25×10^4	7.40×10^4	8.40×10^5	6.80×10^5	4.60×10^6
		0.8	1.00×10^4	5.50×10^4	6.00×10^5	4.90×10^5	3.40×10^6
		1.0	-	-	4.00×10^5	4.10×10^5	2.30×10^6
		1.2	-	-	3.20×10^5	3.20×10^5	2.00×10^6
		1.4	-	-	2.70×10^5	2.60×10^5	1.60×10^6
		1.6	-	-	2.40×10^5	1.95×10^5	1.40×10^6
		1.8	-	-	1.35×10^5	1.32×10^5	8.50×10^5
		2.0	-	-	9.40×10^4	7.80×10^4	7.00×10^5
		2.2	-	-	8.30×10^4	5.50×10^4	7.00×10^5
	12.64	0.1	3.50×10^4	6.50×10^4	5.70×10^5	3.90×10^5	4.10×10^6
		0.2	3.50×10^4	7.10×10^4	8.40×10^5	5.60×10^5	5.80×10^6
		0.3	2.90×10^4	7.90×10^4	1.00×10^6	6.70×10^5	6.70×10^6
		0.4	2.80×10^4	9.80×10^4	1.09×10^6	7.40×10^5	7.30×10^6
		0.5	2.40×10^4	8.20×10^4	1.15×10^6	7.90×10^5	7.80×10^6
		0.6	2.50×10^4	9.40×10^4	1.16×10^6	8.00×10^5	7.70×10^6
		0.7	-	-	1.14×10^6	8.10×10^5	7.50×10^6
		0.8	-	-	1.09×10^6	7.80×10^5	7.20×10^6
		0.9	-	-	1.05×10^6	7.50×10^5	-
		1.0	-	-	9.85×10^5	7.10×10^5	6.60×10^6
		1.2	-	-	8.50×10^5	6.10×10^5	5.70×10^6
		1.4	-	-	6.60×10^5	5.00×10^5	4.40×10^6
		1.6	-	-	4.50×10^5	3.60×10^5	3.30×10^6
		1.8	-	-	2.90×10^5	2.40×10^5	2.20×10^6
		2.0	-	-	1.65×10^5	1.50×10^5	1.75×10^6
		2.2	-	-	1.06×10^5	9.70×10^4	1.45×10^6
		2.4	-	-	8.00×10^4	7.00×10^4	1.03×10^6

Note: The first two channels were barely above signal due to sunlit terrain.

Table 11. Continued

Oxidizer/Fuel Ratio	Contact Area (ft^2)	Time (sec)	Intensity (w/steradian) Channel 1[a] (0.4 to 0.7μ)	Channel 2[b] (0.7 to 1.1μ)	Channel 3[c] (1.8 to 2.7μ)	Channel 4[d] (3 to 5μ)	Channel 5[e] (0.5 to 35μ)
2:1	45.53	0.07	-	-	1.84×10^6	1.36×10^6	2.10×10^6
		0.1	4.10×10^4	2.05×10^5	1.73×10^6	1.34×10^6	8.60×10^6
		0.2	1.83×10^4	9.30×10^4	1.19×10^6	1.02×10^6	5.60×10^6
		0.3	9.90×10^3	5.60×10^4	8.40×10^5	7.40×10^5	3.70×10^6
		0.4	-	-	5.90×10^5	5.40×10^5	3.00×10^6
		0.5	-	-	4.40×10^5	4.20×10^5	2.00×10^6
		0.6	-	-	2.90×10^5	2.90×10^5	1.50×10^6
		0.7	-	-	2.40×10^5	2.30×10^5	1.25×10^6
		0.8	-	-	1.70×10^5	1.86×10^5	1.35×10^6
		1.0	-	-	1.17×10^5	1.30×10^5	6.50×10^5
		1.2	-	-	1.08×10^5	1.05×10^5	7.00×10^5
		1.4	-	-	8.10×10^4	7.30×10^4	5.50×10^5
		1.6	-	-	6.30×10^4	5.70×10^4	6.50×10^5
		Note: Appreciable sunlight component in the first two channel signals.					
	22.90	0.1	5.30×10^4	2.20×10^5	1.96×10^6	1.44×10^6	1.11×10^7
		0.2	5.30×10^4	2.30×10^5	2.10×10^6	1.67×10^6	1.23×10^7
		0.3	4.90×10^4	1.90×10^5	2.05×10^6	1.64×10^6	1.16×10^7
		0.4	3.40×10^4	1.56×10^5	1.87×10^6	1.55×10^6	1.06×10^7
		0.5	-	-	1.70×10^6	1.43×10^6	9.00×10^6
		0.6	2.05×10^4	9.30×10^4	1.50×10^6	1.26×10^6	7.90×10^6
		0.7	-	-	1.30×10^6	1.12×10^6	6.70×10^6
		0.8	1.20×10^4	6.00×10^4	1.19×10^6	9.80×10^5	5.60×10^6
		1.0	1.00×10^4	4.90×10^4	8.10×10^5	7.30×10^5	4.30×10^6
		1.2	-	-	5.80×10^5	5.40×10^5	3.10×10^6
		1.4	-	-	4.50×10^5	4.20×10^5	2.20×10^6
		1.6	-	-	2.70×10^5	2.80×10^5	1.70×10^6
		1.8	-	-	1.65×10^5	1.70×10^5	1.10×10^6
		2.0	-	-	1.05×10^5	1.15×10^5	8.00×10^5
		2.2	-	-	7.00×10^4	7.70×10^4	6.50×10^5
		2.4	-	-	5.20×10^4	6.20×10^4	6.00×10^5
		2.6	-	-	-	-	4.50×10^5
	11.39	0.1	4.00×10^4	6.70×10^4	5.80×10^5	4.10×10^5	3.60×10^6
		0.2	4.80×10^4	9.30×10^4	9.20×10^5	6.90×10^5	6.10×10^6
		0.3	5.10×10^4	1.04×10^5	1.11×10^6	8.40×10^5	7.30×10^6
		0.4	4.50×10^4	1.02×10^5	1.22×10^6	9.30×10^5	8.30×10^6
		0.5	3.90×10^4	1.12×10^5	1.28×10^6	9.90×10^5	8.50×10^6
		0.6	3.80×10^4	1.15×10^5	1.36×10^6	1.04×10^6	9.00×10^6
		0.7	-	-	1.35×10^6	1.07×10^6	-
		0.8	2.60×10^4	6.70×10^4	1.35×10^6	1.08×10^6	9.00×10^6
		0.9	-	-	1.34×10^6	1.09×10^6	-
		1.0	1.78×10^4	6.40×10^4	1.32×10^6	1.09×10^6	8.80×10^6
		1.2	1.33×10^4	6.20×10^4	1.25×10^6	1.05×10^6	8.40×10^6
		1.4	1.29×10^4	6.20×10^4	1.17×10^6	9.90×10^5	8.20×10^6

Table 11. Continued

Oxidizer/Fuel Ratio	Contract Area (ft^2)	Time (sec)	Intensity (w/steradian) Channel 1[a] (0.4 to 0.7μ)	Channel 2[b] (0.7 to 1.1μ)	Channel 3[c] (1.8 to 2.7μ)	Channel 4[d] (3 to 5μ)	Channel 5[e] (0.5 to 35μ)
2:1 (cont)	11.39 (cont)	1.6	1.15×10^4	4.80×10^4	1.04×10^6	8.90×10^5	7.50×10^6
		1.8	1.50×10^4	6.40×10^4	9.30×10^5	7.90×10^5	6.60×10^6
		2.0	9.40×10^3	4.00×10^4	7.60×10^5	6.40×10^5	5.60×10^6
		2.2	1.19×10^4	-	5.90×10^5	5.10×10^5	4.50×10^6
		2.4	4.70×10^3	-	4.30×10^5	3.80×10^5	3.30×10^6
		2.6	-	-	3.00×10^5	2.70×10^5	2.40×10^6
		2.8	-	-	2.00×10^5	1.80×10^5	1.70×10^6
		3.0	-	-	1.30×10^5	1.25×10^5	1.50×10^6
		3.2	-	-	9.00×10^4	1.00×10^5	1.20×10^6
		3.4	-	-	7.70×10^4	-	1.00×10^6
		Note: Appreciable sunlight component in the first two channel signals.					
1:1	35.90	0.1	1.19×10^5	4.00×10^5	2.40×10^6	2.00×10^6	1.92×10^7
		0.13	-	-	2.50×10^6	2.10×10^6	-
		0.2	9.20×10^4	3.60×10^5	2.50×10^6	2.20×10^6	1.95×10^7
		0.3	5.40×10^4	2.50×10^5	2.40×10^6	2.10×10^6	1.80×10^7
		0.4	3.70×10^4	1.84×10^5	2.20×10^6	1.95×10^6	1.62×10^7
		0.5	4.60×10^4	2.10×10^5	2.00×10^6	1.78×10^6	1.45×10^7
		0.6	2.60×10^4	1.48×10^5	1.74×10^6	1.57×10^6	1.27×10^7
		0.7	-	-	1.54×10^6	1.37×10^6	-
		0.8	1.90×10^4	7.80×10^4	1.32×10^6	1.18×10^6	8.90×10^6
		1.0	1.70×10^4	7.50×10^4	9.30×10^5	8.40×10^5	6.30×10^6
		1.2	1.25×10^4	5.10×10^4	6.40×10^5	5.90×10^5	4.50×10^6
		1.4	-	-	4.40×10^5	4.20×10^5	3.50×10^6
		1.6	-	-	2.60×10^5	2.90×10^5	2.50×10^6
		1.8	-	-	1.50×10^5	1.87×10^5	1.70×10^6
		2.0	-	-	1.05×10^5	1.17×10^5	1.50×10^6
		2.2	-	-	7.00×10^4	8.60×10^4	-
	17.96	0.1	4.30×10^4	1.13×10^5	1.87×10^6	1.34×10^6	No data
		0.2	6.00×10^4	1.71×10^5	2.50×10^6	1.95×10^6	
		0.3	6.20×10^4	1.77×10^5	2.70×10^6	2.15×10^6	
		0.4	4.70×10^4	1.59×10^5	2.70×10^6	2.20×10^6	
		0.6	3.40×10^4	1.55×10^5	2.50×10^6	2.00×10^6	
		0.8	1.85×10^4	1.01×10^5	2.20×10^6	1.78×10^6	
		1.0	1.95×10^4	9.50×10^4	1.82×10^6	1.61×10^6	
		1.2	1.55×10^4	7.60×10^4	1.63×10^6	1.34×10^6	
		1.4	-	5.70×10^4	1.52×10^6	1.22×10^6	
		1.6	-	7.70×10^4	1.35×10^6	1.10×10^6	
		1.8	-	5.50×10^4	1.21×10^6	1.02×10^6	
		2.0	-	-	9.90×10^5	8.70×10^5	
		2.2	-	-	6.90×10^5	6.20×10^5	
		2.4	-	-	4.40×10^5	4.10×10^5	
		2.6	-	-	2.70×10^5	2.60×10^5	
		2.8	-	-	1.70×10^5	1.78×10^5	
		3.0	-	-	1.05×10^5	1.38×10^5	
	8.88	No data					

Measurements made with:

a. short wavelength silicon detector
b. long wavelength silicon detector
c. PbS detector
d. PbSe detector
e. bolometer

Table 12. Fireball Spectral Distribution and Intensity - LOX/RP-1.

Oxidizer/Fuel Ratio	Contact Area (ft^2)	Time (sec)	Intensity (w/steradian) Channel 1[a] (0.4 to 0.7μ)	Channel 2[b] (0.7 to 1.1μ)	Channel 3[c] (1.8 to 2.7μ)	Channel 4[d] (3 to 5μ)	Channel 5[e] (0.5 to 35μ)
3.5:1	57.85	0.1	1.47×10^6	7.15×10^5	1.45×10^6	1.31×10^6	1.74×10^7
		0.2	6.90×10^5	4.10×10^5	1.35×10^6	1.29×10^6	1.50×10^7
		0.3	2.50×10^5	1.98×10^5	1.09×10^6	1.07×10^6	1.04×10^7
		0.4	1.89×10^5	1.32×10^5	9.30×10^5	9.30×10^5	8.40×10^6
		0.5	2.80×10^5	1.65×10^5	8.80×10^5	8.50×10^5	7.30×10^6
		0.6	1.75×10^5	9.90×10^4	7.90×10^5	7.90×10^5	6.70×10^6
		0.7	1.45×10^5	8.80×10^4	6.90×10^5	7.30×10^5	6.00×10^6
		0.8	1.12×10^5	7.70×10^4	6.20×10^5	6.60×10^5	5.50×10^6
		0.9	-	-	5.60×10^5	6.20×10^5	4.80×10^6
		1.0	-	-	5.20×10^5	5.80×10^5	3.90×10^6
		1.1	-	-	4.80×10^5	5.20×10^5	3.80×10^6
		1.2	-	-	4.30×10^5	4.80×10^5	3.50×10^6
		1.4	-	-	3.30×10^5	3.80×10^5	2.70×10^6
		1.6	-	-	2.60×10^5	2.50×10^5	2.10×10^6
		1.8	-	-	1.57×10^5	1.95×10^5	1.54×10^6
		2.0	-	-	1.05×10^5	1.42×10^5	1.26×10^6
	32.06	0.1	1.52×10^5	5.60×10^5	1.44×10^6	1.16×10^6	1.43×10^7
		0.2	9.00×10^4	4.80×10^5	1.61×10^6	1.37×10^6	1.59×10^7
		0.3	6.50×10^4	4.00×10^5	1.64×10^6	1.42×10^6	1.53×10^7
		0.4	5.00×10^4	3.10×10^5	1.54×10^6	1.38×10^6	1.38×10^7
		0.5	4.25×10^4	2.70×10^5	1.46×10^6	1.32×10^6	1.21×10^7
		0.6	3.50×10^4	2.20×10^5	1.38×10^6	1.27×10^6	1.12×10^7
		0.7	2.70×10^4	1.65×10^5	1.31×10^6	1.25×10^6	1.08×10^7
		0.8	2.70×10^4	1.44×10^5	1.29×10^6	1.21×10^6	1.01×10^7
		0.9	3.00×10^4	1.44×10^5	1.25×10^6	1.20×10^6	9.80×10^6
		1.0	2.70×10^4	1.24×10^5	1.23×10^6	1.16×10^6	9.20×10^6
		1.1	-	-	1.12×10^6	1.07×10^6	8.20×10^6
		1.2	2.50×10^4	9.30×10^4	1.00×10^6	9.60×10^5	7.30×10^6
		1.3	-	-	8.50×10^5	8.10×10^5	5.90×10^6
		1.4	1.75×10^4	7.20×10^4	7.00×10^5	6.70×10^5	4.75×10^6
		1.5	-	-	5.70×10^5	5.10×10^5	3.60×10^6
		1.6	1.75×10^4	4.10×10^4	4.10×10^5	4.00×10^5	2.70×10^6
		1.7	-	-	2.90×10^5	2.90×10^5	2.60×10^6
		1.8	-	-	2.10×10^5	2.20×10^5	1.73×10^6
		1.9	-	-	1.91×10^5	1.71×10^5	1.30×10^6
		2.0	-	-	1.32×10^5	1.45×10^5	1.15×10^6
		2.1	-	-	1.03×10^5	1.08×10^5	1.15×10^6
	16.02		No data				

Table 12. Continued

Oxidizer/Fuel Ratio	Contact Area (ft^2)	Time (sec)	Intensity (w/steradian) Channel 1[a] (0.4 to 0.7μ)	Channel 2[b] (0.7 to 1.1μ)	Channel 3[c] (1.8 to 2.7μ)	Channel 4[d] (3 to 5μ)	Channel 5[e] (0.5 to 35μ)
2.5:1	59.38	0.1	2.85×10^5	1.04×10^6	1.80×10^6	1.85×10^6	3.20×10^7
		0.2	1.80×10^5	7.50×10^5	1.76×10^6	1.89×10^6	2.90×10^7
		0.3	1.10×10^5	5.60×10^5	1.63×10^6	1.76×10^6	2.60×10^7
		0.4	7.20×10^4	4.20×10^5	1.49×10^6	1.61×10^6	2.60×10^7
		0.5	6.60×10^4	3.70×10^5	1.34×10^6	1.39×10^6	2.00×10^7
		0.6	4.50×10^4	2.90×10^5	1.20×10^6	1.28×10^6	1.60×10^7
		0.7	4.20×10^4	2.40×10^5	-	-	-
		0.8	3.30×10^4	1.70×10^5	8.50×10^5	9.30×10^5	1.10×10^7
		0.9	2.70×10^4	1.35×10^5	-	-	-
		1.0	2.70×10^4	1.10×10^5	6.70×10^5	7.30×10^5	7.7×10^6
		1.1	2.10×10^4	8.30×10^4	-	-	-
		1.2	2.10×10^4	8.30×10^4	5.00×10^5	5.35×10^5	5.50×10^6
		1.3	1.80×10^4	6.20×10^4	-	-	-
		1.4	-	-	3.60×10^5	4.04×10^5	4.20×10^6
		1.6	-	-	2.20×10^5	2.83×10^5	3.10×10^6
		1.8	-	-	1.42×10^5	1.82×10^5	2.20×10^6
		2.0	-	-	8.70×10^4	1.31×10^5	1.80×10^6
		2.2	-	-	6.30×10^4	1.01×10^5	1.50×10^6
		2.4	-	-	4.70×10^4	7.07×10^4	1.30×10^6
	29.65				No data		
	14.83				No data		
1.5:1	50.67	0.1	3.20×10^5	1.30×10^6	3.10×10^6	2.70×10^6	3.50×10^7
		0.2	2.30×10^5	1.00×10^6	3.20×10^6	2.90×10^6	3.30×10^7
		0.3	1.40×10^5	7.10×10^5	3.10×10^6	3.30×10^6	2.90×10^7
		0.4	8.80×10^4	5.10×10^5	2.80×10^6	2.60×10^6	2.80×10^7
		0.5	7.30×10^4	4.90×10^5	2.50×10^6	2.30×10^6	2.20×10^7
		0.6	7.10×10^4	4.00×10^5	2.30×10^6	2.20×10^6	2.00×10^7
		0.8	3.30×10^4	2.50×10^5	2.00×10^6	1.80×10^6	1.40×10^7
		1.0	2.30×10^4	1.40×10^5	1.50×10^6	1.40×10^6	1.20×10^7
		1.2	1.80×10^4	8.40×10^4	1.10×10^6	1.10×10^6	7.00×10^6
		1.4	1.80×10^4	6.50×10^4	8.30×10^5	8.00×10^5	6.20×10^6
		1.6	-	-	7.10×10^5	6.70×10^5	6.20×10^6
		1.8	-	-	6.00×10^5	5.60×10^5	3.70×10^6
		2.0	-	-	4.90×10^5	4.50×10^5	3.70×10^6
		2.2	-	-	3.50×10^5	3.25×10^5	-
		2.4	-	-	2.20×10^5	2.20×10^5	-
		2.6	-	-	1.25×10^5	1.40×10^5	-
		2.8	-	-	5.70×10^4	8.40×10^4	-
		3.0	-	-	3.40×10^4	5.60×10^4	-
	25.35	0.1	2.10×10^5	1.54×10^6	Off Scale	Off Scale	3.20×10^7
		0.2	2.90×10^5	2.03×10^6			-
		0.3	3.20×10^5	2.05×10^6			3.70×10^7
		0.4	2.70×10^5	1.82×10^6			3.50×10^7
		0.5	2.10×10^5	1.61×10^6			3.20×10^7
		0.6	1.58×10^5	1.33×10^6			2.90×10^7

Table 12. Continued

Oxidizer/Fuel Ratio	Contact Area (ft^2)	Time (sec)	Intensity (w/steradian) Channel 1[a] (0.4 to 0.7μ)	Channel 2[b] (0.7 to 1.1μ)	Channel 3[c] (1.8 to 2.7μ)	Channel 4[d] (3 to 5μ)	Channel 5[e] (0.5 to 35μ)
1.5:1 (cont)	25.35 (cont)	0.7	1.24×10^5	1.13×10^6	Off Scale	Off Scale	2.60×10^7
		0.8	9.40×10^4	9.30×10^5			2.40×10^7
		0.9	7.50×10^4	7.40×10^5			2.10×10^7
		1.0	6.10×10^4	6.50×10^5			2.00×10^7
		1.1	-	-			1.90×10^7
		1.2	4.80×10^4	5.30×10^5			1.80×10^7
		1.3	-	-			1.80×10^7
		1.4	4.60×10^4	4.80×10^5			1.80×10^7
		1.5	-	-			1.90×10^7
		1.6	4.00×10^4	4.50×10^5			1.70×10^7
		1.7	-	-			1.60×10^7
		1.8	3.40×10^4	3.60×10^5			1.30×10^7
		1.9	-	-			1.20×10^7
		2.0	2.50×10^4	2.40×10^5			9.40×10^6
		2.1	-	-			8.00×10^6
		2.2	1.72×10^4	1.30×10^5			5.80×10^6
		2.3	-	-			3.90×10^6
		2.4	1.15×10^4	7.30×10^4			3.30×10^6
		2.5	-	-			2.80×10^6
		2.6	1.15×10^4	4.0×10^4			3.10×10^6
		2.7	-	-			1.70×10^6
	12.67				No data		
3:1	Ultimate Mix Test No. 2	0.1	6.70×10^4	4.40×10^5	2.40×10^6	1.40×10^6	1.61×10^7
		0.2	5.20×10^4	4.60×10^5	2.70×10^6	1.44×10^6	1.85×10^7
		0.3	4.80×10^4	4.40×10^5	2.80×10^6	1.87×10^6	1.92×10^7
		0.4	4.60×10^4	4.20×10^5	2.90×10^6	1.97×10^6	1.98×10^7
		0.5	4.50×10^4	4.30×10^5	2.90×10^6	1.97×10^6	1.92×10^7
		0.6	3.20×10^4	3.40×10^5	2.80×10^6	1.87×10^6	1.83×10^7
		0.7	3.20×10^4	3.00×10^5	2.60×10^6	1.73×10^6	1.62×10^7
		0.8	2.50×10^4	2.30×10^5	2.30×10^6	1.56×10^6	1.41×10^7
		1.0	1.80×10^4	1.44×10^5	2.80×10^6	1.19×10^6	1.01×10^7
		1.2	1.25×10^4	8.60×10^4	1.21×10^6	8.00×10^5	6.30×10^6
		1.4	1.21×10^4	5.80×10^4	7.40×10^5	4.80×10^5	3.80×10^6
		1.6	7.30×10^3	3.40×10^4	3.90×10^5	3.00×10^5	2.40×10^6
		1.8	-	-	2.40×10^5	2.05×10^5	1.65×10^6
		2.0	-	-	1.55×10^5	1.40×10^5	1.34×10^6
		2.2	-	-	1.24×10^5	1.21×10^5	-
		2.4	-	-	1.03×10^5	9.30×10^4	-
		2.6	-	-	8.30×10^4	6.50×10^4	-

Measurements made with:

a. short wavelength silicon detector
b. long wavelength silicon detector
c. PbS wavelength silicon detector
d. PbSe wavelength silicon detector
e. bolometer

Table 13. Total Fireball Radiation Yield.

Propellant	Mixture Ratio	Contact Area (ft^2)	Total Yield (j)
N_2O_4/A-50	3:1	51.01	1.8×10^7
		25.44	9.8×10^7
		12.64	1.4×10^8
	2:1	45.53	4.7×10^7
		22.90	2.2×10^8
		11.39	2.4×10^8
	1:1	35.90	2.1×10^8
		17.96	No data
		8.88	No data
LOX/RP-1	3.5:1	57.85	1.5×10^8
		32.06	2.1×10^8
		16.02	No data
	2.5:1	59.38	2.9×10^8
		29.65	No data
		14.83	No data
	1.5:1	50.67	3.6×10^8
		25.35	6.1×10^8
		12.67	No data
	Ultimate Mix Test No. 2	N/A	2.5×10^8

Table 14. Meteorological Data.

Oxidizer/Fuel Ratio	Contact Area (ft^2)	Relative Humidity (%)	Air Temperature (^oF)	Wind Direction	Wind Velocity (mph)	Atmospheric Pressure (in. of Hg)
			LOX/RP-1			
3.5:1	57.85	36	62	Northeast	0-4	29.15
	32.06	58	70	Northeast	0-2	28.94
	16.02	25	70	Northeast	0-3	28.98
2.5:1	59.38	53	53	Northeast	0-2	29.04
	29.65	52	74	Northeast	0-2	28.92
	14.83	38	54	Northeast	0-2	28.97
1.5:1	50.67	66	56	Northeast	0-3	28.86
	25.35	54	54	Northeast	0-2	28.90
	12.67	59	74	Northeast	1-3	28.80
			N_2O_4/A-50			
3:1	51.01	49	63	East	5-10	28.91
	25.44	22	66	Northeast	4-8	28.30
	12.64	19	59	North	0-6	29.00
2:1	45.53	50	58	Northeast	4-8	28.10
	22.90	62	60	Northeast	4-8	28.85
	11.39	28	62	East	0-6	28.99
1:1	35.90	42	61	Northeast	2-9	28.98
	17.96	68	57	East	2-8	28.90
	8.88	23	72	Northeast	0-5	28.82

Table 15. Cryogenic Mixing Test Results.

Test No.	Distance from Event (ft)	Gage No.	Peak Overpressure (psi)	Positive Impulse (psi-msec)	Positive Pulse Duration (msec)	Maximum Radiant Heat Flux (BTU/ft^2-sec)	Maximum Temperature ($^\circ$F)
1	10	1	92.4	111.8	3.8	70.0	2617
		2	130.0	169.0	5.1	80.0	2742
		3	138.8	175.6	3.4	115.0	3180
		4	90.4	152.5	6.9	76.0	2670
		mean	112.9	152.2	4.8		
	25	5	19.8	44.7	6.3	38.0	555
		6	26.0	60.0	6.3	47.5	1973
		7	22.0	49.3	5.5	62.8	2306
		8	22.5	52.3	7.3	37.5	484
		mean	22.6	51.6	6.4		
	40	9	8.1	35.2	10.7	*	342
		10	8.5	29.3	9.0	14.5	452
		11	9.7	40.6	9.2	*	725
		12	11.5	36.9	8.0	9.5	194
		mean	9.5	25.5	9.3		
2	10	1	147.6	205.9	3.6	75.0	1910
		2	113.9	111.1	2.5	60.0	**
		3	157.3	150.1	2.3	110.0	2956
		4	188.7	246.4	2.9	72.0	2331
		mean	151.9	178.4	2.8		
	25	5	29.5	80.9	7.4	51.0	1086
		6	33.6	80.0	8.0	50.0	2650
		7	29.2	80.2	9.0	74.6	1623
		8	40.1	83.6	5.8	56.5	1445
		mean	33.1	81.1	7.6		
	40	9	15.7	48.6	8.1	*	220
		10	12.9	44.3	9.4	8.8	235
		11	13.2	50.0	8.4	*	207
		12	20.2	68.3	8.7	13.5	204
		mean	15.5	52.8	8.7		
3	10	1	218.0	**	**	**	**
		2	202.0	**	**	**	> 902
		3	245.0	**	**	**	> 986
		4	220.0	**	**	**	>1029
		mean	221.0				
	25	5	63.3	**	**	*	**
		6	62.0	**	**	33.0	930
		7	59.9	**	**	*	> 632
		8	60.5	**	**	37.0	661
		mean	61.4				
	40	9	34.8	85.3	5.0	*	749
		10	53.8	74.0	6.2	10.7	557
		11	32.6	72.5	6.6	*	248
		12	34.6	79.4	8.1	11.1	428
		mean	34.0	77.8	6.5		

*No gage
**Gage damaged by fragments or blast yield.

Table 16. Cryogenic Mixing Test Data
(Shockwave Velocities and Rankine-Hugoniot Pressures).

Test No.	Position (Gage No.)	to (Gage No.)	Average Velocity* (ft/sec)	Calculated Shock Overpressure (psi)
1	1	5	2143	44.4
	2	6	2381	58.7
	3	7	2381	58.7
	4	8	2174	46.1
	5	9	1531	14.5
	6	10	1563	15.8
	7	11	1613	17.9
	8	12	1579	16.5
2	1	5	2500	68.5
	2	6	2439	64.3
	3	7	2500	68.5
	4	8	2419	63.0
	5	9	1775	26.0
	6	10	1744	24.5
	7	11	1705	22.6
	8	12	1807	27.6
3	1	5	5000	-
	2	6	5172	-
	3	7	5172	-
	4	8	5000	-
	5	9	2727	77.4
	6	10	2586	68.0
	7	11	2632	70.9
	8	12	2727	77.4

*Shockwave velocities computed from piezoelectric gage data by dividing gage-to-gage distance by gage-to-gage elapsed time.

Table 17. Cryogenic Mixing Test Results (Fireball Size and Duration).

Test No.	Maximum Height (ft)	Maximum Diameter (ft)	Duration (sec)
1	74	86	1.85
2	37	88	1.39
3	50	95	0.64

Table 18. Calculated Fireball Temperatures.

Propellant	Mixture Ratio	Contact Area (ft^2)	Elapsed Time (sec)	Fireball Cross-sectional Area (ft^2)	Peak Intensity (w/steradian x 10^7)	Temperature (°K)
N_2O_4/A-50	3:1	51.01	0.1	1300	0.50	1230
		25.44	0.2	1340	1.11	1490
		12.64	0.5	1200	0.78	1400
	2:1	45.53	0.1	2000	0.86	1270
		22.90	0.2	1730	1.23	1430
		11.39	0.6	2300	0.90	1240
	1:1	35.90	0.2	2500	1.95	1460
LOX/RP-1	3.5:1	57.85	0.1	2200	1.74	1470
		32.06	0.2	3100	1.59	1320
	1.5:1	50.67	0.1	2300	3.5	1740
		25.35	0.3	2800	3.7	1660

Emissivity Correction factors:

if ϵ = 0.75, multiply temperature by 1.07

ϵ = 0.50, multiply temperature by 1.19

ϵ = 0.25, multiply temperature by 1.41

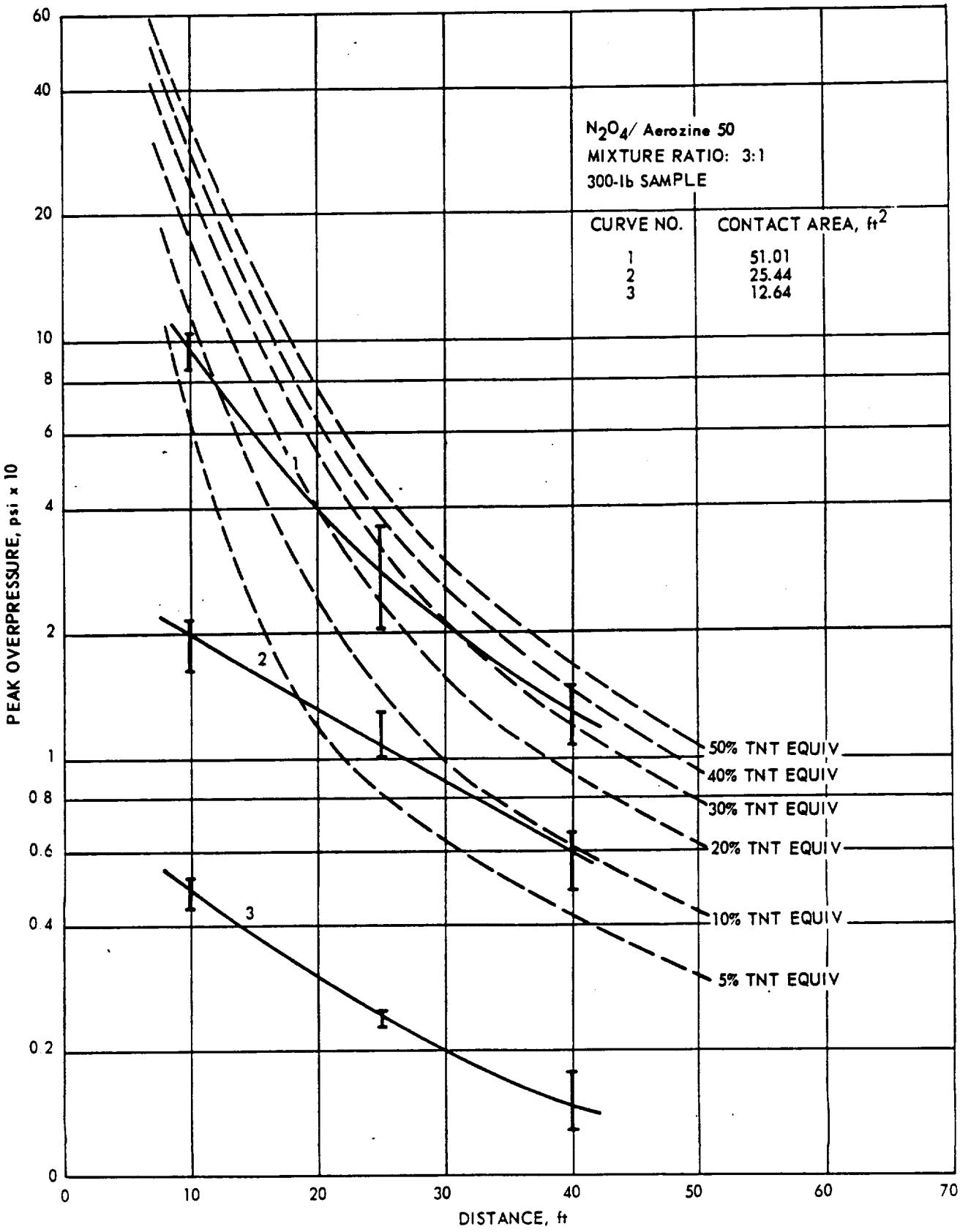

Figure 19. Peak Overpressure Data.

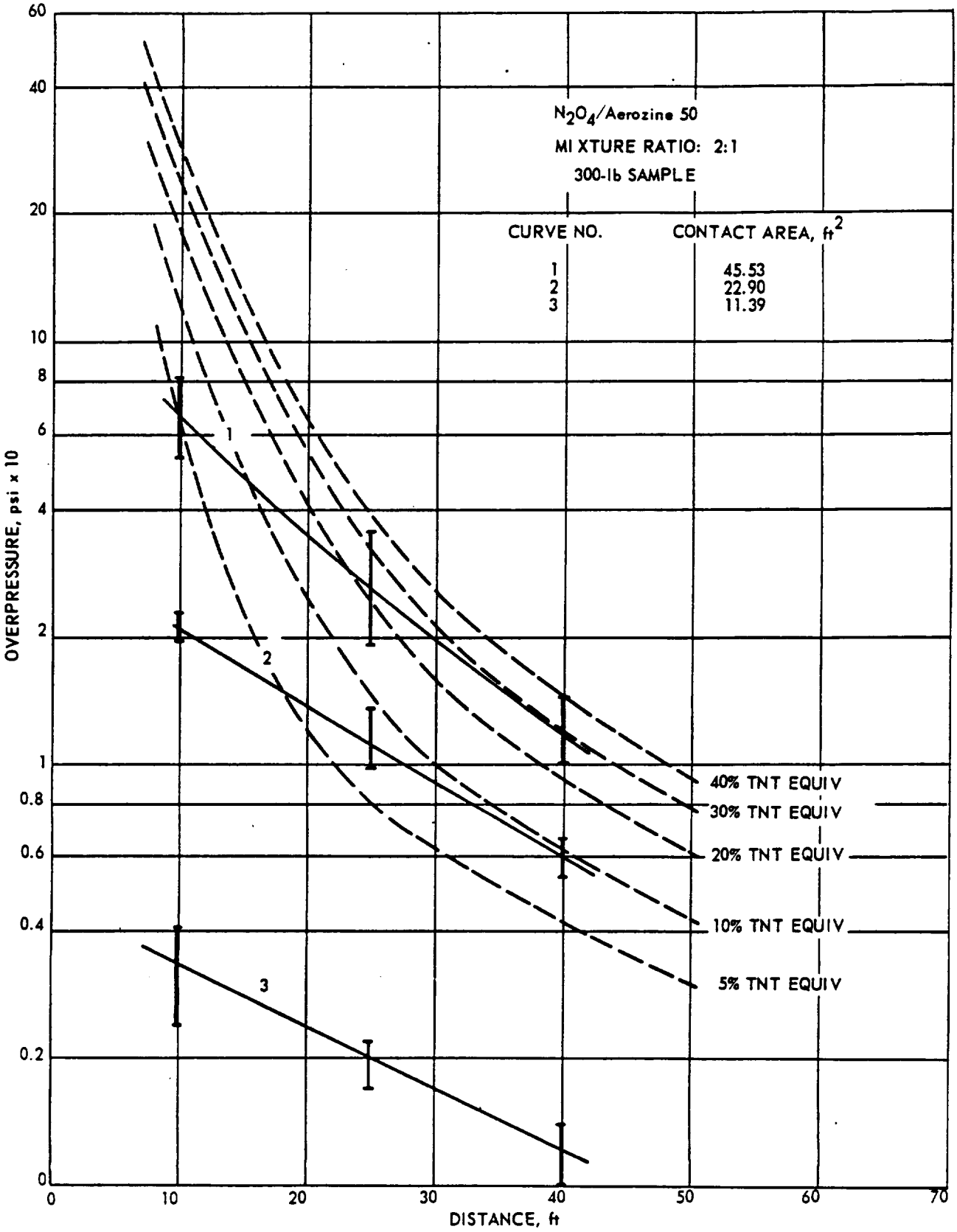

Figure 20. Peak Overpressure Data.

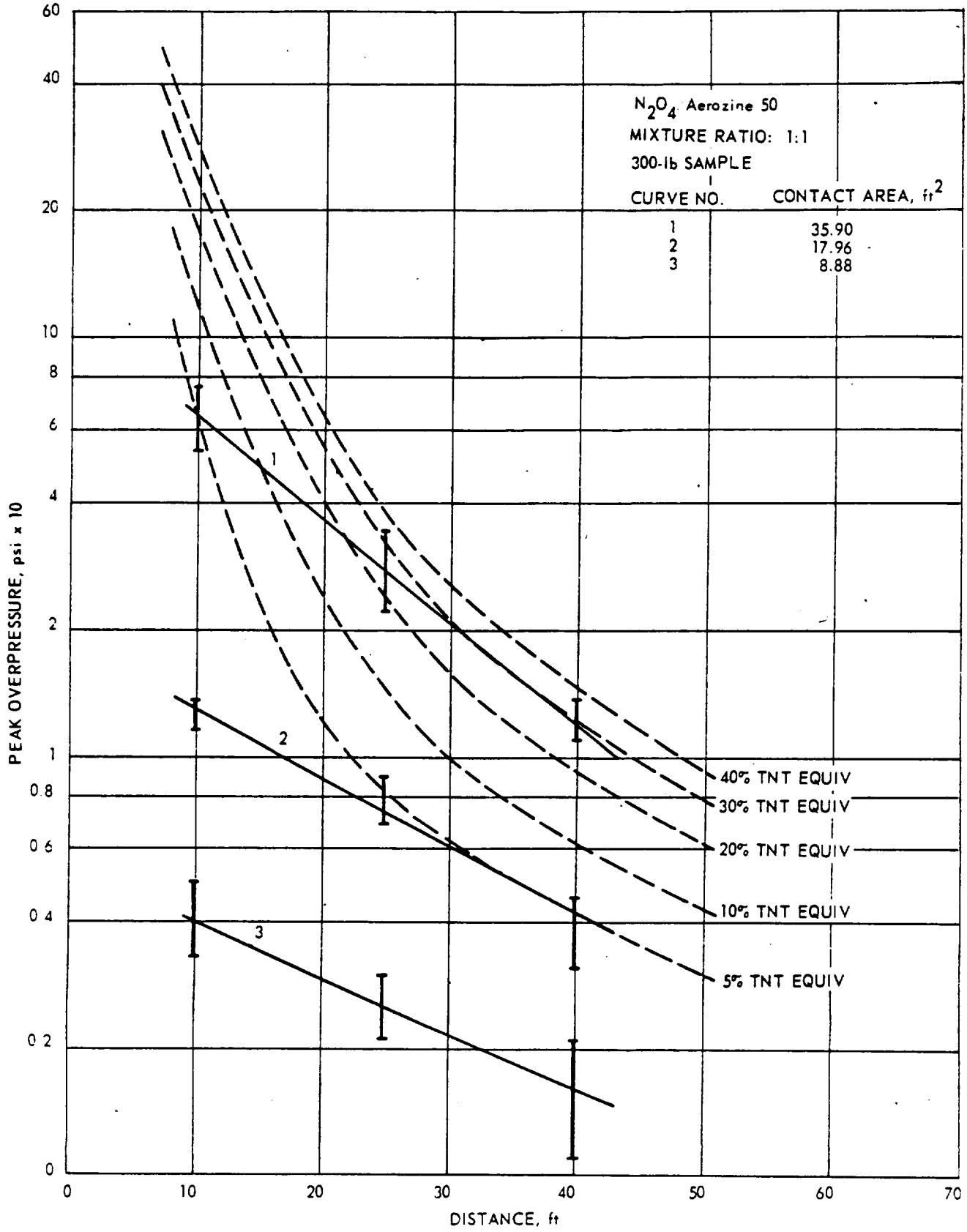

Figure 21. Peak Overpressure Data.

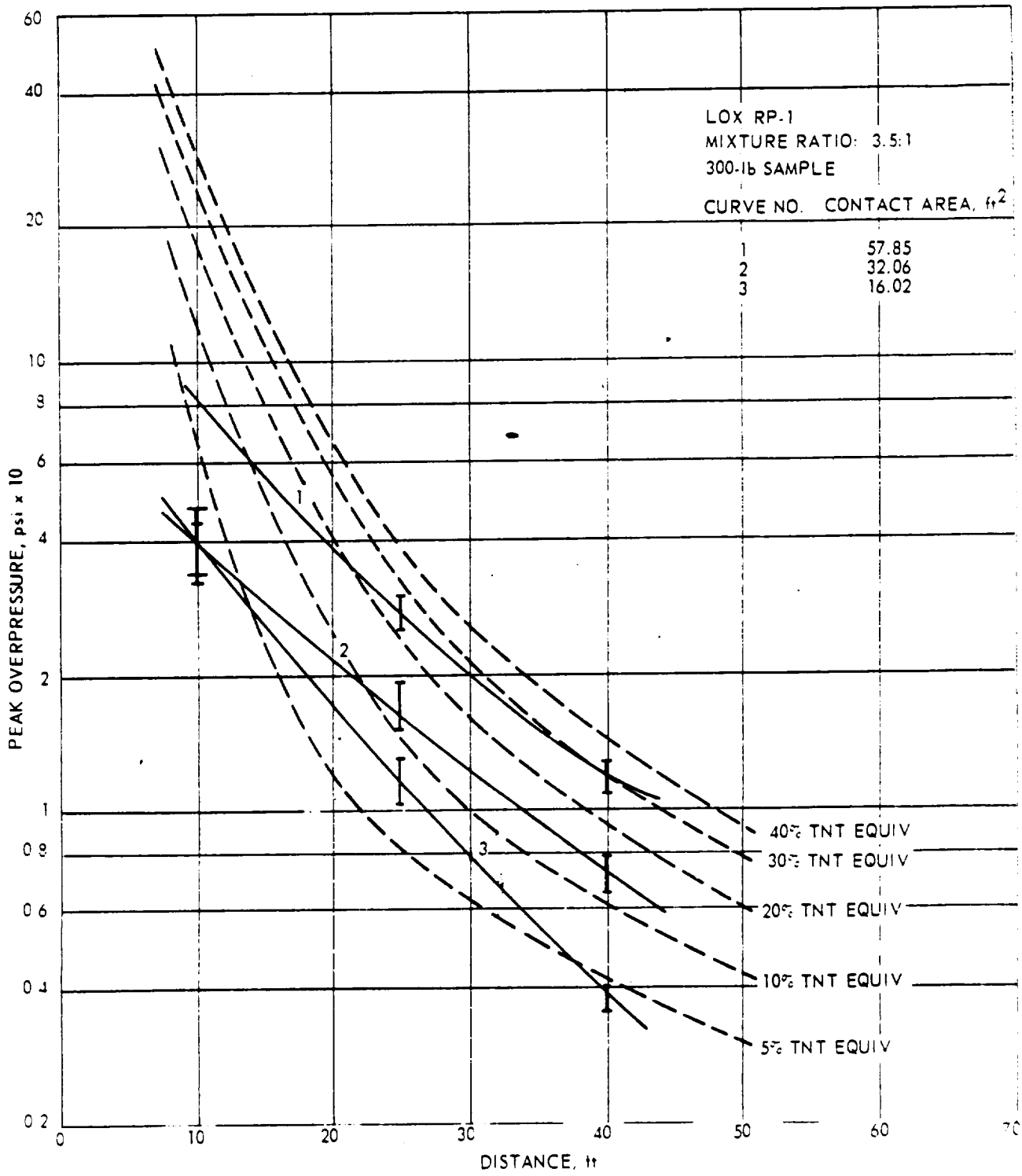

Figure 22. Peak Overpressure Data.

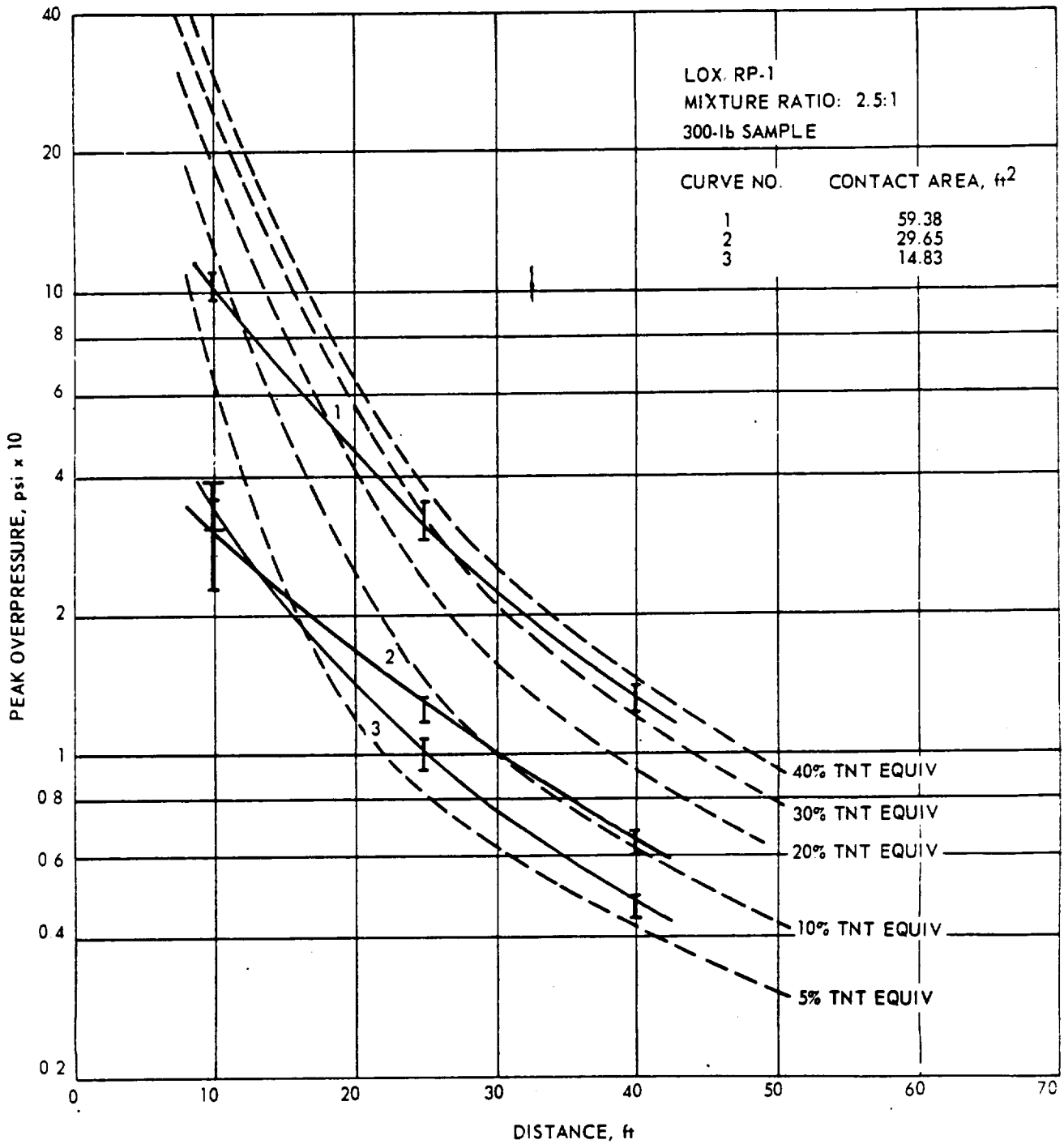

Figure 23. Peak Overpressure Data.

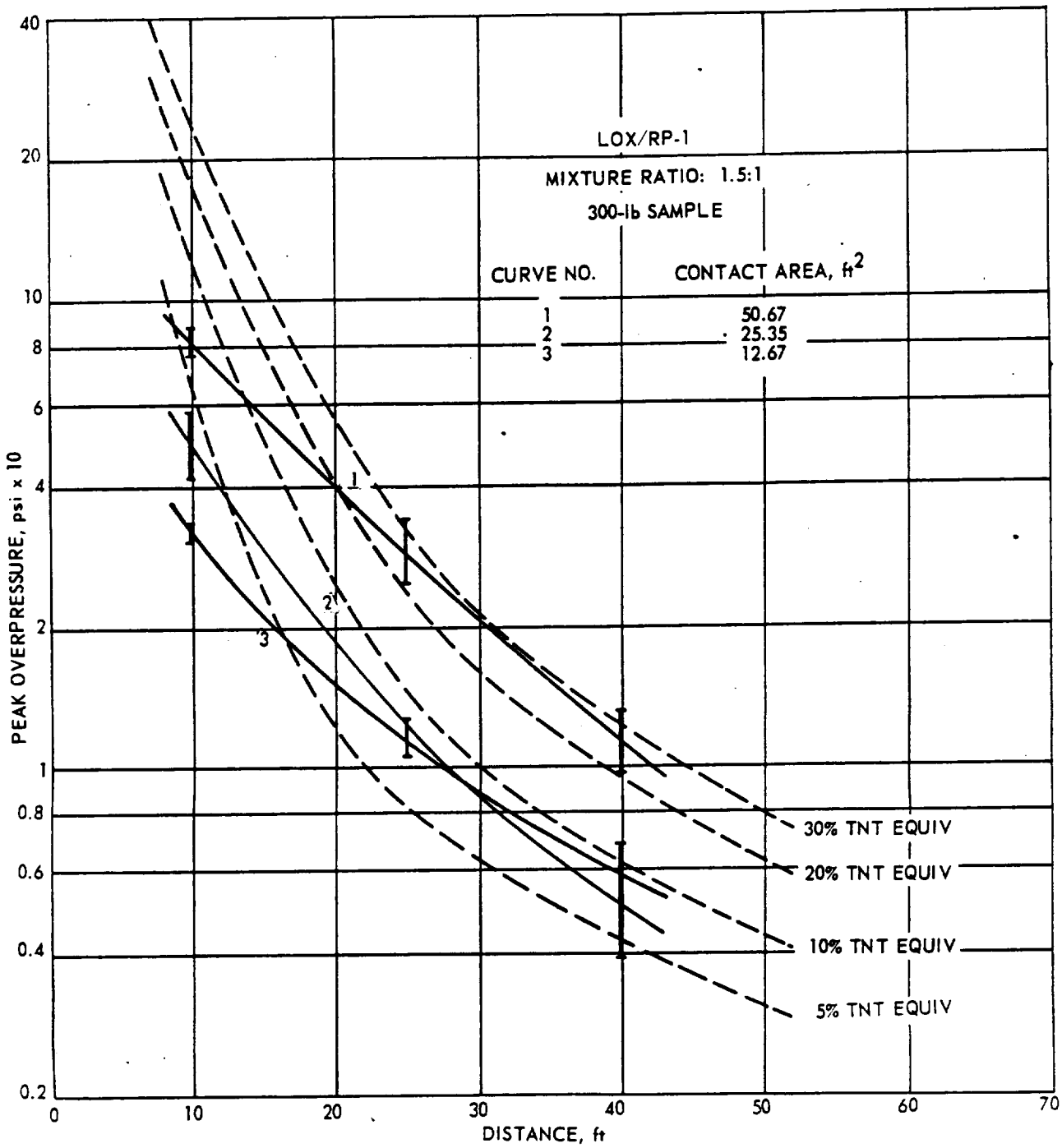

Figure 24. Peak Overpressure Data.

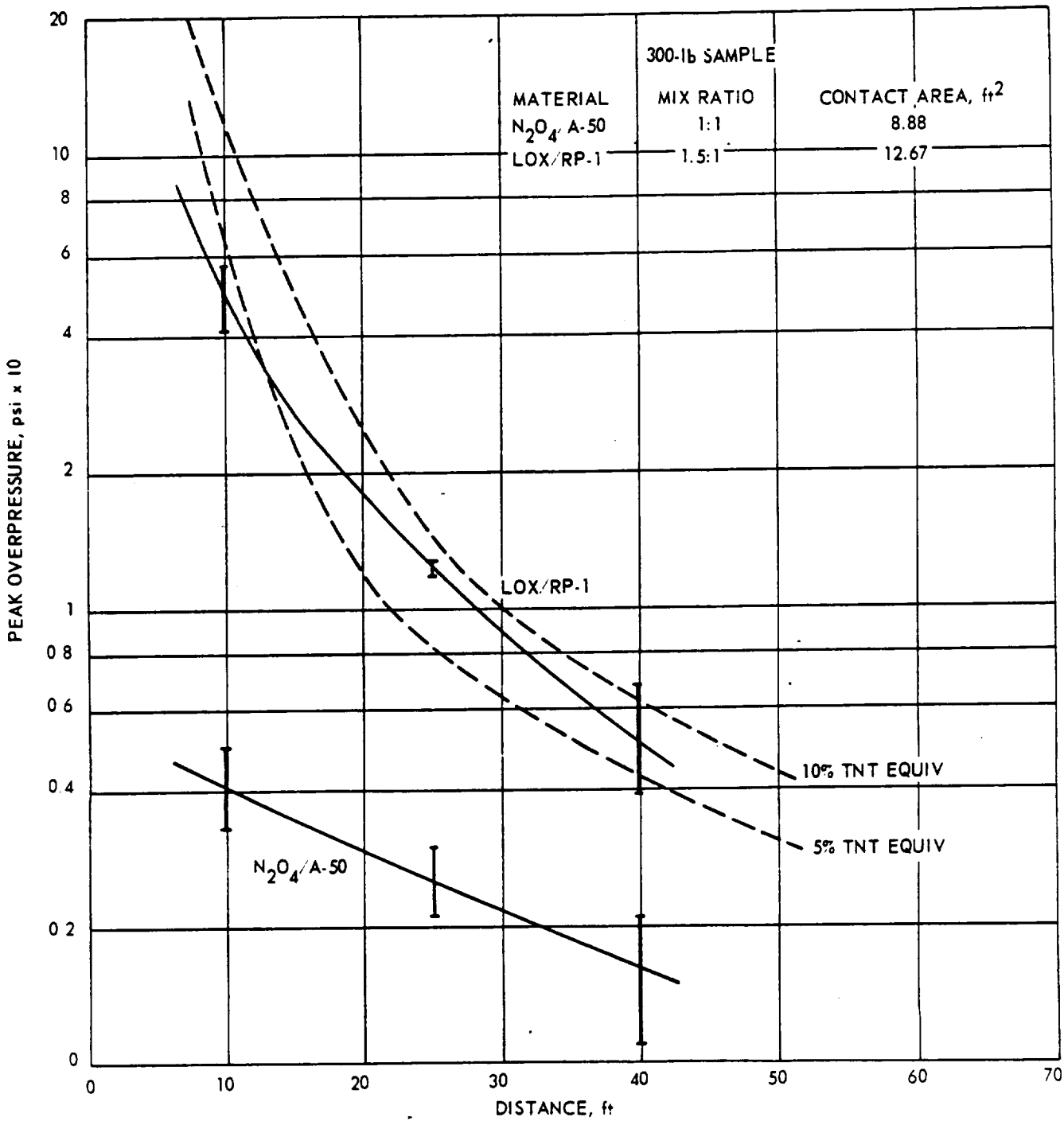

Figure 25. Comparison of Overpressure Data.

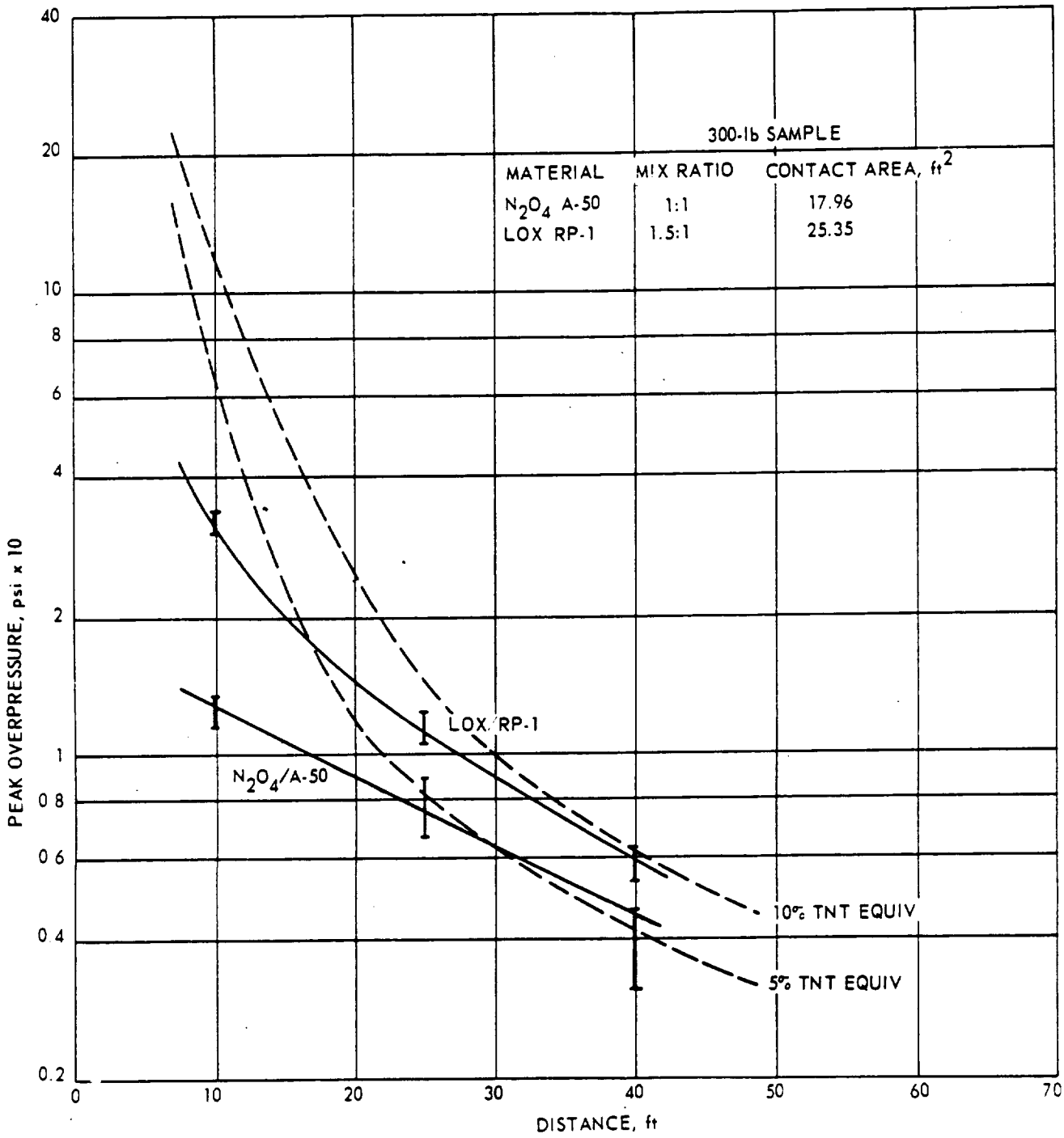

Figure 26. Comparison of Overpressure Data.

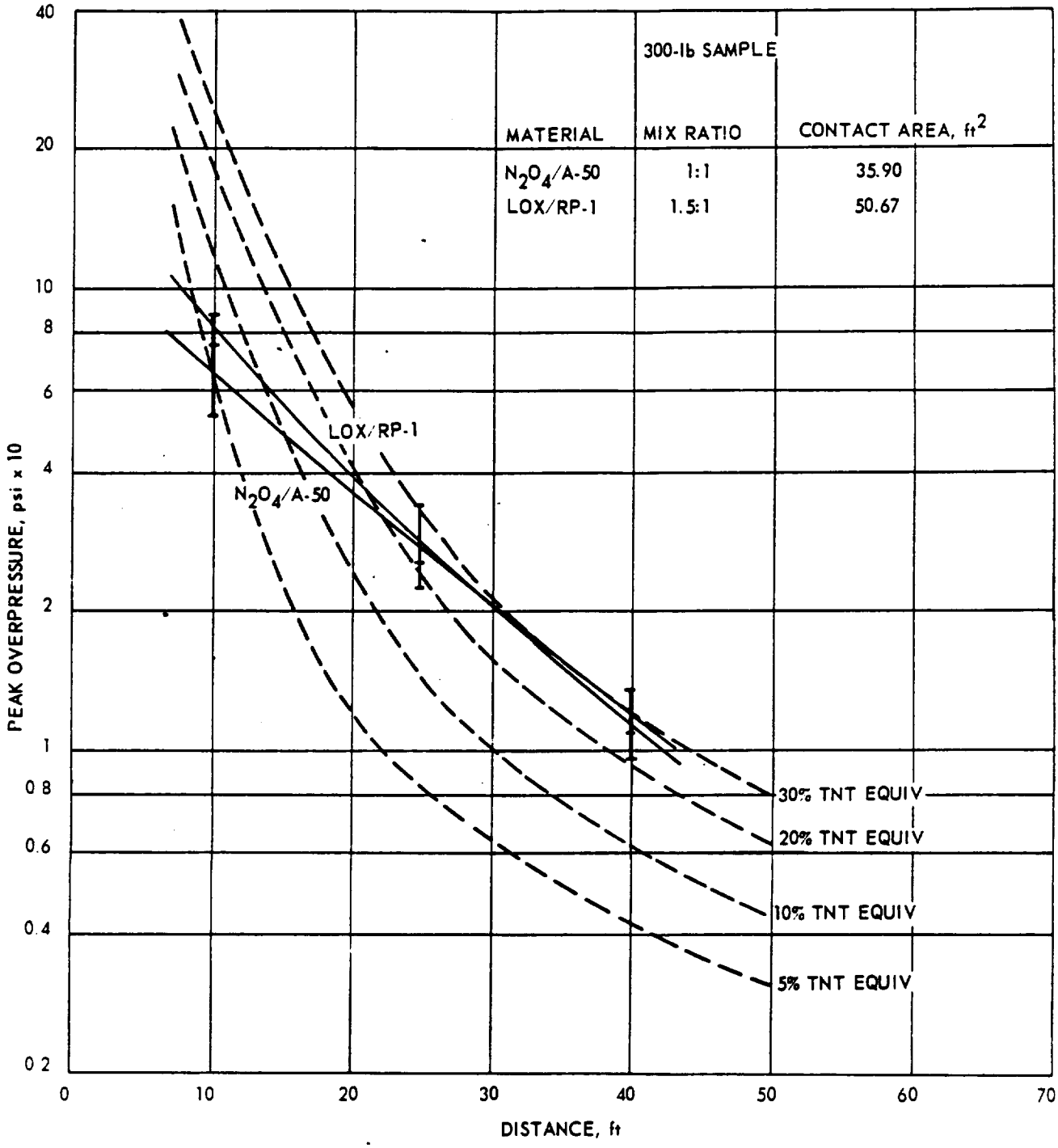

Figure 27. Comparison of Overpressure Data.

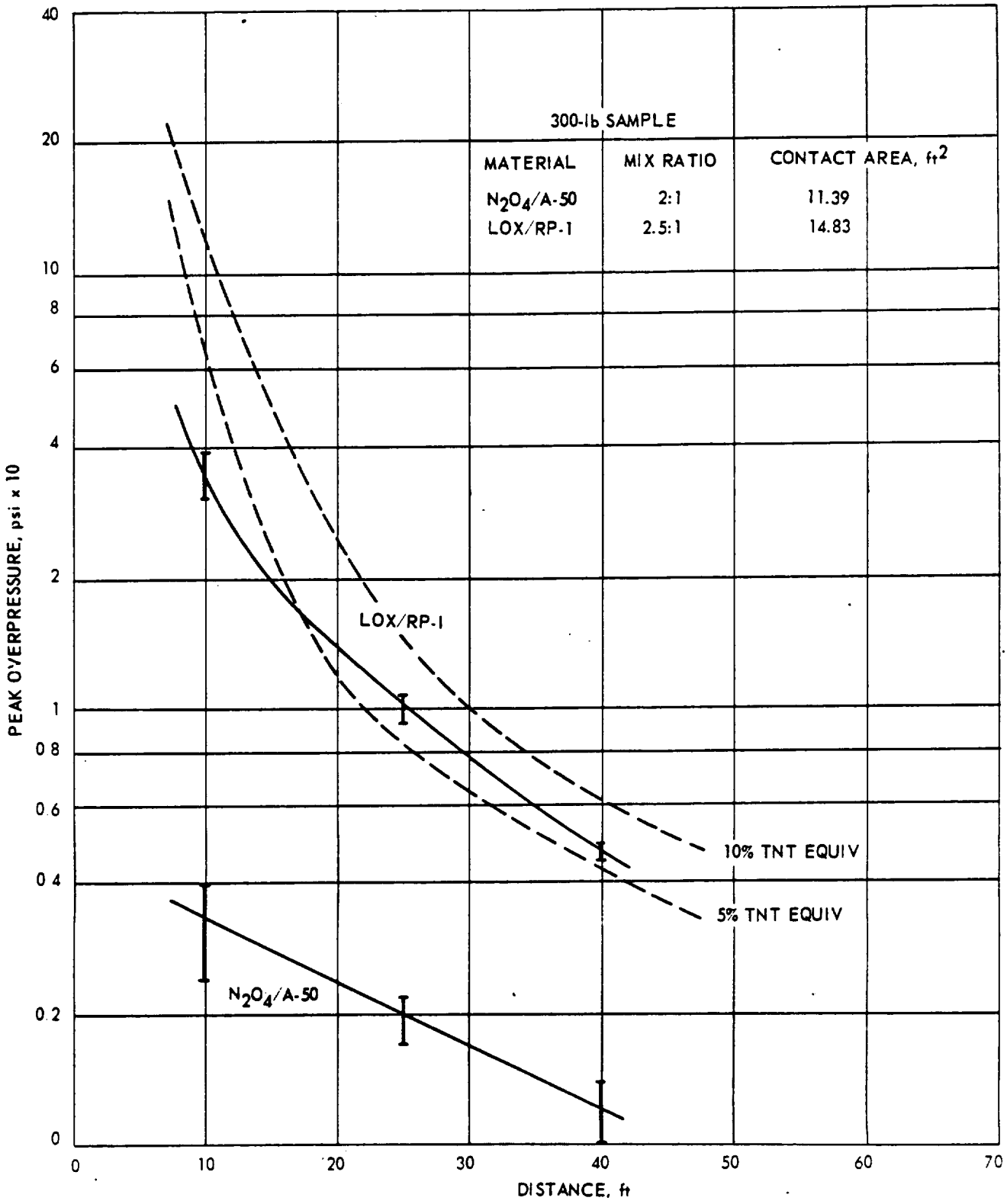

Figure 28. Comparison of Overpressure Data.

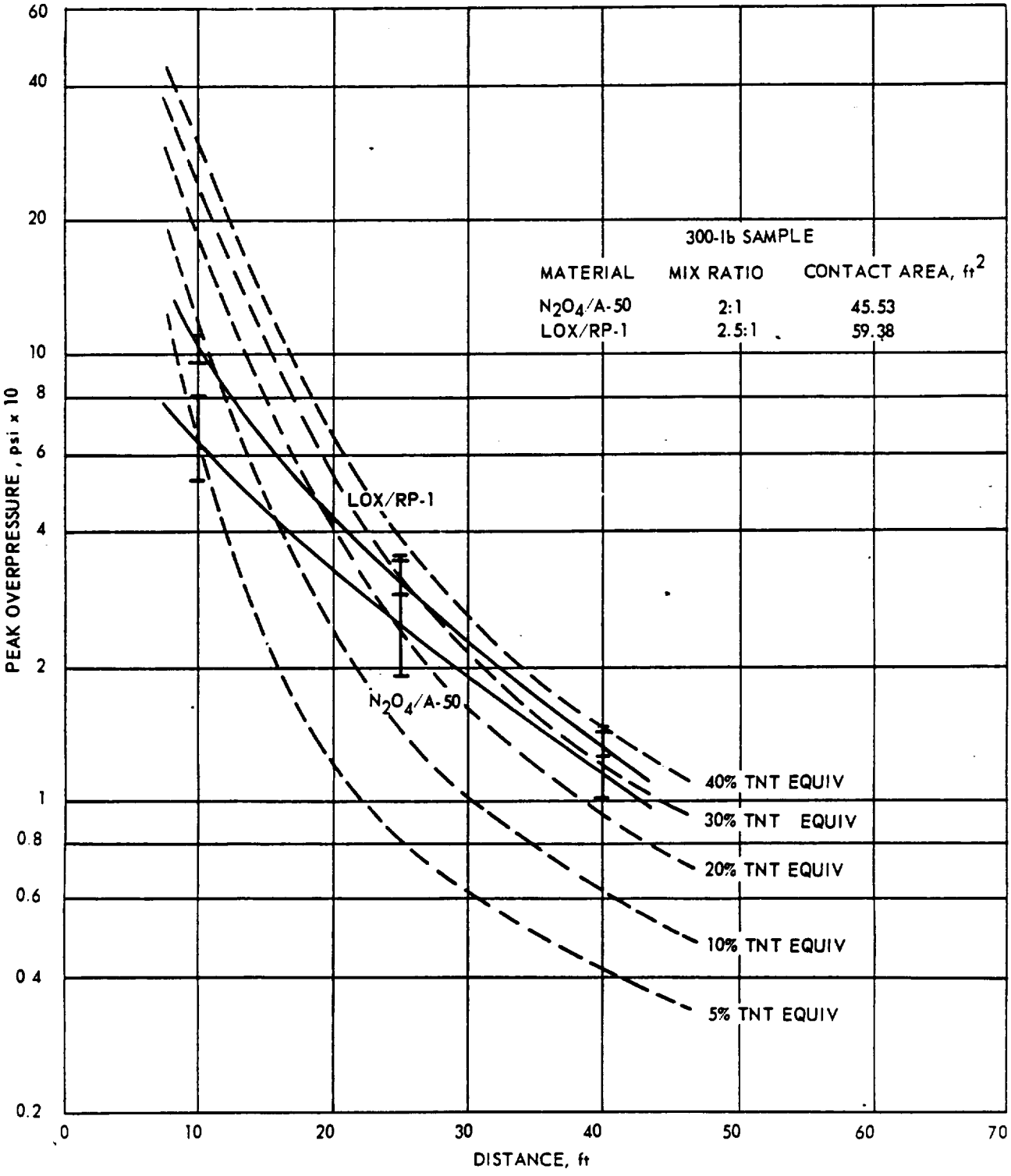

Figure 30. Comparison of Overpressure Data.

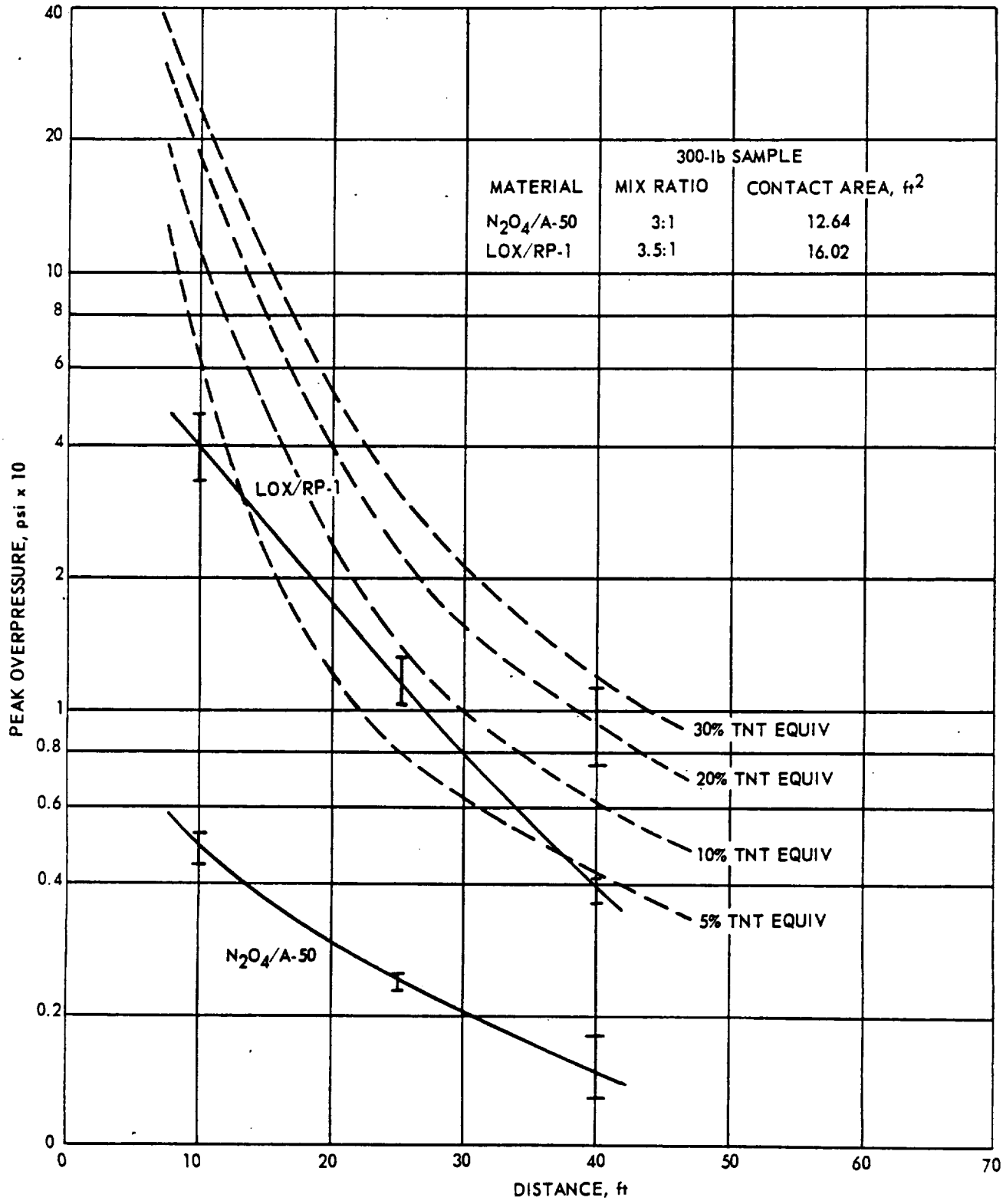

Figure 31. Comparison of Overpressure Data.

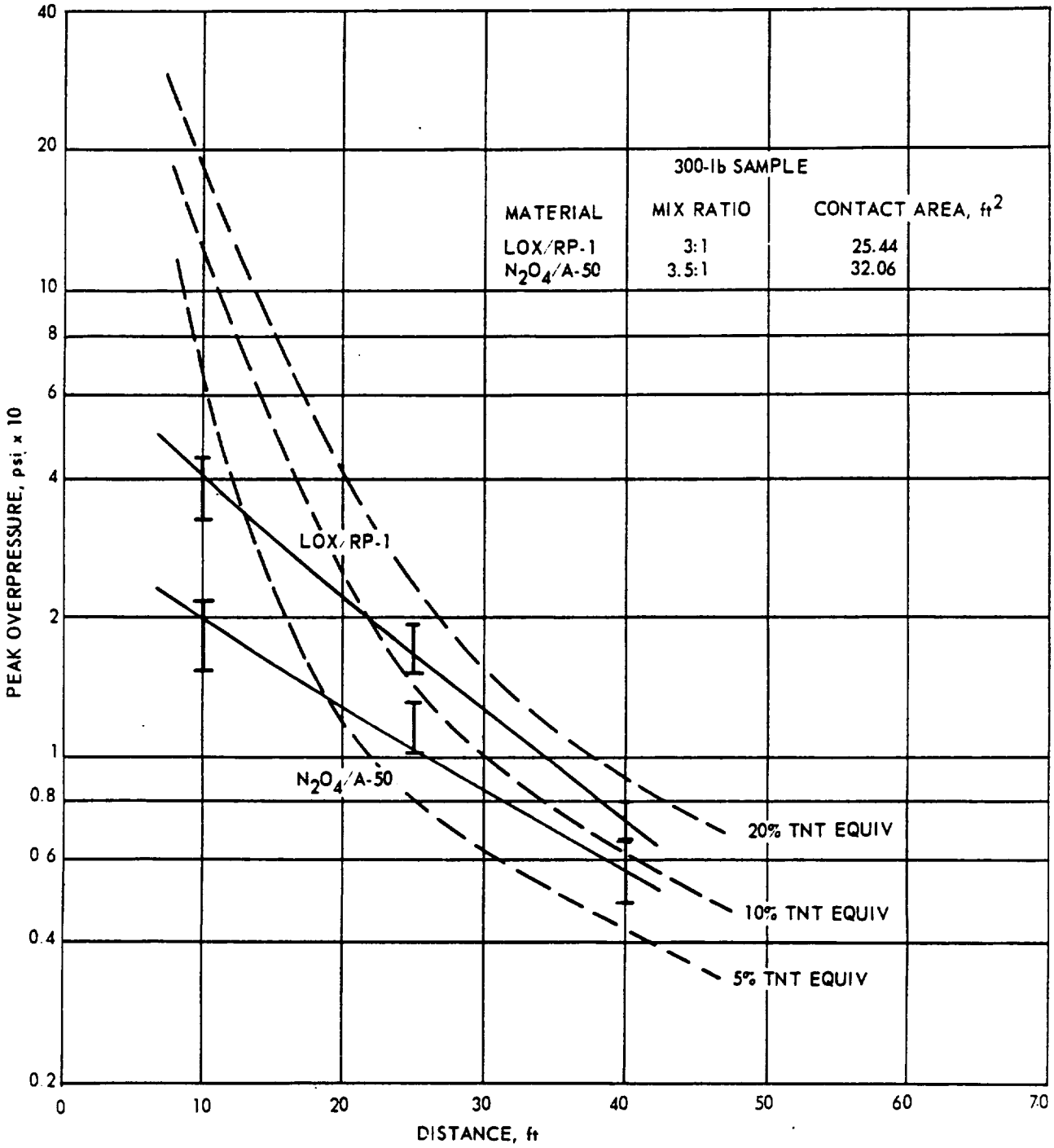

Figure 32. Comparison of Overpressure Data.

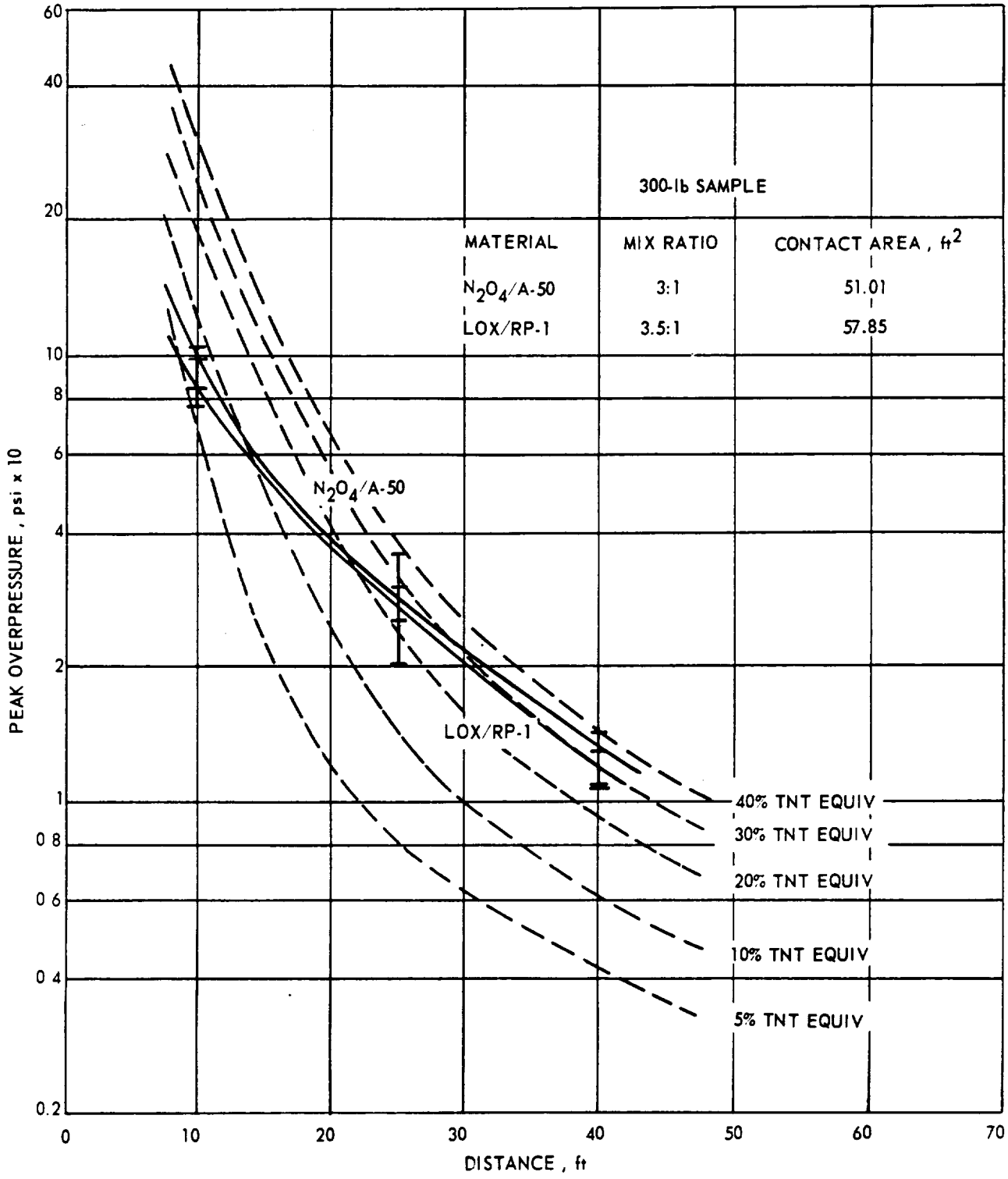

Figure 33. Comparison of Overpressure Data.

The impulse calibration data are presented in Figures 34 through 39 by superimposing the pertinent TNT equivalence curves over the results of the impulse measurements for the various contact areas and mixture ratios. These curves permit a direct evaluation of the TNT impulse equivalences for each test mixture and contact area.

The TNT equivalence comparison of two explosive materials must be made with caution and a simultaneous evaluation of peak overpressure and positive impulse data. The initial air shock produced from an explosive material is increased, by the support it receives from expanding gases and secondary shocks, to a point that it assumes the characteristics of a shockwave produced from a point source. This unsupported shockwave does not form until the shock has traveled beyond the fireball limits.

The propellant tests on this program are examples of nonpoint-source samples; examination of Figures 19 through 39 indicates an increase in TNT equivalence with increased distance. It is apparent that the propellant shockwaves are still in the supported region at the 40-ft-gage position, and that the TNT equivalences could increase at distances beyond this point to a maximum value. Because of the shockwave development as the distance from the sample increased, all TNT comparisons were made with data from the 40-ft-gage data.

4.6.2 Shockwave Pulse Characteristics

Examination of the pressure-pulse records indicates that the pressure-time characteristics of the blast waves were similar to those of conventional explosives for all cryogenic tests and for the high- and intermediate-contact-area hypergolic tests.

The low-contact-area hypergolic tests yielded pulses with a gradual pressure rise at the leading edge instead of the characteristic sharp pressure rise observed in other tests. The rise rate was dependent on the distance of the pressure transducer from the propellant sample. In the low-contact-area tests the shockwave velocity was near the sonic velocity for the atmospheric conditions experienced. The wave velocities for all other tests were above 1200 ft/sec.

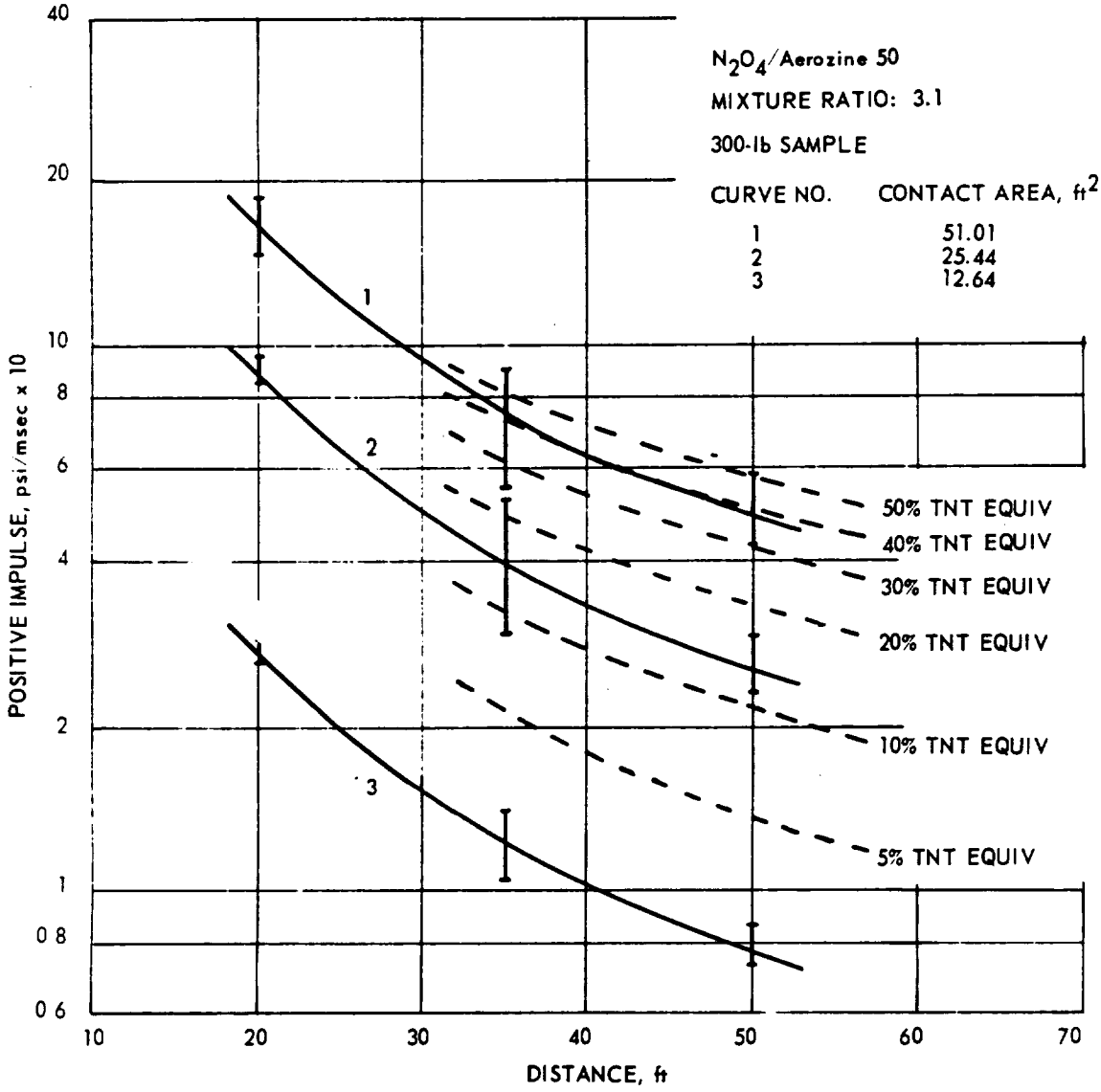

Figure 34. Positive Impulse Data.

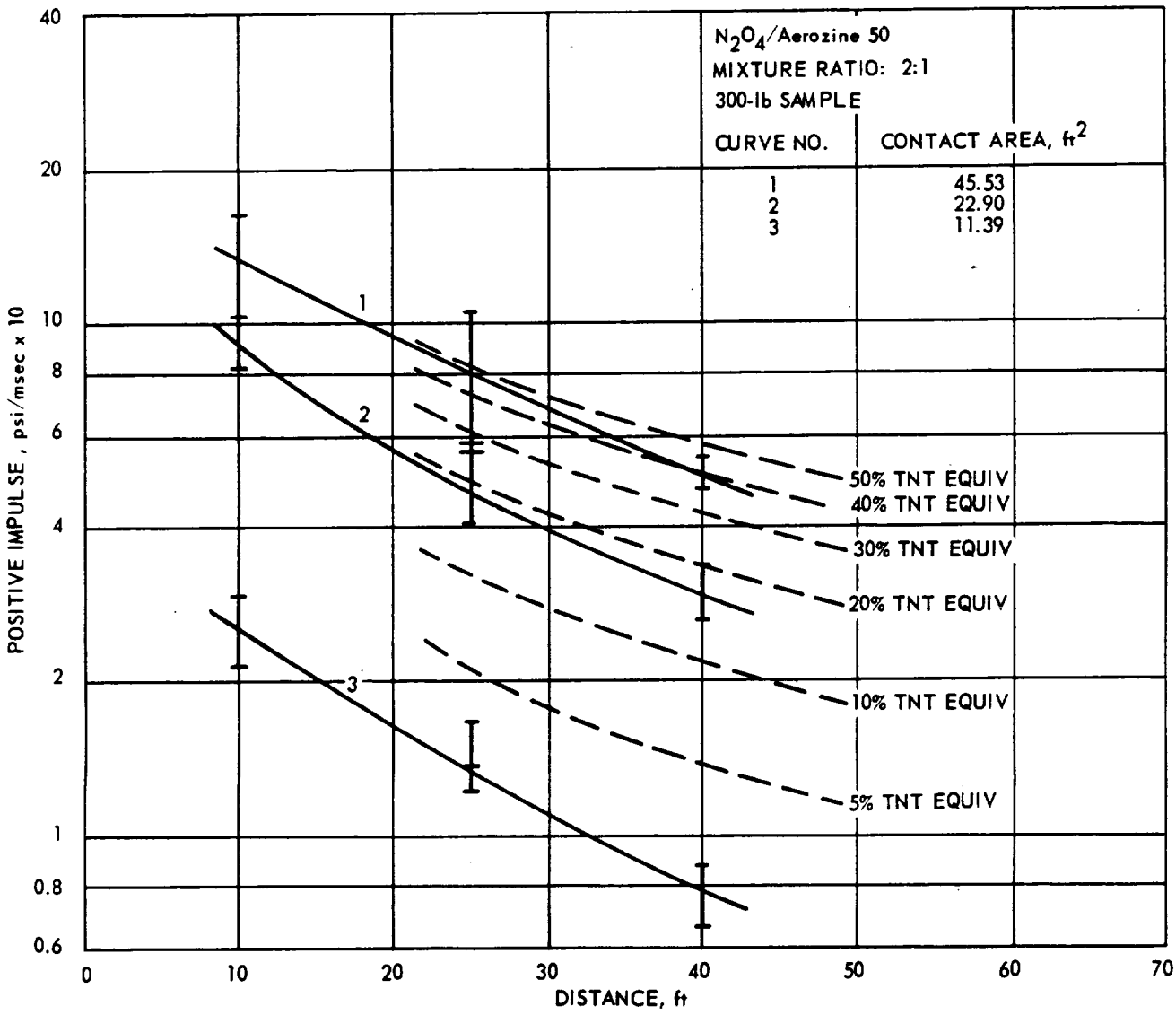

Figure 35. Positive Impulse Data.

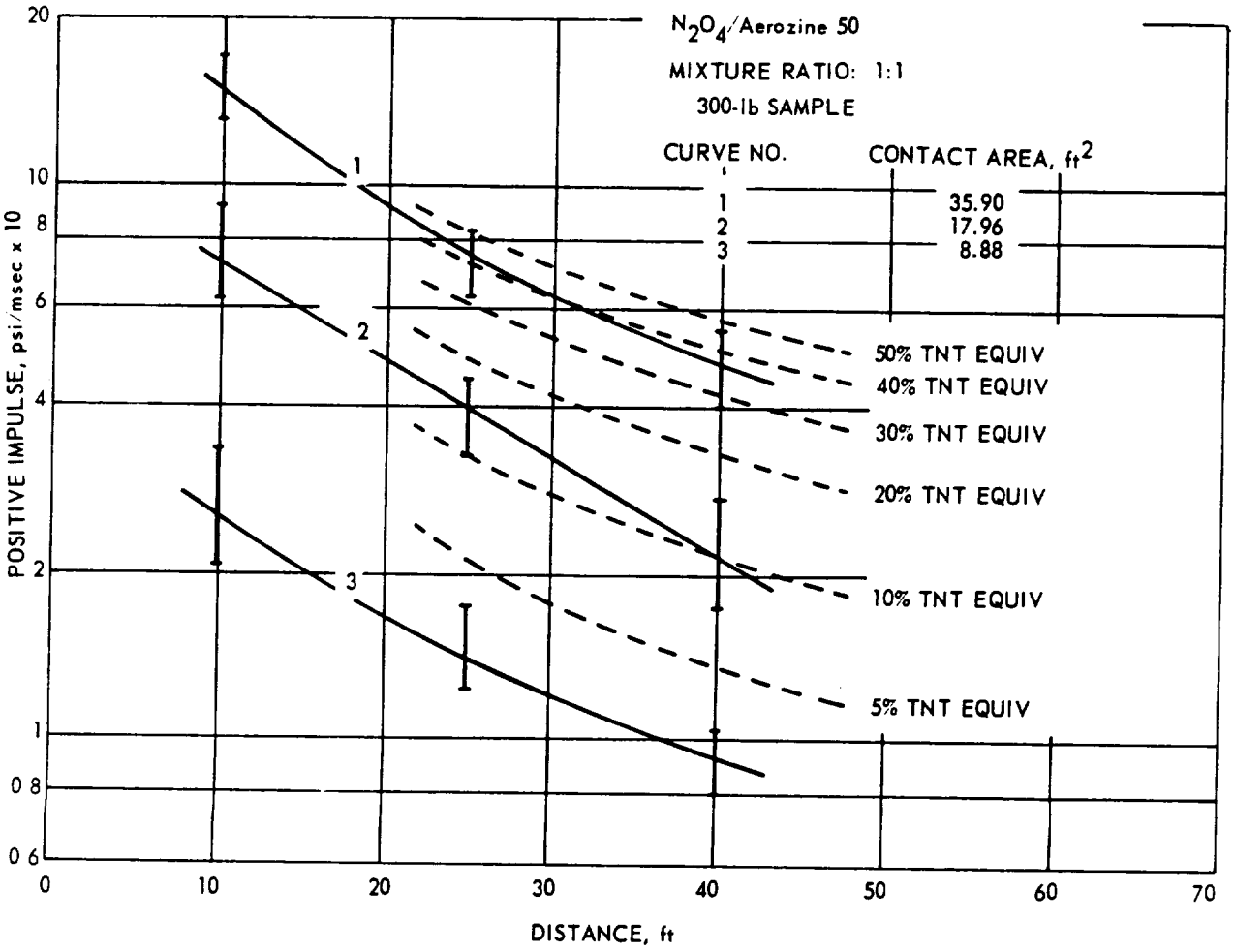

Figure 36. Positive Impulse Data.

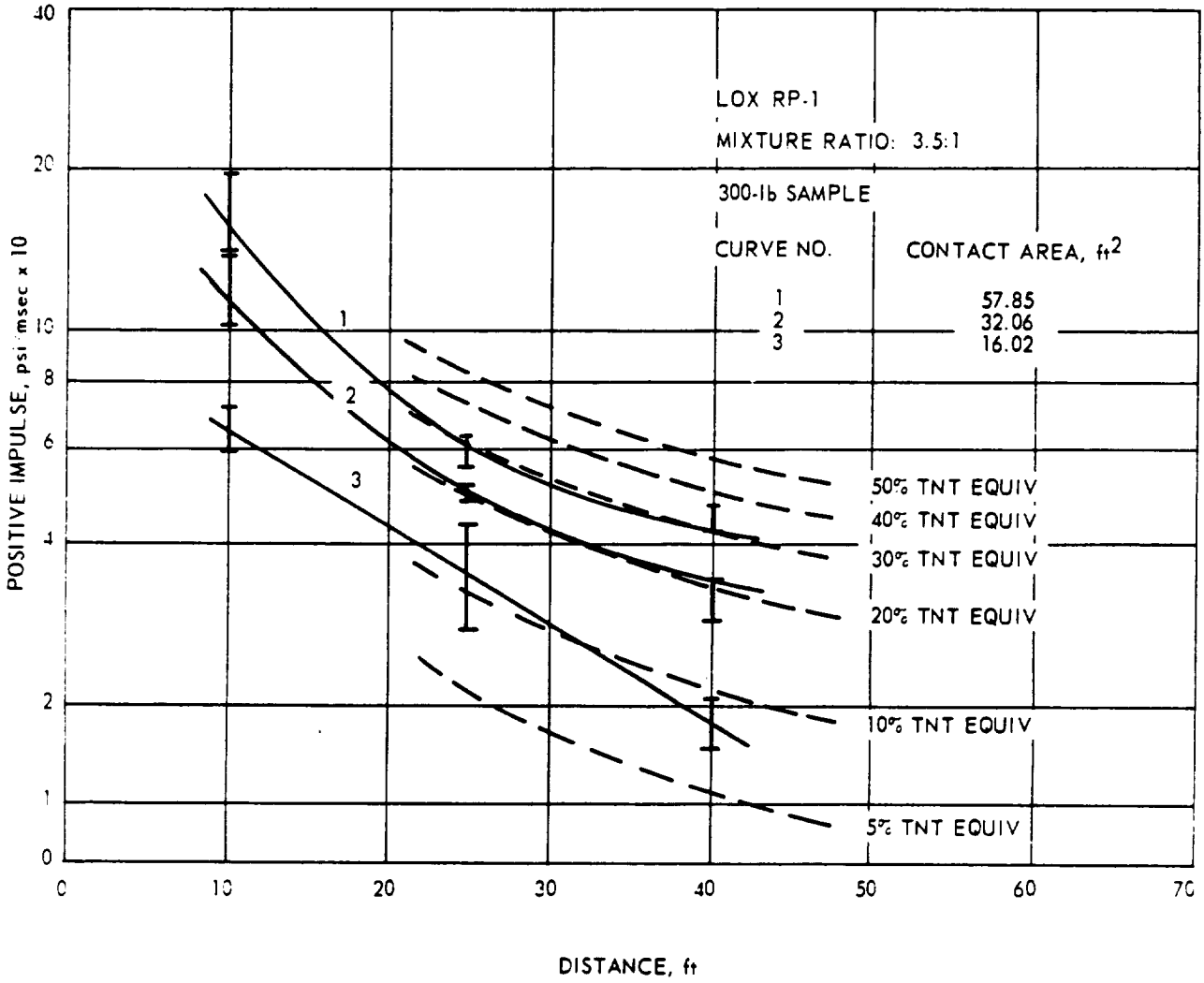

Figure 37. Positive Impulse Data.

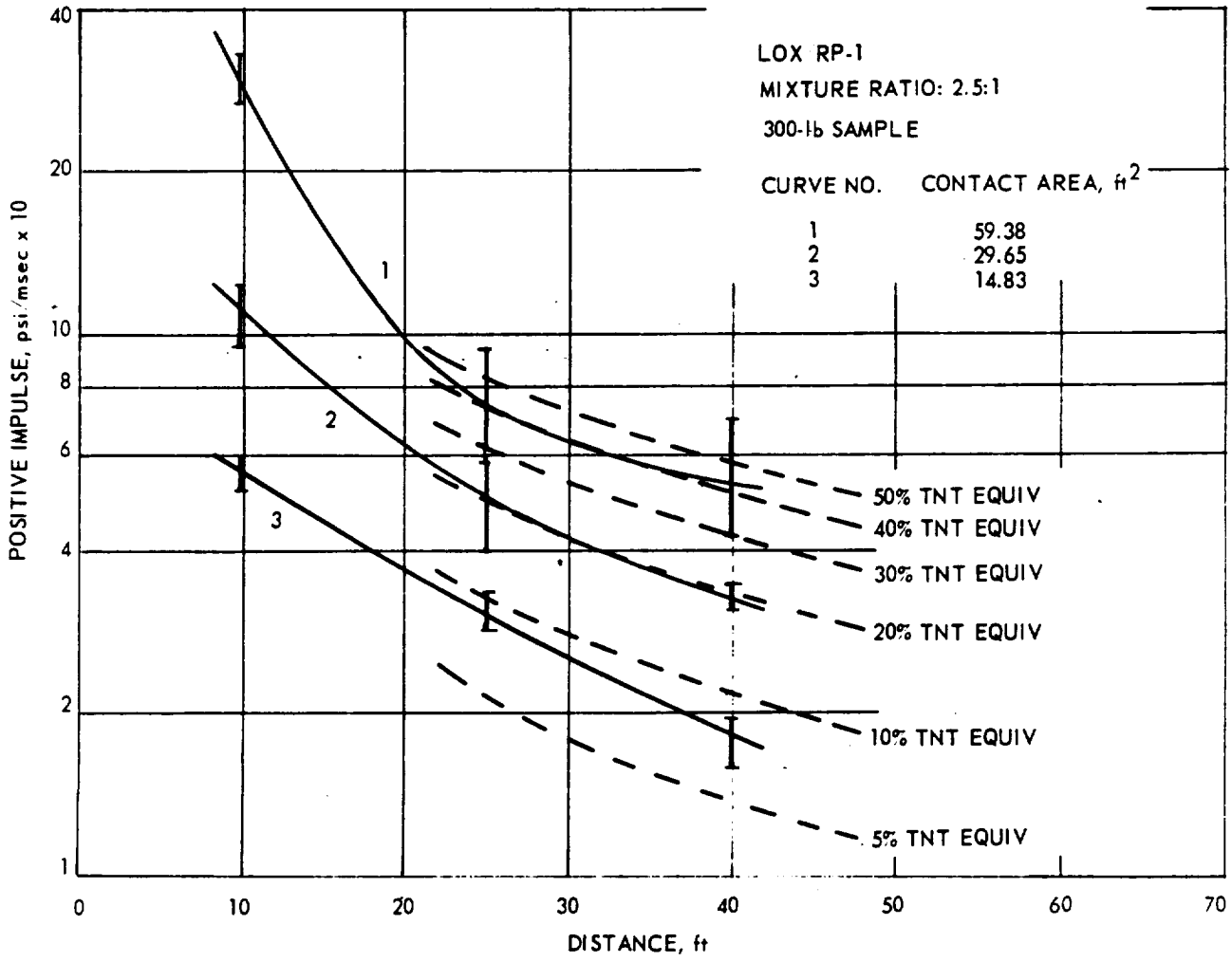

Figure 38. Positive Impulse Data.

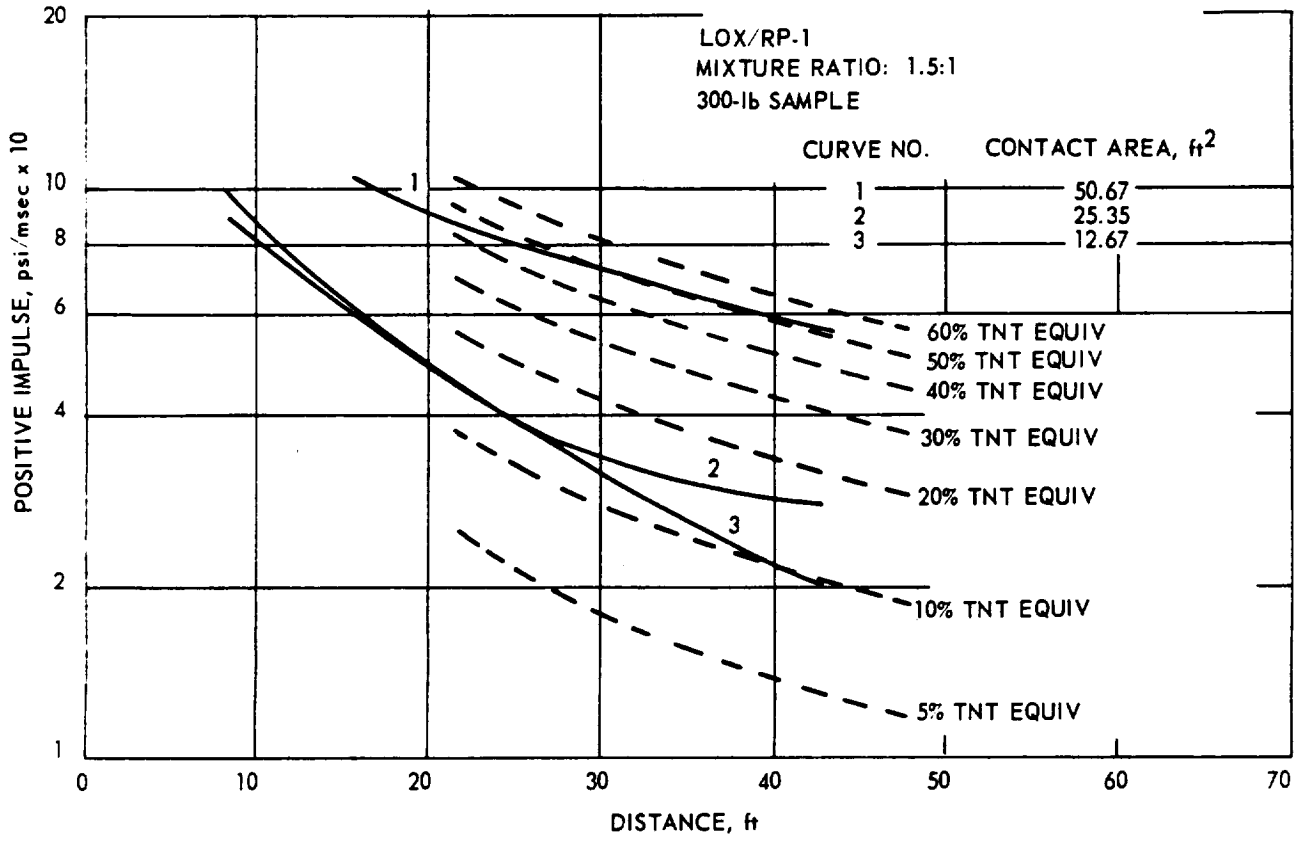

Figure 39. Positive Impulse Data.

4.6.3 Cryogenic Propellant Initiation

The original program for the cryogenic tests included provisions for an initiation delay at a predetermined time after the impact of the dewar/pan assembly. The delay period was intended to permit ultimate participation of the fuel and oxidizer in the explosive reaction. In actual practice, it was found that, at impact, the LOX/RP-1 propellant combinations initiated spontaneously from an undetermined stimulus; thus providing a comparative degree of mixing for both propellant types. The cause of the initiation is not known, but possible causes are: (1) impact-caused implosion of the glass dewars, (2) the compression of the LOX/RP-1 propellant between the glass fragment and the pan wall, or (3) a combination of the two proposed sources of initiation. The spontaneous initiation is evidenced in Figure 18 by a dewar/pan assembly that is in slight motion presumably after impacting against a steel plate. The reaction of the propellants has already commenced, as evidenced by the light reflecting from the top of the drop tower although the dewar pan is still intact.

4.6.4 Blast Results

The test results indicated the blast yield of both the hypergolic and the cryogenic propellant combinations was dependent on the oxidizer/fuel contact area. This is more pronounced in the hypergolic propellant tests. The peak overpressure data indicated a TNT equivalence of less than 0.02 lb of TNT per lb of propellant at the 40-ft-gage stations for a low-contact area and 0.34 lb of TNT per lb of propellant for a high-contact area.

For the hypergolic propellant tests, TNT equivalence from 0.29 to 0.34 lb of TNT per lb of propellant were measured on a overpressure basis for a high-contact area. For an intermediate-contact area, equivalences of 0.05 to 0.09 lb of TNT per lb of propellant were measured. The low-contact area tests yielded equivalences of less than 0.02 lb of TNT per lb of propellant.

The peak overpressure data for the cryogenic tests indicated similar results at the 40-ft-gage location. TNT overpressure equivalences of 0.28 to 0.36 lb of TNT per lb of propellant were determined for the high-contact areas. The immediate-contact-area tests ranged from 0.07 to 0.14 lb of TNT per lb of propellant. For a low contact area, the test results ranged from 0.07 to 0.11 lb of TNT per lb of propellant.

The hypergolic-test results indicated TNT impulse equivalences of from 0.37 to 0.42 lb of TNT per lb of propellant. For an intermediate-contact area, impulse equivalences of 0.10 to 0.17 lb of TNT per lb of propellant were measured. The low-contact-area hypergolic test yielded TNT impulse equivalences of less than 0.03 lb of TNT per lb of propellant.

The high-contact-area cryogenic tests yielded TNT impulse equivalences which ranged from 0.30 to 0.49 lb of TNT per lb of propellant. The impulse data for the intermediate-contact-area-cryogenic tests indicated equivalences of 0.19 to 0.26 lb of TNT per lb of propellant. For a low-contact area, TNT impulse equivalences of 0.06 to 0.10 lb of TNT per lb of propellant were determined.

4.6.5 Fireball History

The results of the fireball size and duration measurements are presented in Figures 40 to 45 and are listed in Table 10. The fireballs produced by the hypergolic propellants in fuel-lean and stoichiometric mixture tests were greatly affected by the contact area. In these tests the fireball duration increased with decreased contact area. The duration ranged from 0.5 sec to 2.15 sec. The maximum fireball diameters varied from 58 to 68 ft, and the maximum height ranged from 31 to 52 ft. Tests with a fuel-rich mixture ratio (1:1) showed no definite relationship between contact areas. The duration ranged between 2.02 and 2.87 sec. The maximum fireball diameter ranged from 69 to 80 ft, and the height ranged between 47 to 59 ft.

A random variation was observed in the fireball size and duration of the cryogenic tests. No definite relationship was observed for the fireball size or duration with contact area and mixture ratio. The durations varied from 1.7 to 2.5 sec. The maximum diameter ranged from 66 to 108 ft, and the height ranged from 30 to 83 ft.

4.6.6 Fragment Impact Test

During the early part of the experimental studies, a malfunction occurred in the pan release mechanism that prevented the assembly from dropping. For safety reasons the filled fixture could not be lowered. Since the test had to be destroyed, it was pertinent to observe the effects of projectile impact through the pan. The pan contained a fuel-lean cryogenic mixture (3.5:1 mixture ratio) with a low-contact area. A 30 caliber bullet was utilized as the projectile. The velocity of the projectile was approximately 2500 fps.

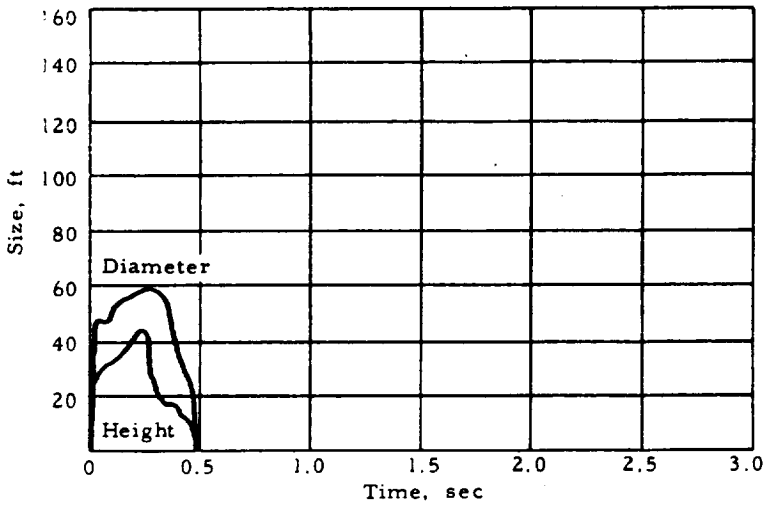

CONTACT AREA: 51.01 ft^2
MAXIMUM HEIGHT: 44 ft
MAXIMUM DIAMETER: 59 ft
DURATION: 0.5 sec

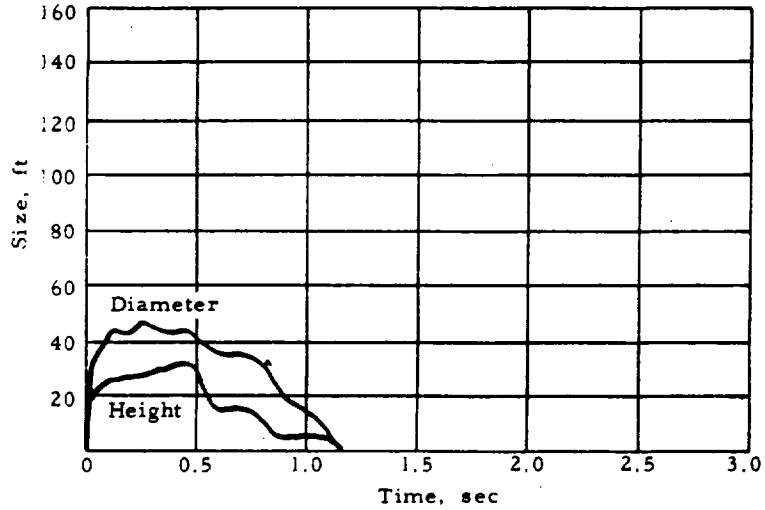

CONTACT AREA: 25.44 ft^2
MAXIMUM HEIGHT: 39 ft
MAXIMUM DIAMETER: 58 ft
DURATION: 1.15 sec

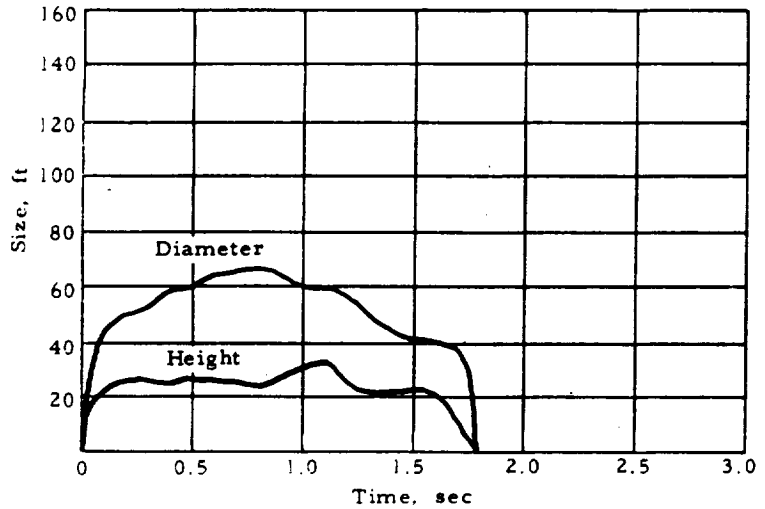

CONTACT AREA: 12.64 ft^2
MAXIMUM HEIGHT: 33 ft
MAXIMUM DIAMETER: 66 ft
DURATION: 1.78 sec

Figure 40. Fireball History - N_2O_4/ \-50; MR = 3:1.

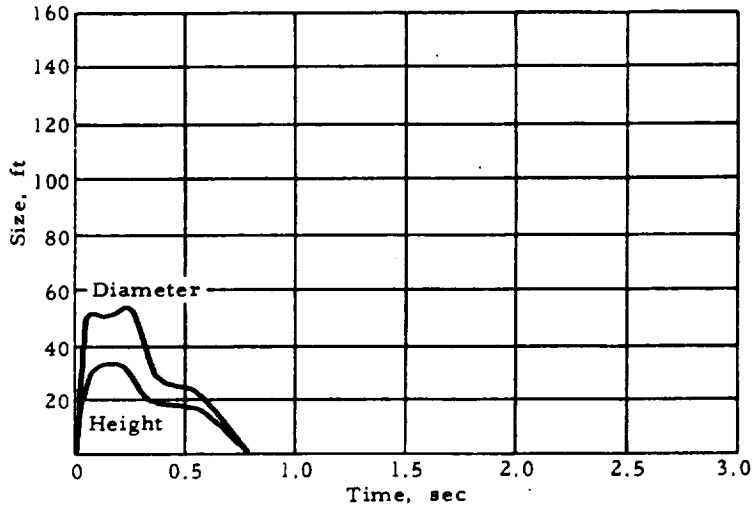

CONTACT AREA: 45.53 ft^2
MAXIMUM HEIGHT: 41 ft
MAXIMUM DIAMETER: 67 ft
DURATION: 0.8 sec

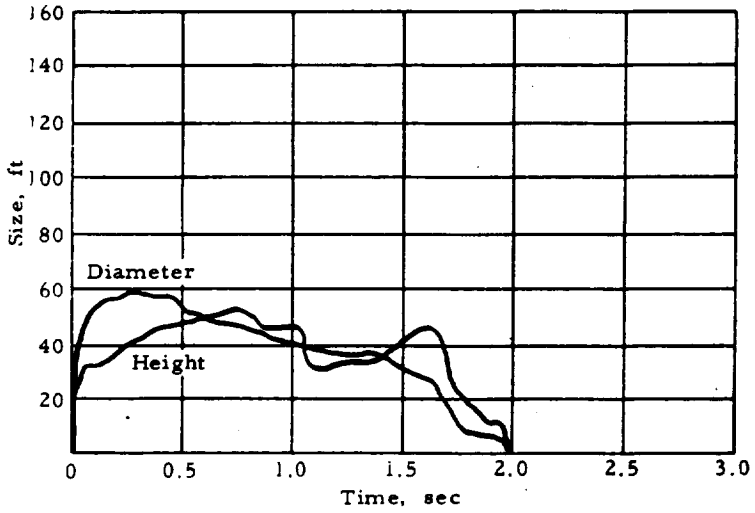

CONTACT AREA: 22.90 ft^2
MAXIMUM HEIGHT: 52 ft
MAXIMUM DIAMETER: 58 ft
DURATION: 1.97 sec

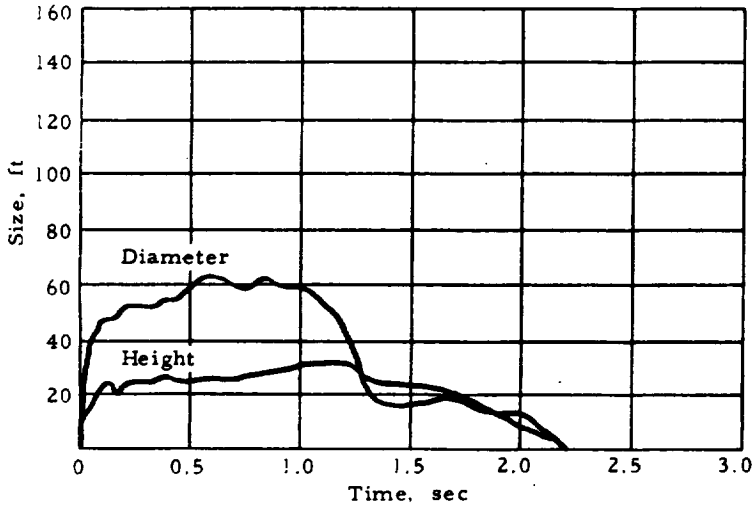

CONTACT AREA: 11.39 ft^2
MAXIMUM HEIGHT: 31 ft
MAXIMUM DIAMETER: 62 ft
DURATION: 2.2 sec

Figure 41. Fireball History - N_2O_4/A-50; MR = 2:1.

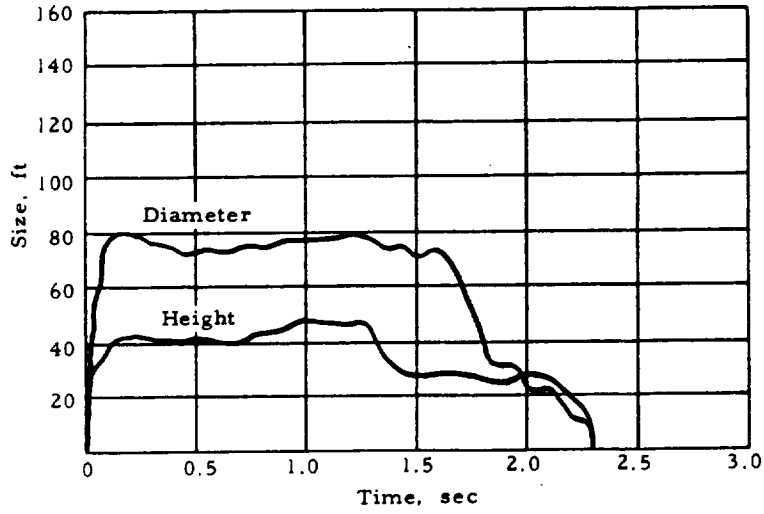

CONTACT AREA: 35.90 ft^2
MAXIMUM HEIGHT: 47 ft
MAXIMUM DIAMETER: 80 ft
DURATION: 2.29 sec

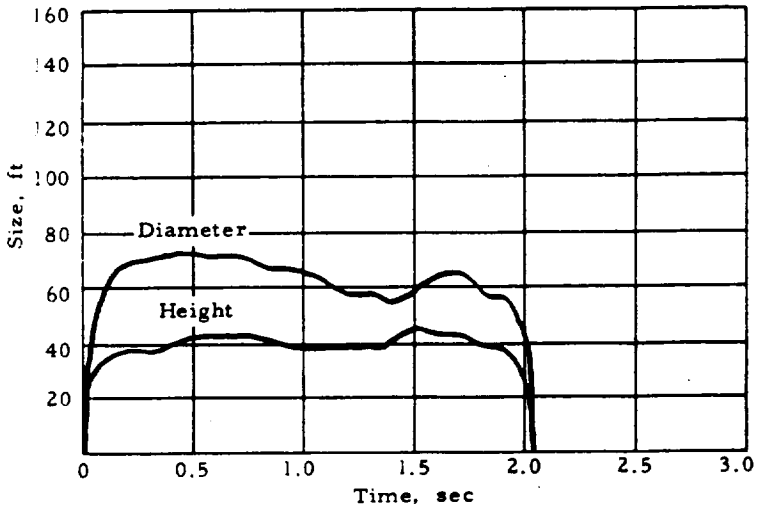

CONTACT AREA: 17.96 ft^2
MAXIMUM HEIGHT: 44 ft
MAXIMUM DIAMETER: 74 ft
DURATION: 2.02 sec

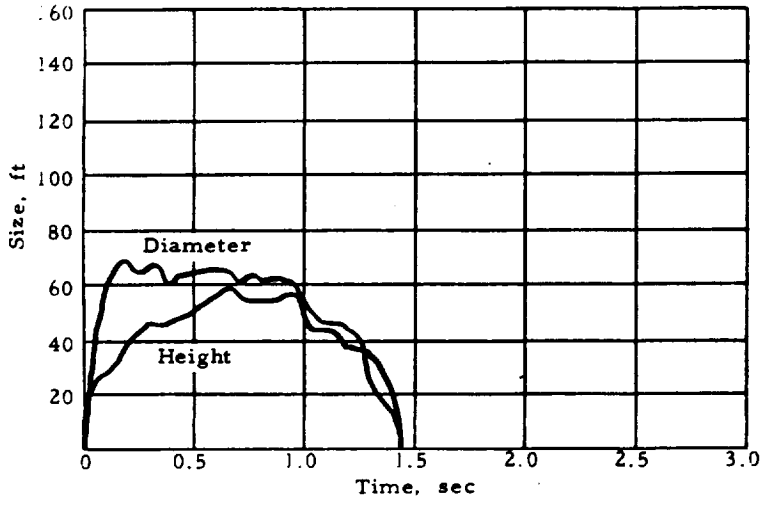

CONTACT AREA: 8.88 ft^2
MAXIMUM HEIGHT: 59 ft
MAXIMUM DIAMETER: 70 ft
DURATION: 2.87 sec

Figure 42. Fireball History - N_2O_4/A-50; MR = 1:1.

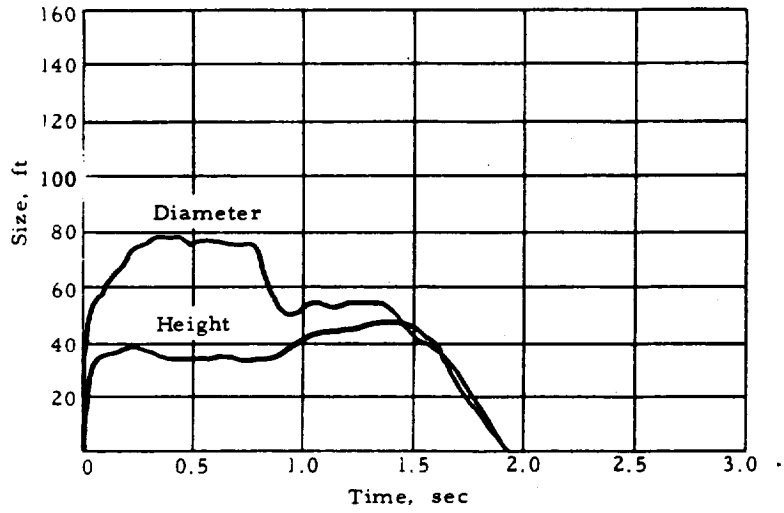

CONTACT AREA: 57.85 ft^2
MAXIMUM HEIGHT: 48 ft
MAXIMUM DIAMETER: 79 ft
DURATION: 1.90 sec

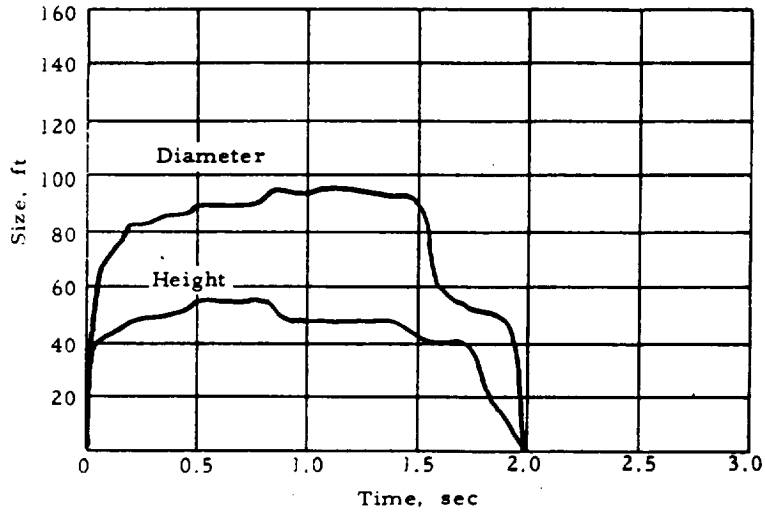

CONTACT AREA: 32.06 ft^2
MAXIMUM HEIGHT: 55 ft
MAXIMUM DIAMETER: 97 ft
DURATION: 1.99 sec

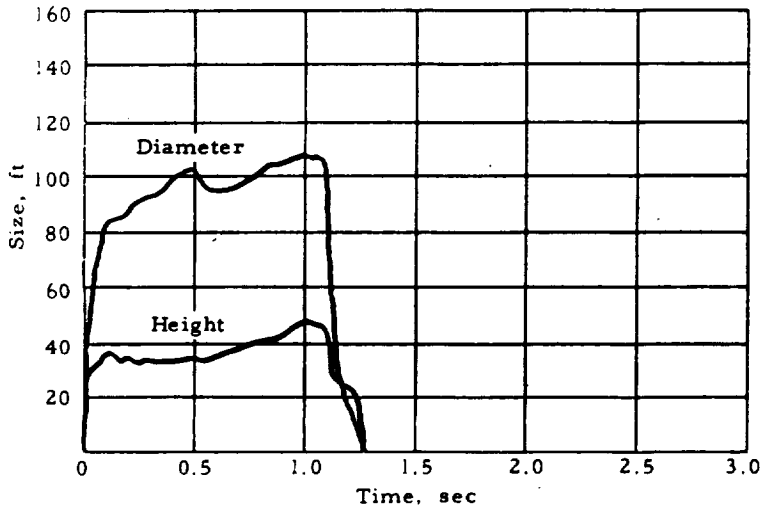

CONTACT AREA: 16.02 ft^2
MAXIMUM HEIGHT: 57 ft
MAXIMUM DIAMETER: 108 ft
DURATION: 2.55 sec

Figure 43. Fireball History - LOX-RP-1; MR = 3.5:1.

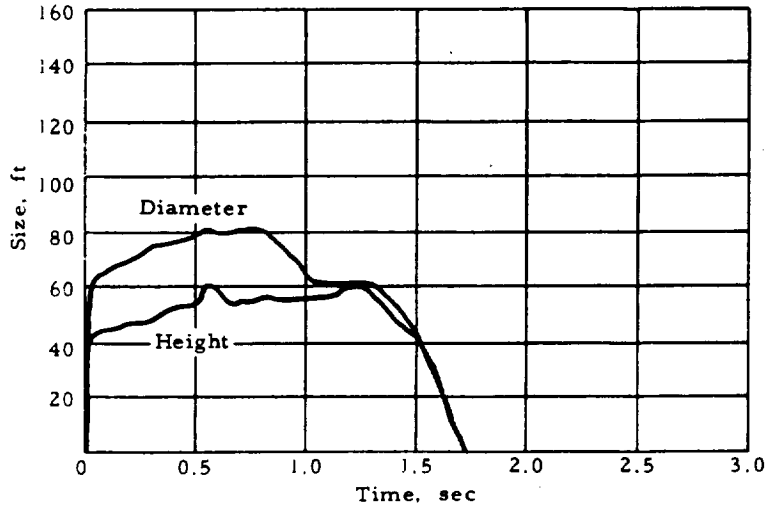

CONTACT AREA: 59.38 ft^2
MAXIMUM HEIGHT: 60 ft
MAXIMUM DIAMETER: 80 ft
DURATION: 1.70 sec

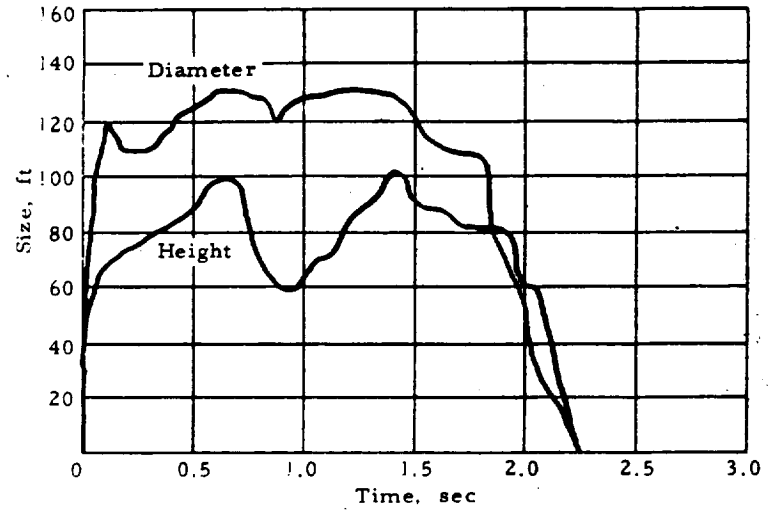

CONTACT AREA: 29.65 ft^2
MAXIMUM HEIGHT: 51 ft
MAXIMUM DIAMETER: 66 ft
DURATION: 2.25 sec

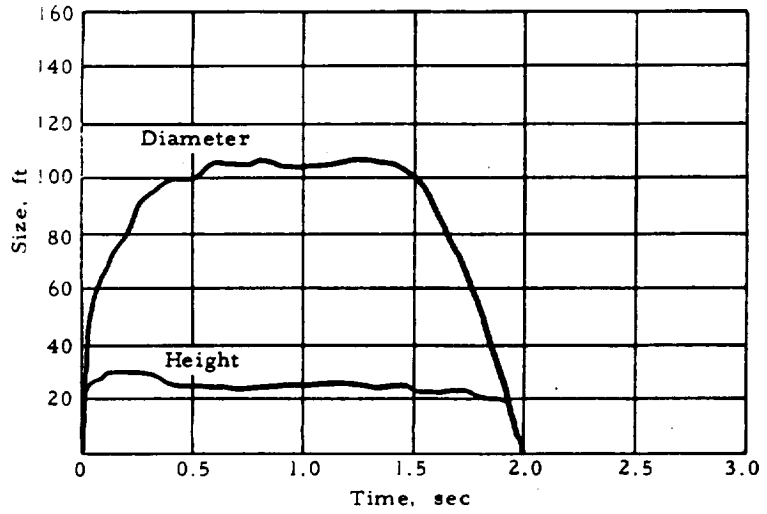

CONTACT AREA: 14.83 ft^2
MAXIMUM HEIGHT: 30 ft
MAXIMUM DIAMETER: 107 ft
DURATION: 1.99 sec

Figure 44. Fireball History - LOX/RP-1; MR = 2.5:1.

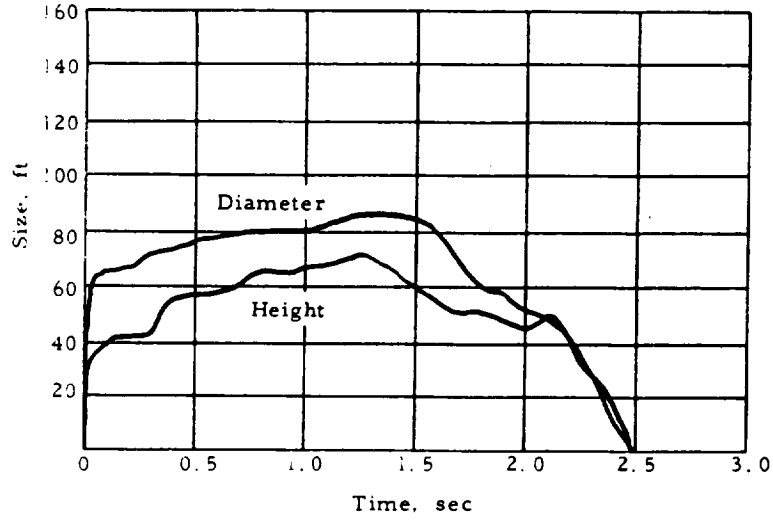

CONTACT AREA: 50.67 ft^2
MAXIMUM HEIGHT: 71 ft
MAXIMUM DIAMETER: 85 ft
DURATION: 2.50 sec

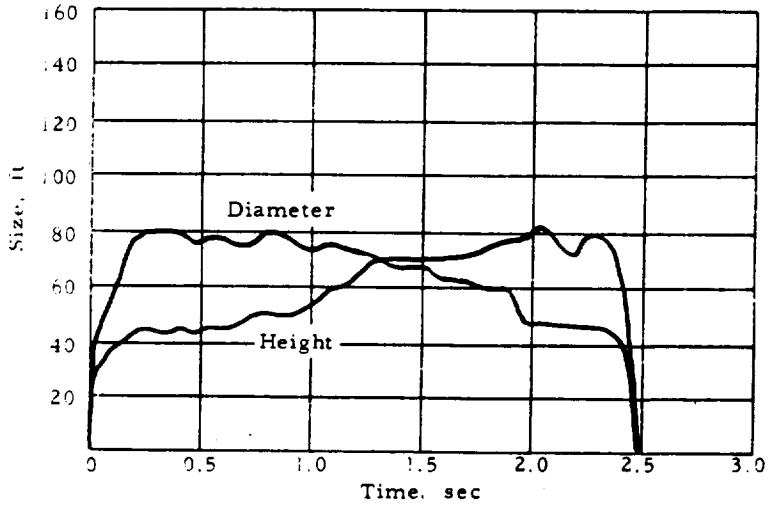

CONTACT AREA: 25.35 ft^2
MAXIMUM HEIGHT: 83 ft
MAXIMUM DIAMETER: 81 ft
DURATION: 2.49 sec

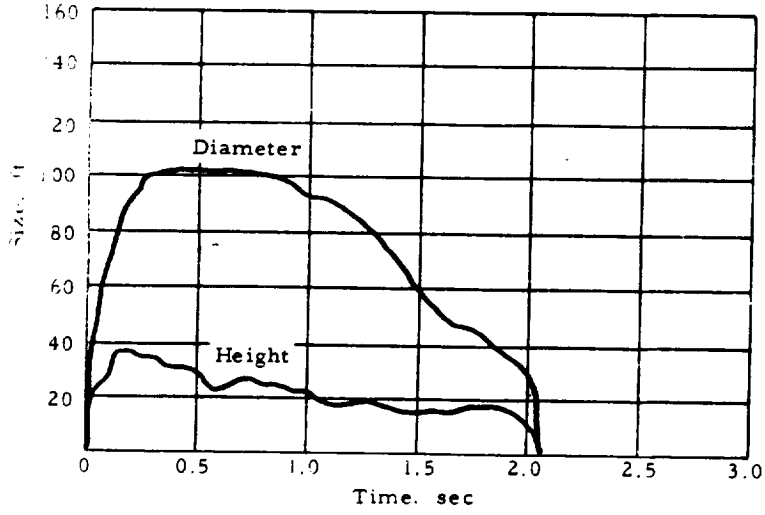

CONTACT AREA: 12.67 ft^2
MAXIMUM HEIGHT: 36 ft
MAXIMUM DIAMETER: 102 ft
DURATION: 2.07 sec

Figure 45. Fireball History - LOX/RP-1; MR = 1.5:1.

Immediately after impact a series of "pops" and "cracks" were heard and several streams of liquid and gas sprayed from the pan. Approximately 1 sec after impact, initiation occurred with a reaction comparable to the drop tests. It is significant that the projectile initiated the liquid oxygen and RP-1 propellant, in that if a similar projectile or fragment should strike a fueled launch vehicle, the results would be catastrophic.

4.6.7 Nitrogen Tetroxide Vapor Reaction

A preignition of the oxidizer and fuel was experienced during the fourth test with the hypergolic propellants. The ignition occurred during the early part of the fuel transfer operation and was attributed to a N_2O_4 vapor and an A-50 liquid reaction that ignited the A-50 in the pan. The air temperature during the test contributed to the preignition by causing excessive vaporization of the N_2O_4.

The ambient temperature at test time was 75°F, and the relative humidity was 24%. The wind velocity during the loading operation varied from 0 to 2 mph, which contributed to the accumulation of N_2O_4 vapor in the pan. The first evidence of an abnormal reaction was the emission of heat waves from the pan. The waves continued for approximately 1 min before the heat probably caused one or more of the dewars to shatter, thus permitting direct contact of the two hypergolic liquids with a subsequent destructive explosion and loss of the test items.

To prevent recurrence of the preignition, a stopper (a Saran-covered cork) was placed in each dewar to contain the nitrogen tetroxide vapors. A plywood cover was placed on top of the stoppers and secured to the sides of the pan as in all previous tests.

The first test with the cork stoppers was conducted without difficulty; however, the following tests again resulted in a preignition of the propellants during fuel loading operations. To prevent any further preignition of the propellants, three added precautions were taken. The cork stoppers were replaced with a Saran-covered, foam rubber stopper with a greater contact area between the stopper and the dewar wall. The N_2O_4 was also cooled by passing the fill line through an ice bath during loading to reduce vaporization, and nitrogen gas was used to flood the interior of the entire pan assembly after the dewars were loaded with the oxidizer. No further difficulty was experienced with any tests that utilized the modified test assembly. These additions did not affect the test functions.

4.6.8 Ultimate Mix Tests

The initiation of the LOX/RP-1 test on impact did not permit an evaluation of the explosive yield from a well-mixed cryogenic sample. A test was designed to determine the effect good mixing of the RP-1 in the LOX would have on the blast characteristics.

The test fixture was an insulated aluminum pan (30 in. x 30 in. x 16 in.) located on a steel plate in the center of the test area. The mixture ratio desired was 2.5:1 LOX/RP-1. The pan was filled with the quantity of LOX, and the necessary quantity of RP-1 was placed in a metal barrel that was located above and to the side of the LOX pan (Figure 46). The barrel was designed to empty into the pan by means of a hinge on its bottom. This test configuration allowed the RP-1 to dump into the LOX by a remotely actuated release mechanism, while also permitting a predetermined delay before mixture initiation.

Visual observation and high-speed camera coverage of the test indicated that, during the pouring operation, part of the incoming RP-1 was ejected from the pan by the extremely high vaporization rate of the LOX. In addition, RP-1 vaporized an unknown quantity of the LOX. The mixing procedure thus resulted in an unknown quantity of LOX and RP-1 in the pan. The propellant was initiated with a No. 8 electric blasting cap (EBC), centered in the pan, 0.5 sec after the completion of the RP-1 pouring operation.

The results of the test are presented in Table 15 as Ultimate Mixing Test No. 1.

The high-speed camera coverage indicated ≈50% of the LOX and RP-1, or 150 lb, were remaining after the mixing operation. Allowing for this approximate weight and for the overpressure measurements at 40 ft, the sample yielded a TNT equivalence of ≈42%.

To prevent the mixing losses observed in the first mix test, a new technique was devised to add a sufficient quantity of LOX to allow for boil-off. An insulated 55-gal steel drum was used to hold the desired mixture. The amount of LOX required to compensate for the RP-1 quantity was determined by a trial mix with LN_2 and RP-1. The heats of vaporization for the two liquids are similar. The RP-1 was pumped into the barrel (Figure 47) through a 3/8-in.-diameter line that terminated approximately 3 in. above the surface of the LOX. This technique provided partial success. The RP-1 froze on contact with the LOX and formed a layer of solid RP-1 on the surface of the LOX in the barrel. This prevented

Figure 46. Preliminary Cryogenic Mixing Test
(Note Solid RP-1 on Ground).

Figure 47. Ultimate Mixing Test Fixture - RP-1 Induced at top of LOX.

an undetermined amount of RP-1 from combining with the LOX. An attempt to agitate the mixture with nitrogen gas resulted in a loss of part of the frozen RP-1. The propellant remaining in the barrel was initiated with two No. 8 EBC located at the center of the fixture. Results of the test are presented in Table 15 as Ultimate Mixing Test No. 2.

High-speed camera coverage of the test indicated approximately 60% of the RP-1 was lost during the loading operation and the attempted agitation. Assuming a test sample weight of ≈35 lb of RP-1 and ≈ 250 lb of LOX, the overpressure test results indicate a TNT equivalence of approximately 49% at a distance of 40 ft from the sample.

The third test to determine the effect of mixing involved a different RP-1 to LOX induction method. An insulated 55-gal steel drum was fitted with 3/8-in. tubing on the bottom. A 3/8-in. -diameter U-trap and check valve was placed in the line to the fuel pump line. A small quantity of RP-1 was placed in the U-trap and frozen with liquid nitrogen. A thermocouple was attached to the pumping line to provide an indication as to when the RP-1 was flowing.

A quantity of LOX (450 lb) in slight excess of the amount required to provide a 2.5:1 mixture when mixed with the RP-1 was placed in the barrel. Two screens were positioned under the surface of the LOX to restrain the frozen RP-1 from rising to the top. A 18-in.-diameter by 5-in. -high dome-shaped screen was placed approximately 5 in. from the bottom of the barrel and a flat horizontal screen 22 in. in diameter was located above it at the 15-in. level (Figure 48). Both screens were secured to the sides of the barrel. Two No. 8 EBC, located between the screens, were used to initiate the sample.

Camera coverage indicated the final liquid quantity in the barrel after the addition of the RP-1 was composed of approximately 255 lb of LOX and 86 lb of RP-1; a mixture ratio of 3:1. The results of the test, presented in Table 15 as Ultimate Mixing Test No. 3, indicated a TNT equivalence, (based on overpressure data of 40 ft) of approximately 120%. The blast yield from the reaction was sufficient to project the 3.0-in. -diameter by 25-ft-long steel tower legs as far as 175 ft.

The results of the third ultimate mix test indicate that the degree of mixing between the fuel and oxidizer has considerable affect on the explosive yield. The theoretical equivalent TNT energy for an oxidizer/fuel ratio of 3:1 is approximately 170%, assuming a TNT heat of explosion of 1060 cal/gm and a heat of explosion of ≈ 1800 cal/gm for the propellant.

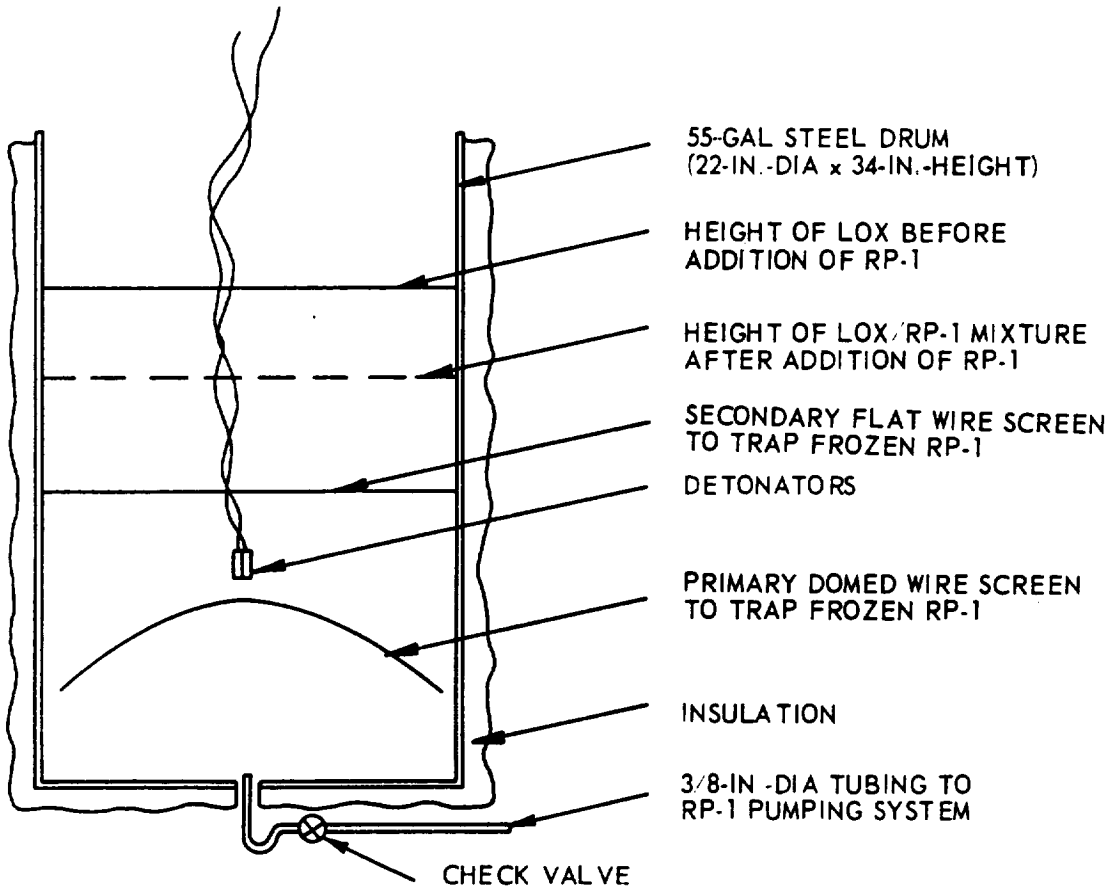

Figure 48. Ultimate Mix Test Fixture
(RP-1 Induced Beneath LOX).

4.6.9 Radiation Tests

The results of the thermal-radiation measurements are presented in Tables 11 and 12 in the form of apparent effective fireball radiant intensity vs time for each of the five spectral regions. The units of intensity are given in watts per steradian; i.e., power emitted per unit solid angle. These values may be converted to irradiance (incident power per unit area) through dividing by the range squared.

The integrated total flux is reported for each test in Table 13. These values were calculated by numerical integration of the total intensity vs time, assuming spherical symmetry for the radiation; i.e., the integral was multiplied by 4π.

The radiant intensity data were presented in order of increasing wavelength. Channel 1 corresponds to the short wavelength silicon detector-filter combination shown in Figure 14. Channel 2 to Figure 15; Channel 3 to Figure 16; Channel 4 to Figure 17; and Channel 5 to the thermistor bolometer.

Data from the low-contact-area LOX/RP-1 tests for mixture ratios of 3.5:1 and 1.5:1 and from a medium-contact area 2.5:1 mixture ratio test are not reported. In these tests, conducted early in the program, the amplifier gains had not yet been chosen properly and the data were lost due to tape recorder overload. Most measurements for the 2.5:1 mixture ratio test of LOX/RP-1 with a low-contact area were lost due to a power failure following the pan assembly impact. No measurements were obtained for the 1:1 mixture ratio N_2O_4/A-50 test with a low-contact area because inclement weather prevented transportation of the instrument van to the site.

The results of the radiation measurements indicated an apparent decrease in radiation yield with increased contact area between the oxidizer and fuel for the cryogenic and hypergolic propellant systems. This is shown in Table 13 by the 3:1 mixture ratio N_2O_4/A-50 tests, which liberated total energies of 1.8×10^7, 9.8×10^7, and 1.4×10^8 joules for contact areas of 51.01, 25.44, and 12.64 ft^2. A similar relationship was observed for the other test mixtures and contact areas.

A comparison of the radiation yields on a mixture ratio basis indicates an increase in radiation yield with a decrease in the oxidizer/fuel ratio although the contact area between the oxidizer and fuel also decreased. A comparison of the radiation energy data and the blast data showed a partitioning of energy between blast and radiation yields; i.e., the higher the blast yield the lower the radiation yield.

The LOX/RP-1 propellant tests yielded higher radiation energies than the N_2O_4/A-50 tests for comparative contact surface areas. The LOX/RP-1 samples produced from 1.5×10^8 to 6.1×10^8 joules, while the N_2O_4/A-50 tests had yields ranging from 1.8×10^7 to 2.4×10^8 joules. The maximum yield for the LOX/RP-1 tests would probably have been higher if radiation data had been obtained for the low-contact-area samples.

The total radiation yields of the hypergolic propellant tests indicated a relationship between contact area and time-to-maximum intensity after impact of the dewar/pan assembly. The radiation yields for the hypergolic tests are presented in Figure 49 in the form of radiant intensity (w/ steradian) vs time (sec). Maximum intensity occurred between 0.1 and 0.2 sec after impact for the high-contact-area tests. Examination of the intermediate- and low-contact-area test results indicated the maximum intensity occurred approximately 0.2 sec after impact for the intermediate-contact-area tests and from 0.5 to 0.6 sec after impact for the low-contact-area tests.

A definite relationship between time-to-maximum radiation intensity and contact area was not established for the cryogenic tests, although the limited data tend to indicate the higher the contact area the shorter the time to maximum radiation intensity. The radiation data for the cryogenic tests are presented in Figure 50.

The results of the heat-flux gage measurements are reported in Tables 4 through 9 in terms of the maximum recorded energy observed at each gage station. Examination of the gage results indicates a wide variation in the recorded values depending on the position of the gage in reference to the fireball growth and wind drift. The N_2O_4/A-50 test results indicated maximum flux values which varied from 2.8 to 80.0 BTU/ft^2-sec. The duration from impact of the dewar/pan assembly to maximum heat flux varied with the contact area. Typical low- and high-contact-area heat-flux test records are presented in Figures 51 and 52. Examination of these records indicates the maximum heat-flux values occurred from 0.5 to 1.0 sec after impact of the dewar/pan assembly for low-contact-area tests and from 0.08 to 0.25 sec after impact for high-contact-area tests.

The LOX/RP-1 tests yielded heat-flux values ranging from 9.2 to 236 BTU/ft-sec. The effect of contact area is illustrated in Figures 53 and 54 for typical tests. The maximum heat-flux values occurred from 0.2 to 0.7 sec after impact of the pan assembly for low-contact-area tests and approximately 0.1 sec after impact for high-contact-area tests.

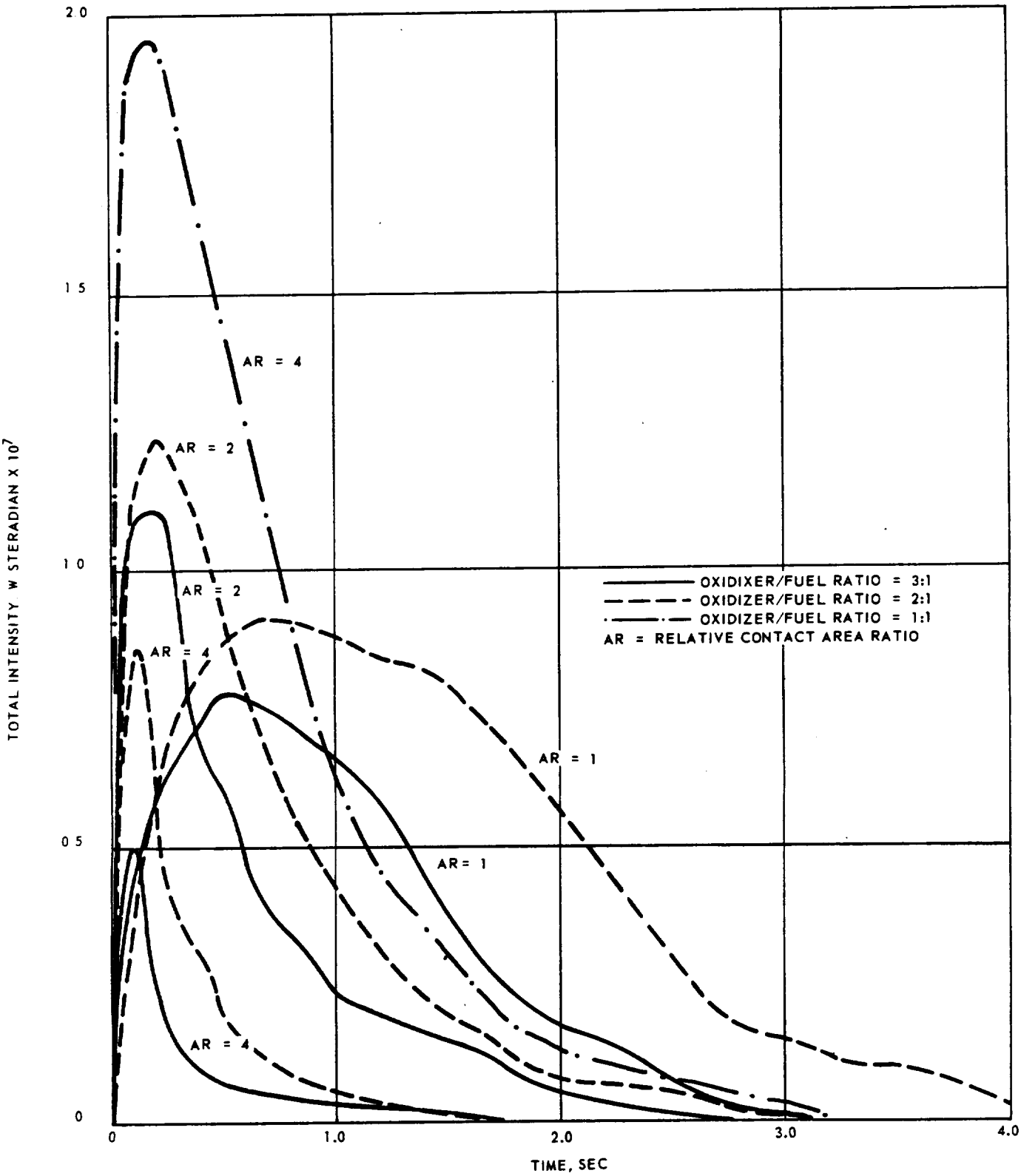

Figure 49. Radiation Intensity N_2O_4/A-50.

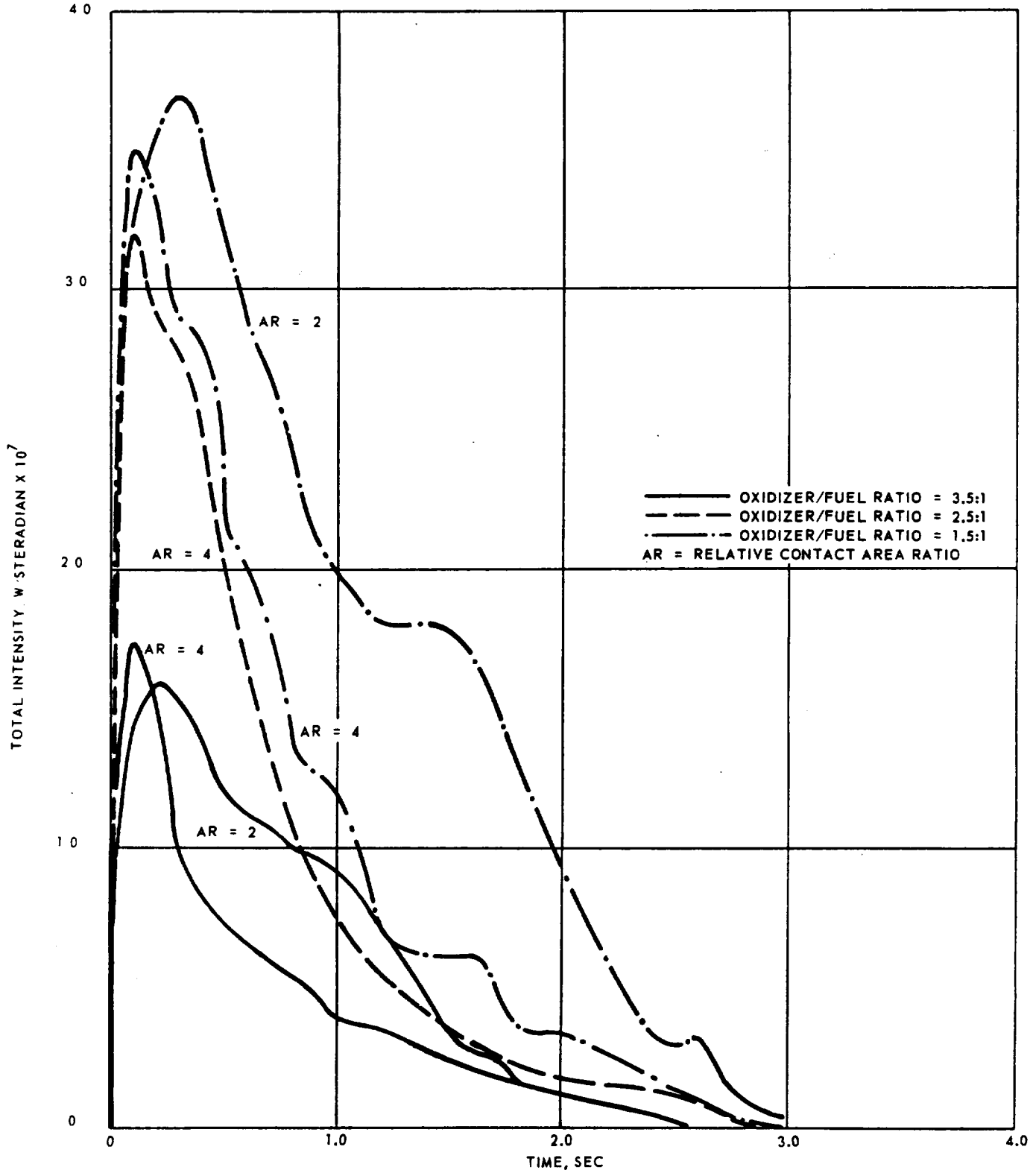

Figure 50. Radiation Intensity LOX/RP-1.

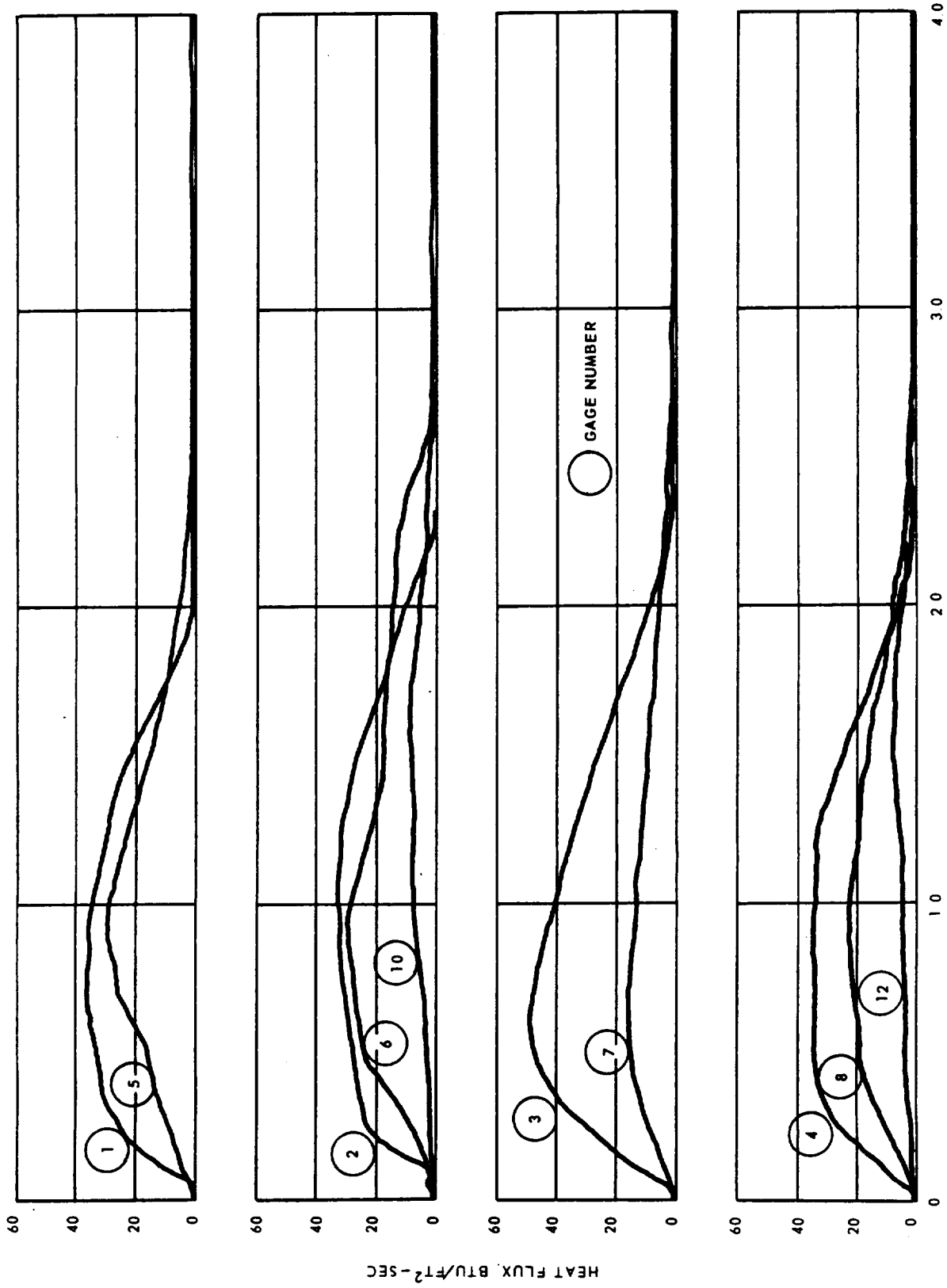

Figure 51. Typical N_2O_4/A-50 Heat Flux Record - Low Contact Area.

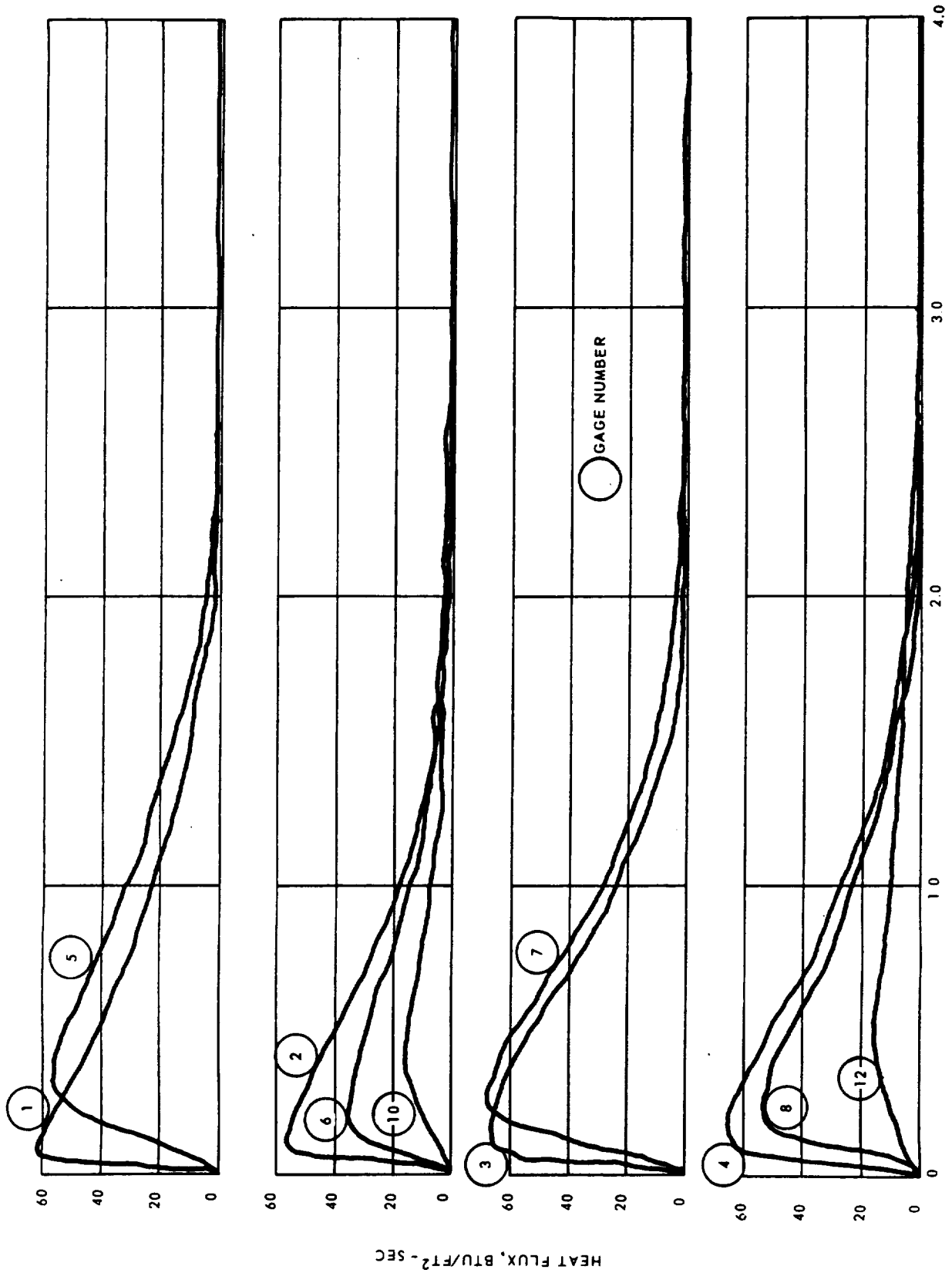

Figure 52. Typical N_2O_4/A-50 Heat-Flux Record - High Contact Area.

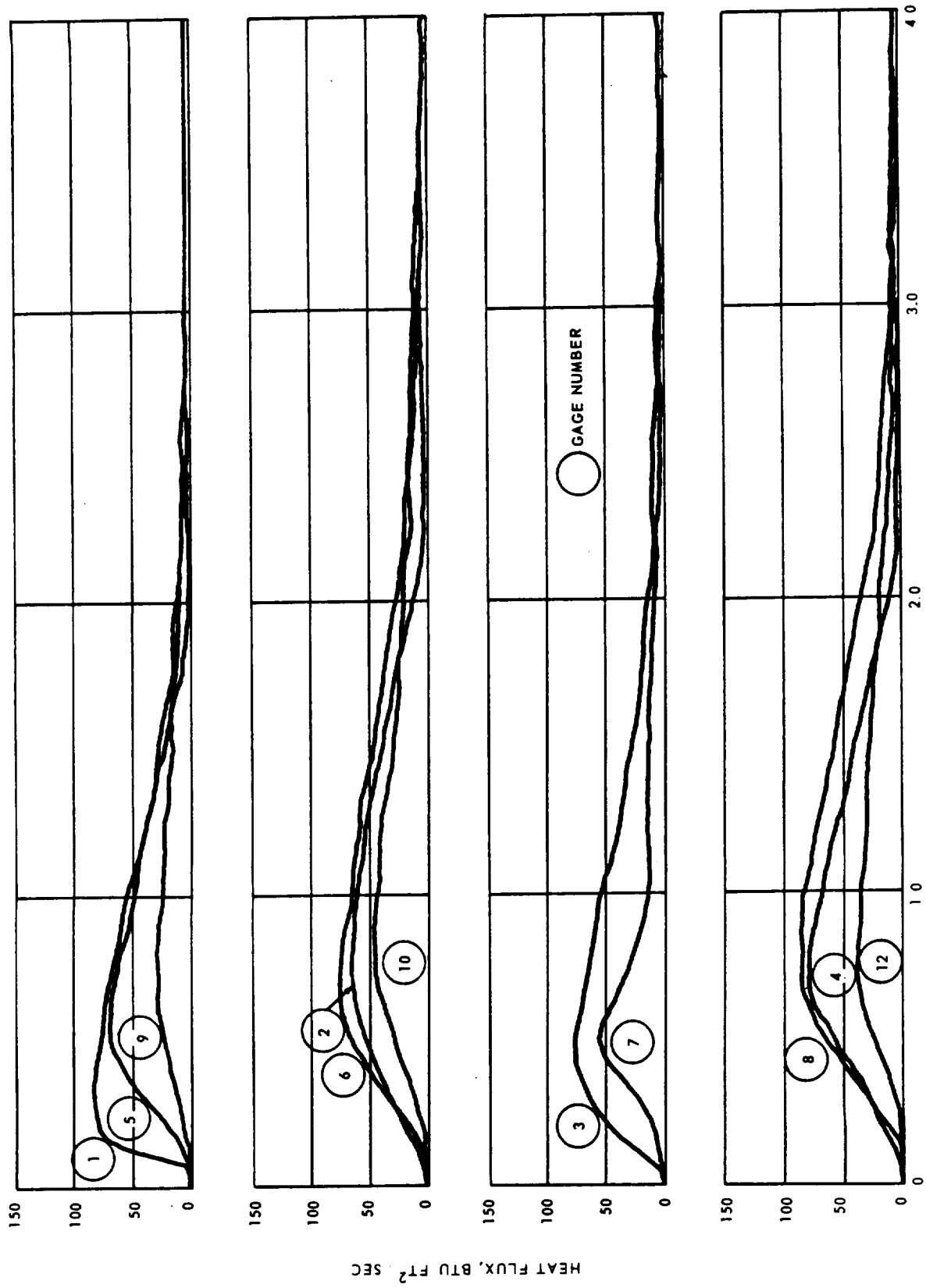

Figure 53. Typical LOX/RP-1 Heat-Flux Record - Low Contact Area.

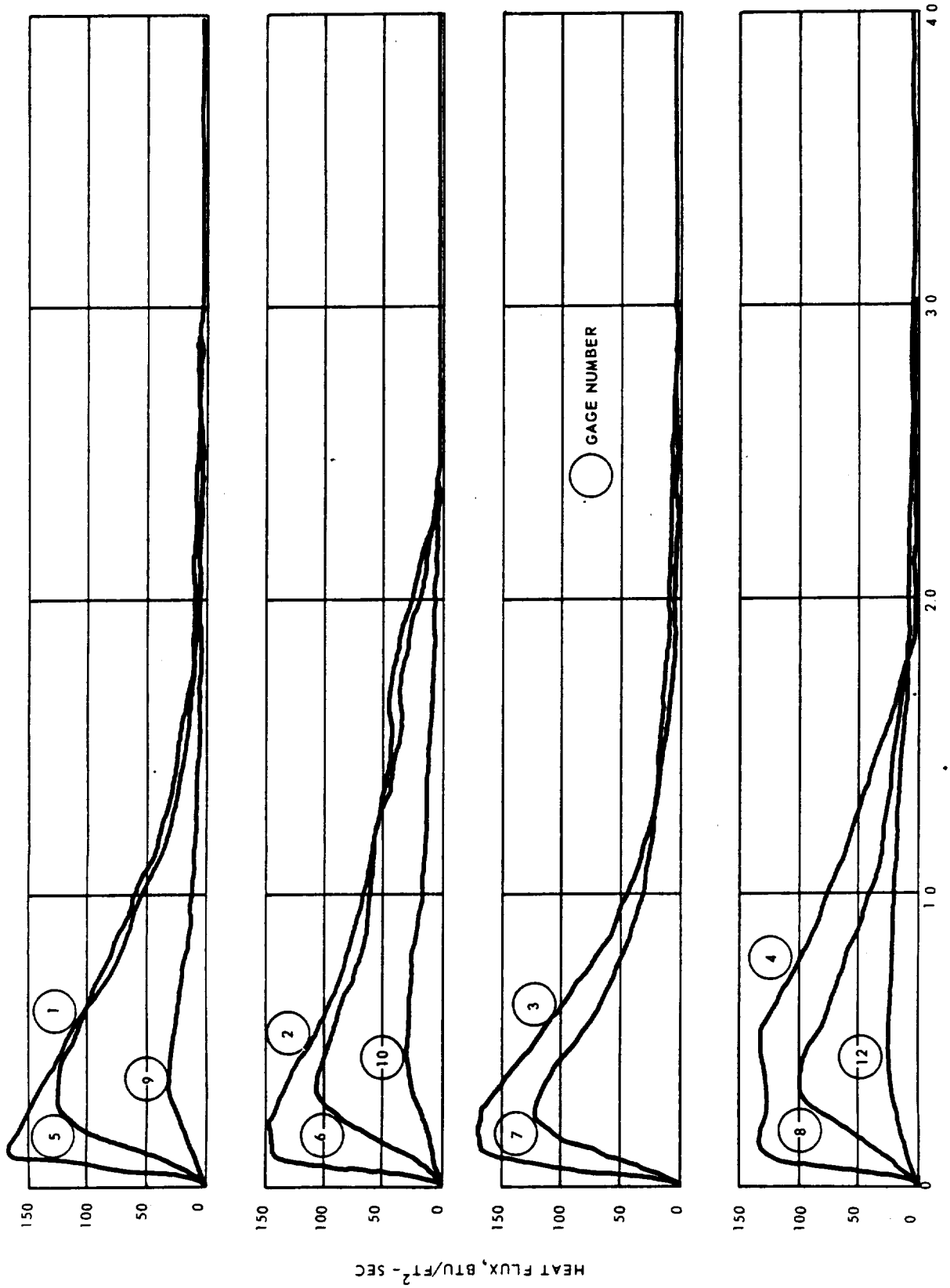

Figure 54. Typical LOX/RP-1 Heat-Flux Record - High Contact Area.

The test results did not indicate a definite relationship between maximum heat flux and mixture ratio for either the hypergolic or the cryogenic propellants.

4.6.10 Fireball Temperature

The maximum temperature measurements were reported in Tables 4 through 9 as the maximum observed value in degrees Fahrenheit at each gage station. Examination of the temperature data indicates a variation in the recorded values depending on the position of the thermocouples in reference to the fireball growth and wind drift. No definite relationship was observed between maximum temperature and other test parameters. The maximum hypergolic temperature was 3070°F and the maximum cryogenic temperature was 3380°F.

Typical hypergolic and cryogenic temperature records are presented in Figures 55 to 58 for high- and low-contact areas. As illustrated in Figures 55 and 56, the maximum temperatures occurred from 0.9 to 1.6 sec after impact of the dewar/pan assembly for low-contact-area N_2O_4/A-50 tests and from 0.2 to 0.45 sec after impact for high-contact-area N_2O_4/A-50 tests. The cryogenic tests yielded maximum temperature values from 0.3 to 0.6 sec after impact for both low-contact-area (Figure 57) and high-contact-area (Figure 58) tests.

The calculated temperatures from the radiation measurements are presented in Table 18. Comparison of the calculated temperature values with the measured temperature values indicates a emissivity factor between 0.4 and 0.7 is required for agreement of the two temperature sources for the hypergolic tests. A similar comparison for the cryogenic tests indicates emissivity factors from 0.25 to 0.60 are required.

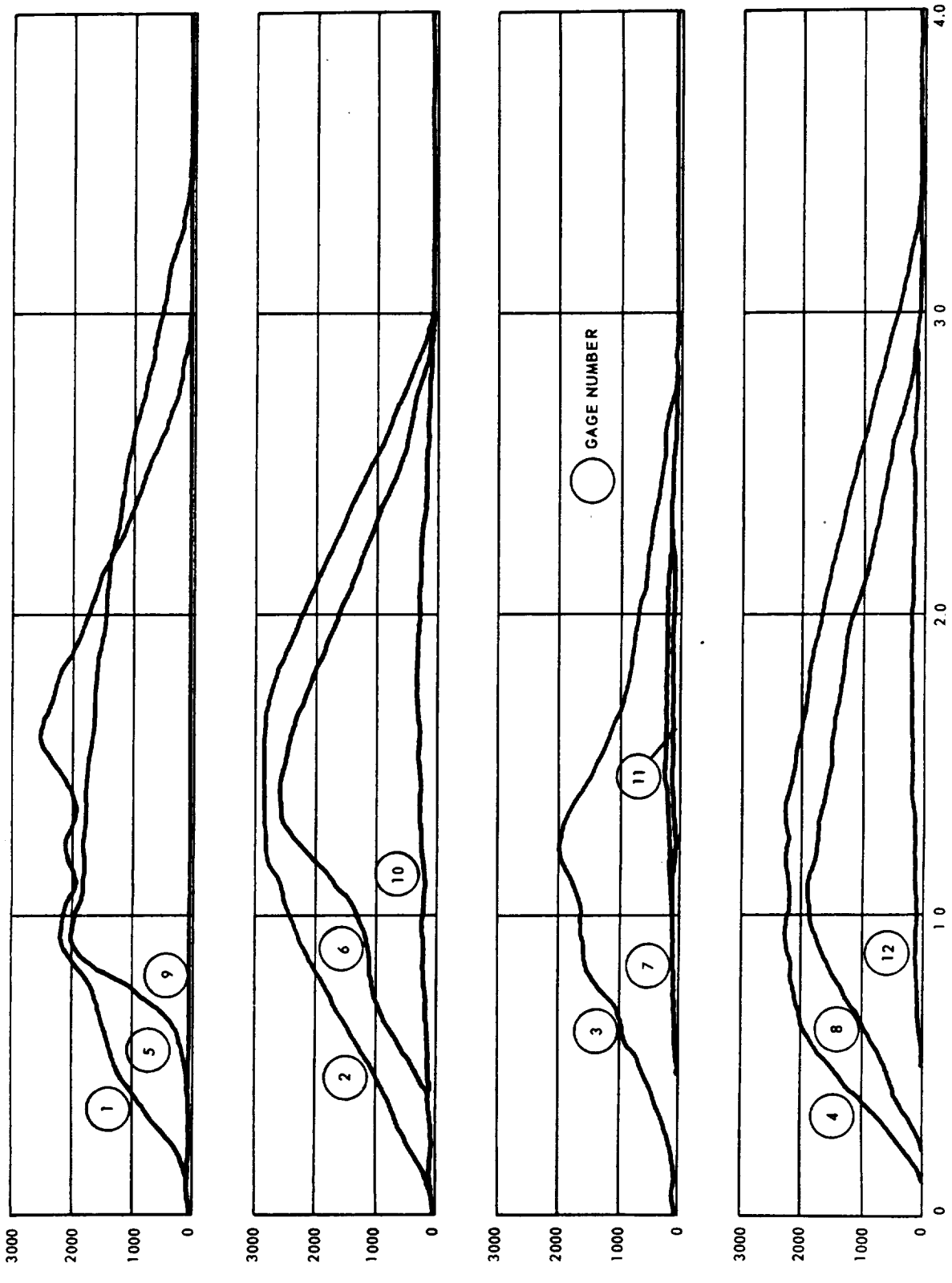

Figure 55. Typical N_2O_4/A-50 Temperature Record -- Low Contact Area.

Figure 56. Typical N_2O_4/A-50 Temperature Record - High Contact Area.

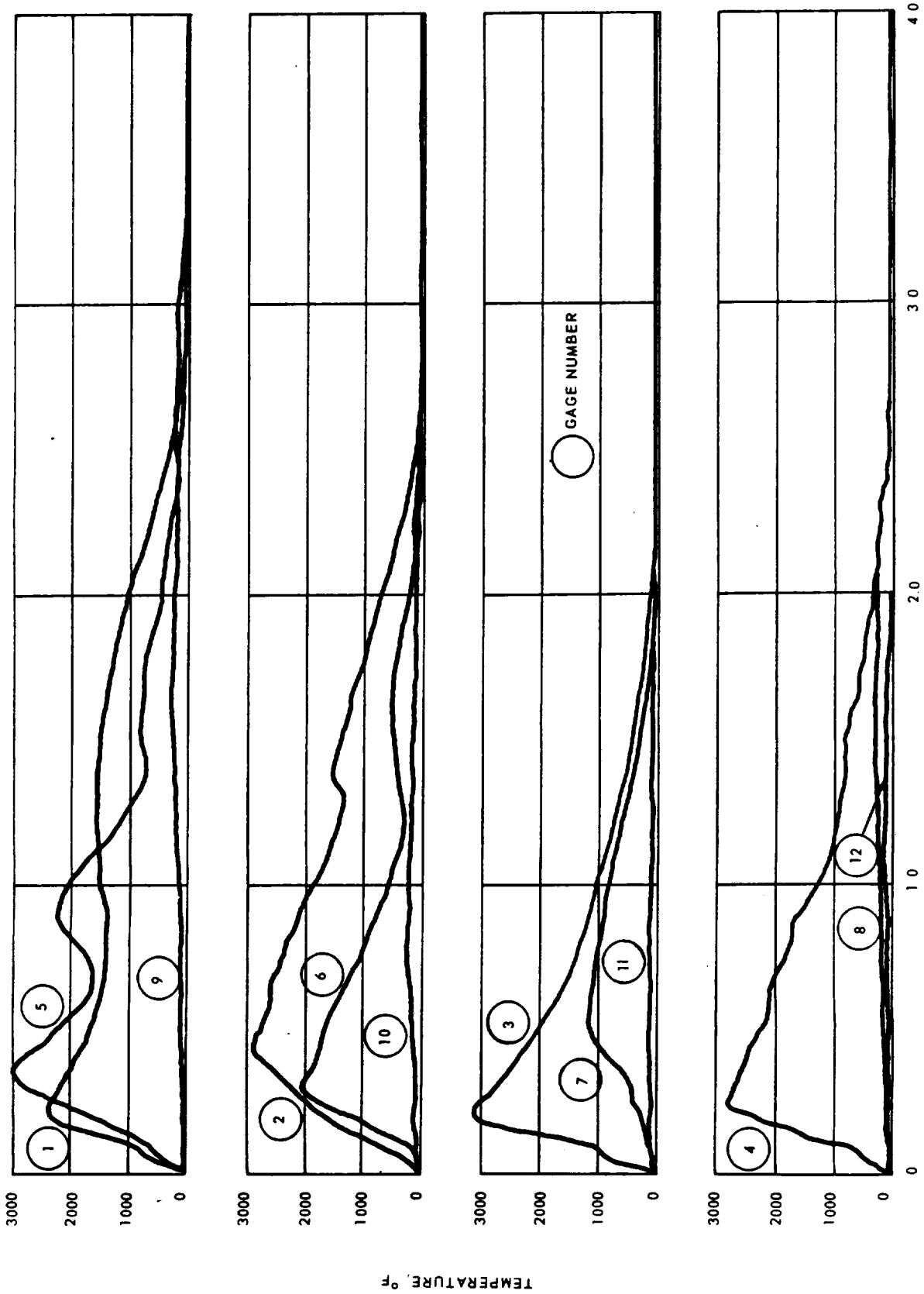

Figure 57. Typical LOX/RP-1 Temperature Record - Low Contact Area.

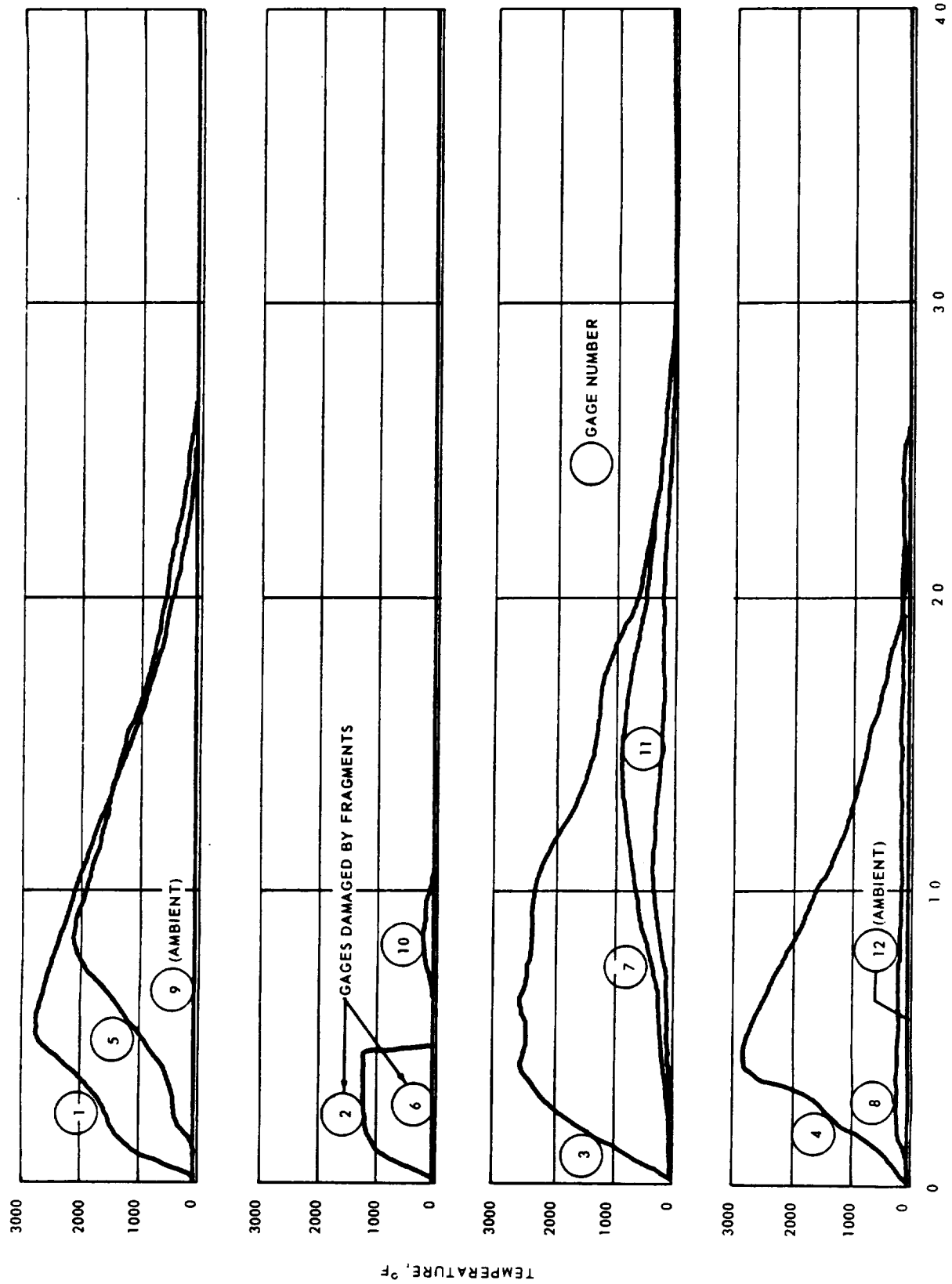

Figure 58. Typical LOX/RP-1 Temperature Record -- High Contact Area.

5. CONCLUSIONS

Based on the results of the experimental studies conducted on this program, the following conclusions are made.

5.1 BLAST YIELD

The explosive yields of the LOX/RP-1 and N_2O_4/A-50 tests were directly related to the contact area between the oxidizer and fuel. The TNT equivalences based on peak overpressure data for the N_2O_4/A-50 samples varied from 0.29 to 0.34 lb of TNT per lb of propellant for a high-contact area and to less than 0.02 lb of TNT per lb of propellant for a low-contact area. A similar comparison for the LOX/RP-1 tests indicated TNT equivalences from 0.28 to 0.36 lb of TNT per lb of propellant for a high-contact area and 0.04 to 0.07 lb of TNT per lb of propellant for a low-contact area.

A comparison of impulse data for the two propellant systems also indicated a direct relationship between positive impulse and contact area, in that the higher explosive yields resulted from the higher contact area. The TNT equivalences based on impulse data for the N_2O_4/A-50 samples varied from 0.37 to 0.42 lb of TNT per lb of propellant for a high-contact area to less than 0.02 lb of TNT per lb of propellant for a low-contact area. The cryogenic test results indicated TNT equivalences on an impulse basis from 0.30 to 0.42 lb of TNT per lb of propellant for a high-contact area to 0.08 lb of TNT per lb of propellant for a low-contact area.

The oxidizer/fuel ratio did not have an appreciable effect on the blast yield of the hypergolic propellant samples. The cryogenic propellant test results were affected to a minor degree by the mixture ratio on a peak overpressure basis. Considerable effect was noticed on impulse by the mixture ratio, but due to variations in the data, it was not possible to establish a definite relationship between the three ratios evaluated.

The explosive yields of both the hypergolic and cryogenic propellant tests varied with distance from the center of the explosion. This variation was attributed to the basic characteristics of the shockwave produced by the reaction of the propellants. The overpressure TNT-equivalences for the hypergolic and cryogenic tests increased with increased distance from the test fixture within the limits of the program.

The magnitude of the blast yielded by the LOX/RP-1 propellant tests was directly affected by the mixing efficiency and duration. A peak overpressure equivalence of approximately 1.2 lb of TNT per lb of propellant was indicated for a well-mixed propellant sample, as compared to a maximum equivalence of 0.36 lb of TNT per lb of propellant for a dewar/pan configuration with essentially no mixing duration.

5.2 FIREBALL SIZE AND DURATION

The fireballs produced by the various propellant combinations were essentially symmetrical and dependent on the height of the liquid in the pan configuration. The tests with the 30-in.-high pan assembly produced a relatively flat fireball compared to the fireballs produced by the other pan configuration, but because of the temporal nature of the fireball, it was impossible to establish a definite relationship between the fireball shape and other test parameters. The maximum diameters of the fireballs were established at 80 ft for the hypergolic propellant tests and 107 ft for the cryogenic propellant tests.

The fireball duration was dependent on the contact area for the fuel-lean and stoichiometric mixture-ratio hypergolic tests; shorter durations resulted from the higher contact areas. The fuel-rich mixture ratio tests yielded durations that were 4 to 5 times greater than the minimum duration from a fuel-lean test and 2.5 to 3.5 times greater than the minimum duration from a stoichiometric mixture-ratio test.

A comparison of the cryogenic-fireball data did not indicate a definite relationship between duration or size and other test parameters.

5.3 MAXIMUM FIREBALL TEMPERATURE

The hypergolic and cryogenic tests produced maximum temperatures of 3070°F and 3380°F, respectively. The N_2O_4/A-50 test results indicated a definite relationship between contact area and the time to maximum temperature after impact of the dewar/pan. The high-contact-area hypergolic tests had shorter time durations to maximum values than did those of low-contact area. The cryogenic test results did not indicate a definite relationship between maximum temperature and contact area. No definite relationship was observed between maximum temperature and other test parameters.

5.4 RADIATION YIELD

The radiation yield of both propellant systems was directly related to the contact area between the oxidizer and fuel. An increase in the contact area decreased the radiation yield of the test samples. A comparison of the blast and radiation yields for an individual test indicated a partitioning of energy between the two parameters in that the higher the radiation yield the lower the blast yield.

A comparison of the radiant-heat-flux values from the hypergolic and cryogenic tests indicated a definite relationship between the time-to-maximum-flux after impact of the dewar/pan assembly and contact area. The high-contact-area tests indicated shorter time duration to maximum intensity than did the low-contact-area tests.

REFERENCES

1. Research on Hazard Classification of New Liquid Rocket Propellants, Rocketdyne, a Division of North American Aviation, Inc., Final Report AF/SSD-TR-61-40, Volume II, Contract AF33(616)-6939, October 1961.

2. Titan II - Dyna-Soar Destruct Test and Analysis Report, Martin-Marietta Corporation, Report ER12269, Contract AF04(695)-54, 15 March 1962.

3. Evaluation of Radiant Heat Flux and Toxicity in Dyna-Soar - Titan II Destruct Tests, Bureau of Mines, Technical Documentary Report ASD-TDR-62-221, May 1962.

4. A Study of Explosions Induced by Contact of Hydrazine-Type Fuels with Nitrogen Tetroxide, Atlantic Research Corporation, 7th Quarterly Progress Report, Contract AF 33(616)-6918, 31 August 1961.

5. Storable Propellant Data for the Titan II Program, Bell Aerosystems Company, Report 8182-933001, AFBMD TR-61-55, Contract AF04(647)-846, July 1961.

6. Storable Propellant Data for the Titan II Program, Bell Aerosystems Company, Report 8182-933002, AFBSD TR-61-35, Contract AF 04(694)-72, November 1961.

7. Summary Report on a Study of the Blast Effect of a Saturn Vehicle, A. D. Little, Inc., Report C-63850, Contract NAS 8-523, Feburary 1962 (CONFIDENTIAL).

8. Kingery, C., and B. Pannil, Peak Overpressure vs Scaled Distance, BRL Memo Report 1518, April 1964.

9. Kalavski, P. Z., A High-Speed Recording System Using the Velocity Method to Determine the Peak Pressure Produced in Air by Explosives, U. S. Naval Ordnance Laboratory, NAVORD Report 2167.

10. Kingery, C., Informal notes, Ballistic Research Laboratories, Aberdeen Proving Grounds, Maryland (being compiled for publication).

APPENDIX A

COMPUTER PROGRAM FOR SELECTION OF DEWAR FLASKS AND PAN GEOMETRY

A-1. INTRODUCTION

Test conditions required that a number of dewar flasks holding a fixed volume of one liquid be placed in a pan holding a fixed volume of another liquid with the following stipulations:

- The surface level of both liquids must be at the same height after dewar immersion.
- The mean area of contact between the flasks and the pan liquid must be in the ratios of 1:2:4.
- Three weight ratios of the two-liquid systems must be tested. The weight ratio of the liquid in the flask to the liquid in the pan must be 1.5, 2.5, and 3.5 to 1 and 1.0, 2.0, and 3.0 to 1.

A-2. OBJECTIVES

An analytical equation, or set of equations, must be determined to provide the necessary dewars and pans dimensions with the following conditions:

- The height of the liquid in the dewars must be maintained as near the top as practical to minimize the number of dewars.
- The dewars must fit into a pan with vertical sides. The base of the pan may be rectangular or any regular polygon with any desired side lengths.
- The dewars are cylindrical with a hemispherical base both inside and outside. The radius of the hemispherical base is one-half the diameter of the cylindrical section. A small glass tip protrudes from the base of the dewars. The volume of the tip is assumed to be negligible; the height of the tip is not negligible.
- The total cost must be as low as possible.

NOMENCLATURE

A-3. DERIVATION

A	=	Total area, $in.^3$
a	=	Area of one dewar, $in.^2$
D	=	Diameter, in.
H	=	Height of dewar, in.
h	=	Height (a variable), in.
N	=	Integer number of dewars
n	=	Variable number of dewars
r	=	Ratio of mean surface areas - one dewar to smaller dewar
V	=	Total volume, $in.^3$
v	=	Volume of one dewar (V = nv), $in.^3$

SUBSCRIPTS

b	=	base
c	=	cylindrical section of dewar
i	=	the inside of dewar
j	=	liquid in dewars
k	=	liquid in pans
l	=	any commercially available dewar
m	=	mean value determined from the dewar wall thickness
o	=	outside of dewar
p	=	pan
pl	=	per unit length
t	=	height of blown-glass tip of given dewar
x, y, z	=	different commercially available dewars
1, 2, 3, etc.	=	different, listed commercially available dewars

A-3.1 CONSERVATION OF VOLUME

Consideration must be given first to dewars in the pan. The following equation represents the volume contained by the pan.

$$V_p = V_r + V_{b_o} + V_{c_o} \tag{1}$$

that is,

$$V_p = f(V_{b_o}, V_{c_o}) \tag{2}$$

Therefore,

$$A_{b_p} h_p = V_k + N v_{b_o} + N v_{c_o} \tag{3}$$

The volume of the dewar glass tip will be negligible since $v_x >> v_t$.

$$A_{b_p} (h_b + h_c + h_t) = V_k + N(v_{b_o} + v_{c_o}) \tag{4}$$

Since the pan liquid height equals the dewar liquid height

$$A_{b_p} (\frac{D_o}{2} + h_o + h_t) = V_k + \frac{V_j}{v_i}(v_{b_o} + v_{c_o}) \tag{5}$$

Since n is defined as the number of dewars required to hold the volume of liquid V_j.

$$A_{b_p} (\frac{D_o}{2} + h_c + h_t) = V_k + V_j (\frac{v_{b_o} + v_{c_o}}{v_{b_i} + v_{c_i}}) \tag{6}$$

$$A_{b_p} = \frac{2}{D_o + 2h_o + 2h_t} \left[V_k + V_j \frac{\frac{\pi D_o^3}{12} + \frac{\pi D_o^2 h_c}{4}}{\frac{\pi D_i^3}{12} + \frac{\pi D_i^2 h_c}{4}} \right] \quad (7)$$

where

$$h_{c_i} = h_{c_o} = h_{c_m} = h_c$$

Therefore,

$$A_{b_p} = \frac{2}{D_o + 2h_c + 2h_t} \left[V_k + V_j \frac{D_o^3 + 3D_o^2 h_c}{D_i^3 + 3D_i^2 h_c} \right] \quad (8)$$

and

$$A_{b_p} = f(h_c) \quad (9)$$

Thus, for a given dewar size, where the pan liquid height is equal to the dewar liquid height, the area of the base of the pan must be the area determined from Equation 9.

NOTE: V_j and V_k are constants during a given test. D_o and D_i are limited to commercially available dewars only, and therefore, are constants with a few different values. The only variables are A_{b_p} and h_c.

$$A_{b_p} = f(h_c)$$

A-3.2 SURFACE AREA AND VOLUME CONDITIONS

It is necessary to make a table of available dewars, with calculations to show their volume and surface area characteristics. It can be observed immediately that the larger a dewar is, with the minimum number of dewars holding liquid V_j, the smaller the surface area is.

The surface area conditions state the following:

$$A_{m_x} = \frac{1}{r} (A_{m_y} + A_{m_z}) \tag{10}$$

$$N_x a_{m_x} = \frac{1}{r} (n_y a_{m_y} + n_z a_{m_z}) \tag{11}$$

where dewar x has the larger volume and represents one test configuration. Dewars y and z are mixed in another pan and represent another separate test condition related by the value of r.

$$r N_x (a_{b_{m_x}} + a_{c_{m_x}}) = n_y (a_{b_{m_y}} + a_{c_{m_y}}) + n_z (a_{b_{m_z}} + a_{c_{m_z}}) \tag{12}$$

Since x is a selected large dewar, N_x is a fixed number that is dependent only on the constant volume V_j. Therefore, solve for

$$n_y = f (n_z, h_{c_y}, h_{c_z}). \tag{13}$$

$$n_y = \frac{r N_x (a_{b_{m_x}} + a_{c_{m_x}}) - n_z (a_{b_{m_z}} + a_{c_{m_z}})}{(a_{b_{m_y}} + a_{c_{m_y}})} \tag{14}$$

$$n_y = \frac{r N_x \left(\frac{\pi D_{m_x}^2}{2} + \pi D_{m_x} h_{c_x}\right) - n_z \left(\frac{\pi D_{m_z}^2}{2} + \pi D_{m_z} h_{c_z}\right)}{\frac{\pi D_{m_y}^2}{2} + \pi D_{m_y} h_{c_y}} \tag{15}$$

$$n_y = \frac{r N_x (D_{m_x}^2 + 2 D_{m_x} h_{c_x}) - n_z (D_{m_z}^2 + 2 D_{m_z} h_{c_z})}{D_{m_y}^2 + 2 D_{m_y} h_{c_y}} \quad (16)$$

The quantities D_{m_x}, D_{m_y}, and D_{m_z} are the given mean dewar diameters and are constants. Also, r is constant.

The quantities N_x and h_{c_x} can be predetermined by specifying a desirable large dewar as dewar x, and selecting a V_j.

Since dewars y and z are mixed in the same pan,

$$h_{t_y} + \frac{D_{o_y}}{2} + h_{c_y} = h_{t_z} + \frac{D_{o_z}}{2} + h_{c_z} \quad (17)$$

and the quantities h_{c_y} and h_{c_z} can be made constants by selecting a dewar height near the top of the shortest dewar.

Therefore, only two variables remain in this equation, and they are n_y and n_z. Notice that n_y is linear with respect to n_z in Equation 16.

A second equation, $n_y = f(n_z)$, can be written, because as the mixture satisfies the area conditions, it must also satisfy the volume, V_j, conditions where

$$V_j = V_{i_y} + V_{i_z} \quad (18)$$

$$V_j = n_y v_{i_y} + n_z v_{i_z} \quad (19)$$

Solving for n_y,

$$n_y = \frac{V_j - n_z v_{i_z}}{v_{i_y}} \quad (20)$$

$$n_y = \frac{V_j - n_z (v_{i_{b_z}} + v_{i_{c_z}})}{v_{i_{b_y}} \quad v_{i_{c_y}}} = \frac{V_j - n_z \left(\frac{\pi D^3_{i_z}}{12} + \frac{\pi D^2_{i_z} h_{c_z}}{4}\right)}{\frac{\pi D^3_{i_y}}{12} + \frac{\pi D_{i_y}^2 h_{c_y}}{4}} \quad (21)$$

$$n_y = \frac{\frac{12}{\pi} V_j - n_z (D_{i_z}^3 + 3 D_{i_z}^2 h_{c_z})}{D_{i_y}^3 + 3 D_{i_y}^2 h_{c_y}} \quad (22)$$

and again the dewar liquid heights are interdependent and are set near the top of the shortest dewar.

Any intersection in the positive quadrant of Equations 16 and 22 are satisfactory solutions. Since two lines can only intersect once, only one solution for each condition of dewars is possible for a fixed V_j and the cylindrical height of the shortest dewar. However, n_y and n_z will not be integers unless h_{c_y} and h_{c_z} are allowed to vary again and even then, they might not ever both be integer values.

Regardless of this fact, at the point of intersection, the variable n_y of Equation 16 is equal to n_y of Equation 22. Therefore,

$$\frac{r N_x (D_{m_x}^2 + 2 D_{m_x} h_{c_x}) - n_z (D_{m_z}^2 + 2 D_{m_z} h_{c_z})}{D_{m_y}^2 + 2 D_{m_y} h_{c_y}}$$

$$= \frac{\frac{12}{\pi} V_j - n_z (D_{i_z}^3 + 3 D_{i_z}^2 h_{c_z})}{D_{i_y}^3 + 3 D_{i_y}^2 h_{c_y}} \quad (23)$$

Solve for n_z.

Cross multiply.

$$r\,N_x\,(D_{m_x}^{\,2} + 2\,D_{m_x}\,h_{c_x})(D_{i_y}^{\,3} + 3\,D_{i_y}^{\,2}\,h_{c_y}) - n_z\,(D_{m_z}^{\,2} + 2\,D_{m_z}\,h_{c_z})(D_{i_y}^{\,2} + 3\,D_{i_y}^{\,2}\,h_{c_y}$$

$$= \frac{12}{\pi}\,V_j\,(D_{m_y}^{\,2} + 2\,D_{m_y}\,h_{c_y}) - n_z\,(D_{m_y}^{\,2} + 2\,D_{m_y}\,h_{c_y})\,(D_{i_z}^{\,3} + 3\,D_{i_z}^{\,2}\,h_{c_z}) \quad (24)$$

and

$$n_z = \frac{\frac{12}{\pi}\,V_j\,(D_{m_y}^{\,2} + 2\,D_{m_y}\,h_{c_y}) - r\,N_x\,(D_{m_x}^{\,2} + 2\,D_{m_x}\,h_{c_x})(D_{i_y}^{\,3} + 3\,D_{i_y}^{\,2}\,h_{c_y})}{(D_{m_y}^{\,2} + 2\,D_{m_y}\,h_{c_y})(D_{i_z}^{\,3} + 3\,D_{i_z}^{\,2}\,h_{c_z}) - (D_{m_z}^{\,2} + 2\,D_{m_z}\,h_{c_z})(D_{i_y}^{\,3} + 3\,D_{i_y}^{\,2}\,h_{c_y})} \quad (25)$$

Therefore, if the largest dewar, x, is filled with V_j and placed in one pan with height, h_{p_x}, dewars y and z, placed in another pan with height, $h_{p_{y,z}}$ will have a mean surface area such that $A_x = \frac{1}{r}(A_y + A_z)$. Providing that n_z from Equation 25 is positive and that n_y from either Equations 16 or 22 is also positive, the n_z and n_y calculated are the number of each dewar to be used.

Equation 9 now must be rewritten in terms of Equation 25.

$$V_p = V_k + V_{b_{o_y}} + V_{c_{o_y}} + V_{b_{o_z}} + V_{c_{o_z}} \quad (26)$$

$$A_{b_p}\,h_p = V_k + n_y\,(v_{b_{o_y}} + v_{c_{o_y}}) + n_z\,(v_{b_{o_z}} + v_{c_{o_z}}) \quad (27)$$

$$A_{b_p}\,(\frac{D_{o_y}}{2} + h_{c_y} + h_{t_y}) = V_k + n_y\,(\frac{\pi}{12}\,D_{o_y}^{\,3} + \frac{\pi}{4}\,D_{o_y}^{\,2}\,h_{c_y}) \quad (28)$$

$$+ n_z\,(\frac{\pi}{12}\,D_{o_z}^{\,3} + \frac{\pi}{4}\,D_{o_z}^{\,2}\,h_{c_z}) \quad (29)$$

$$A_{b_p} = \frac{2}{D_{o_y} + 2h_{c_y} + 2h_{t_y}} \left\{ V_k + \frac{\pi}{12} \left[n_y \left(D_{o_y}^{\ 3} + 3 D_{o_y}^{\ 2} h_{c_y} \right) + n_z \left(D_{o_z}^{\ 3} + 3 D_{o_z}^{\ 2} h_{c_z} \right) \right] \right\} \quad (30)$$

As in Equation 9, Equation 30 determines the area of the base of the pan for a combination of dewars y and z.

A-3.3 DIMENSIONS OF THE PAN BASE

If the dewars y and z are allowed a square area each, i.e., arranged evenly in the pan, the total area needed to hold the dewars will be given by

$$\left\{ \begin{array}{l} \text{Total cross-section area of dewars y and z} \\ \text{with a square permitted around each} \end{array} \right\} = D_{o_y}^{\ 2} n_y + D_{o_z}^{\ 2} n_z \quad (31)$$

If the pan construction is simple,

$$D_{o_y}^{\ 2} n_y + D_{o_z}^{\ 2} n_z < A_{b_p} \quad (32)$$

as calculated in Equation 30, and the dewar will fit in the pan with room to spare. If

$$D_{o_y}^{\ 2} n_y + D_{o_z}^{\ 2} n_z > A_{b_p} \quad (33)$$

an irregular arrangement of dewars may trim down some of the corner area allowed and the dewars may or may not fit into the calculated pan base area.

However, the arrangement of the dewars in the pan with such a base area will be complex. Graphical checking to assure that the dewars will fit into the area calculated should be employed prior to constructing the pans. If the dewars will not fit into the A_{b_p} calculated, then the following approach must be taken.

No arrangement of the dewars in the calculated pan base area is possible when

$$\frac{\pi}{4}\left(D_{o_y}^{2}\, n_z + D_{o_z}^{2}\, n_z\right) > A_{b_p} \tag{34}$$

and the pan bases must, of course, be constructed larger than the calculated A_{b_p}. When the pans must be larger than the calculated A_{b_p}, the liquid level in the pan will not be the same height as the liquid level in the dewars, unless a volume of filler, or ballast material (e.g., marbles, metal rods, etc.) is added to the pan interior. The volume of such material to be added will be given by:

$$\text{Filler volume} = h_p\,(\text{Actual } A_{b_p} - \text{calculated } A_{b_p}) \tag{35}$$

A-3.4 COST

The total cost of any quantity of dewars calculated by Equations 16, 22, and 25 will be given by:

$$\text{Total cost} = \text{Cost}_y\, N_y + \text{Cost}_z\, N_z \tag{36}$$

where $N_y + N_z$ have been refined as nearly as possible to integer values.

A-4. APPLICATION SUMMARY

In view of the number of calculations necessary to arrive at a suitable commercially available combination of inexpensive dewars, a computer program was prepared in Fortran for an IBM Model 1620 digital computer to perform the following step by step functions.

A-4.1 STEP 1

Commercially available dewar dimensions are inputs, along with the desired quantities of V_j, V_k, r and with the total number of dewars defined as L. Note: From three to no more than fifteen different dewars can be input into this computer program, which is Aerojet-categorized as 190.

A-4.2 STEP 2

The data array of Table A-1 is prepared and stored for each dewar.

Table A-1. Dewar Data Array.

NR	Quantity	Definition	Fortran Symbol (not used)	How Obtained	Fortran Storage Location
1	D_{o_x}	Outside Diameter (in.)	DO	Input	PF(1, J)
2	D_{i_x}	Inside Diameter (in.)	DI	Input	PF(2, J)
3	H_{c_x}	Commercial height of cylindrical section (in.)	HHC	Input	PF(3, J)
4	h_{t_x}	Tip height (in.)	HT	Input	PF(4, J)
5	$Cost_x$	Unit cost ($)	COST	Input	PF(5, J)
6	D_{m_x}	Mean Diameter (in.)	DM	$\frac{D_{o_x} + D_{i_x}}{2}$	PF(6, J)
7	h_{b_x}	height of base (in.)	HB	$\frac{D_{o_x}}{2}$	PF(7, J)
8	$a_{b_{mx}}$	Mean area of the dewar base (in.)	AMB	$\frac{\pi}{2} D^2_{m_x}$	PF(8, J)
9	$a_{c_{m_{x_{pl}}}}$	Mean area per unit length of the dewar cylindrical section (in.)	ACMPL	πD_{m_x}	PF(9, J)
10	$v_{b_{i_x}}$	Internal volume of the base of the dewar (in.)	VBI	$\frac{\pi}{12} D^3_{i_x}$	PF(10, J)
11	$v_{c_{i_{xpl}}}$	Internal volume per unit length of the dewar cylindrical section (in.)	VCIPL	$\frac{\pi}{4} D^2_{i_x}$	PF(11, J)
12	$v_{b_{o_x}}$	Outside volume of the dewar base (in.)	VBO	$\frac{\pi}{12} D^3_{o_x}$	PF(12, J)
13	$v_{c_{i_{xpl}}}$	Outside volume per unit length of the dewar cylindrical section (in.)	VCOPL	$\frac{\pi}{4} D^2_{o_x}$	PF(13, J)

Table A-1. (Continued).

NR	Quantity	Definition	Fortran Symbol (not used)	How Obtained	Fortran Storage Location
14	N_x	The minimum integer number of the largest dewar size that will hold V_j	ENX	$n_x = \frac{V_j}{v_{b_{i_x}} + v_{c_{i_{xpl}}} H_{c_x}}$ $N_x = n_x$ truncated + 1	PF(14, J)
15	h_{c_x}	The height of V_j in the cylindrical section of the dewar (in.)	HCX	$h_{c_x} = \frac{V_j - N_x v_{b_{i_x}}}{N_x v_{c_{i_{xpl}}}}$	PF(15, J)
16	A_{m_x}	The total mean surface area at height h_{c_x} of N_x dewars (in.)	AMX	$A_{m_x} = N_x (a_{b_{m_x}} + a_{c_{m_{xpl}}} h_{c_x})$	PF(16, J)

A-4.3 STEP 3

To preclude calculating meaningless,data, a series of numerical comparisons are made between the parameter values of Table A-1. These comparisons are programed as "IF" statements and allow the machine (figuratively) to decide logically what to do. In this program the following main "IF" statements were used.

a. If the total mean surface area of the smallest dewar is less than the desired surface area ratio, r, times the total mean surface area of the largest flask, then no mixture of dewars can produce the desired surface r. Therefore,

(1) IF $A_{m_z} - r A_{m_x}$ = negative number then stop.

(2) IF $A_{m_z} - r A_{m_x}$ = zero, then the smallest dewar is perfectly suited to provide r.

(3) IF $A_{m_z} - r A_{m_x}$ = positive, then the smallest dewar will mix with a larger dewar, and the "IF" statement must be repeated for each larger dewar. The command to stop must be changed to compute only when a negative result is obtained and for each negative thereafter until several combinations have been computed.

b. To equalize the height in the mixed dewars, the following is required:

$$\text{IF } (H_{b_{o_y}} + H_{c_y} + H_{t_y}) - (H_{b_{o_z}} + H_{c_z} + H_{x_z}) \text{ is:} \tag{37}$$

(1) Positive, then

$$h_{c_z} = H_{c_z} - 1 \text{ (to lower the height 1 in. below the top of the shortest dewar and} \tag{38}$$

$$h_{c_y} = h_{c_z} + H_{b_{o_z}} + H_{t_z} - (H_{b_{o_y}} + H_{t_y}) \tag{39}$$

(2). zero, then the heights are equal, and

$$h_{c_z} = H_{c_z} - 1 \tag{40}$$

$$h_{c_y} = H_{c_y} - 1 \tag{41}$$

(3). and negative, then $h_{c_y} = H_{c_y} - 1$

$$h_{c_z} = h_{c_y} + H_{b_{o_y}} + H_{t_y} - (H_{b_{o_z}} + H_{t_z}) \tag{42}$$

A-4.4 STEP 4

The necessary information for computing is now available, and the following quantities are calculated using the following shortened forms of Equations 22, 25, 30, 31, 32, 34, and 36. The equations were shortened due to the calculations of the data array in Table A-1. From Equation 25,

$$n_z = \frac{V_j (a_{b_{m_x}} + a_{c_{m_{ypl}}} h_{c_y}) - r N_x (a_{b_{m_x}} + a_{c_{m_{xpl}}} h_{c_x})(v_{i_{b_y}} + v_{i_{c_{ypl}}} h_{c_y})}{(a_{b_{m_y}} + a_{c_{m_{ypl}}} h_{c_y})(v_{i_{b_z}} + v_{i_{c_{zpl}}} h_{c_z}) - (a_{b_{m_z}} + a_{c_{m_{zpl}}} h_{c_z})(v_{i_{b_y}} + v_{i_{c_{ypl}}} h_{c_y})} \tag{43}$$

From Equation 23,

$$n_y = \frac{V_j - n_z (v_{i_{b_z}} + v_{i_{c_{zpl}}} h_{c_z})}{v_{i_{b_y}} + v_{i_{c_{ypl}}} h_{c_y}} \tag{44}$$

The height of the liquid in the pan is given by

$$h_p = h_{c_y} + H_{b_{o_y}} + H_{t_y} \tag{45}$$

From Equation 30,

$$A_{b_p} = \frac{V_k + n_y (v_{b_{o_y}} + v_{c_{o_{ypl}}} h_{c_y}) + n_z (v_{b_{o_z}} + v_{c_{o_{zpl}}} h_{c_z})}{h_p} \quad (46)$$

From Equation 31,

$$\overline{DDN} = D_{o_y}^2 n_y + D_{o_z}^2 n_z \quad (47)$$

From Equation 32,

$$\overline{TST\ 1} = A_{b_p} - \overline{DDN} \quad (48)$$

From Equation 34,

$$\overline{TST\ 2} = A_{b_p} - \frac{\pi}{4} \overline{DDN} \quad (49)$$

From Equation 36,

$$\text{Total cost} = \text{cost}_y N_y + \text{Cost}_z N_z \quad (50)$$

A-4.5 STEP 5

Refinement of n_y and n_z to integers would require varying the heights h_{c_y} and h_{c_z} and was considered impractical. Analysis of the output data would yield sufficient comparisons of the dewars mixture costs. A variance of up to 2.5% in liquid heights was considered acceptable.

A-4.6 STEP 6

Additional cycling of the equations is incorporated into the computer program for all the dewars, along with test conditions inputs, by means of additional flow control "IF" statement.

A-5. CONCLUSIONS

The output data of the equations represented satisfactory data from which the minimum costing dewar combinations could be selected and from which the pan dimensions could be easily derived.

APPENDIX B

BALLISTIC RESEARCH LABORATORY BLAST MEASUREMENTS

B-1 INTRODUCTION

The program objectives required a redundant method of measuring peak overpressure, positive impulse, and pressure pulse duration. The Ballistic Research Laboratories (BRL) have developed and used a self-contained mechanical pressure-time gage (PNS) for obtaining blast measurements from explosive tests. This gage provided a contrast to the piezoelectric gages used elsewhere on the program and permitted a cross-check of the pressure-measuring instrumentation.

The BRL provided six PNS gages and necessary operating personnel from 6 January 1964 to 10 March 1964. All gages and personnel were provided cost free to the program.

B-2 GAGE DESCRIPTION

The PNS gage contains a single diaphragm sensor that scratch-records on a negator-spring motor recorder in response to the pressure phenomena. Sensors are fabricated of Ni Span C and are welded into a mounting ring. A section of thin-wall stainless steel tubing is bonded, by epoxy, to the center of the diaphragm; the free end of the tube passing through an oline jewel bearing fixed to the top section of the mounting ring. A flat 5/16-in. -long section of phosphor bronze, containing an osmium-tipped 1/32-in. -long stylus, is soldered in the tubing. An O-ring serves as a pressure seal, and two alignment pins facilitate a mounting in the gage. Sensors are 1-5/16-in. in diameter and are interchangeable, covering a pressure spectrum of 0 to 1000 psi in 15 pressure ranges. A sensor is shown in Figure B-1.

The general characteristics of the pressure sensors are presented in Table B-1. Average deflection at rated pressure is 0.020 in., hysteresis is less than 1% and the linearity is less than 5%. The natural frequency ranges from 1 to 7000 cps. Damping is accomplished by an orifice plate mounted in the face plate of the gage. Rise times of from 0.3 to 0.5 msec have been achieved in shocktube and field-test programs.

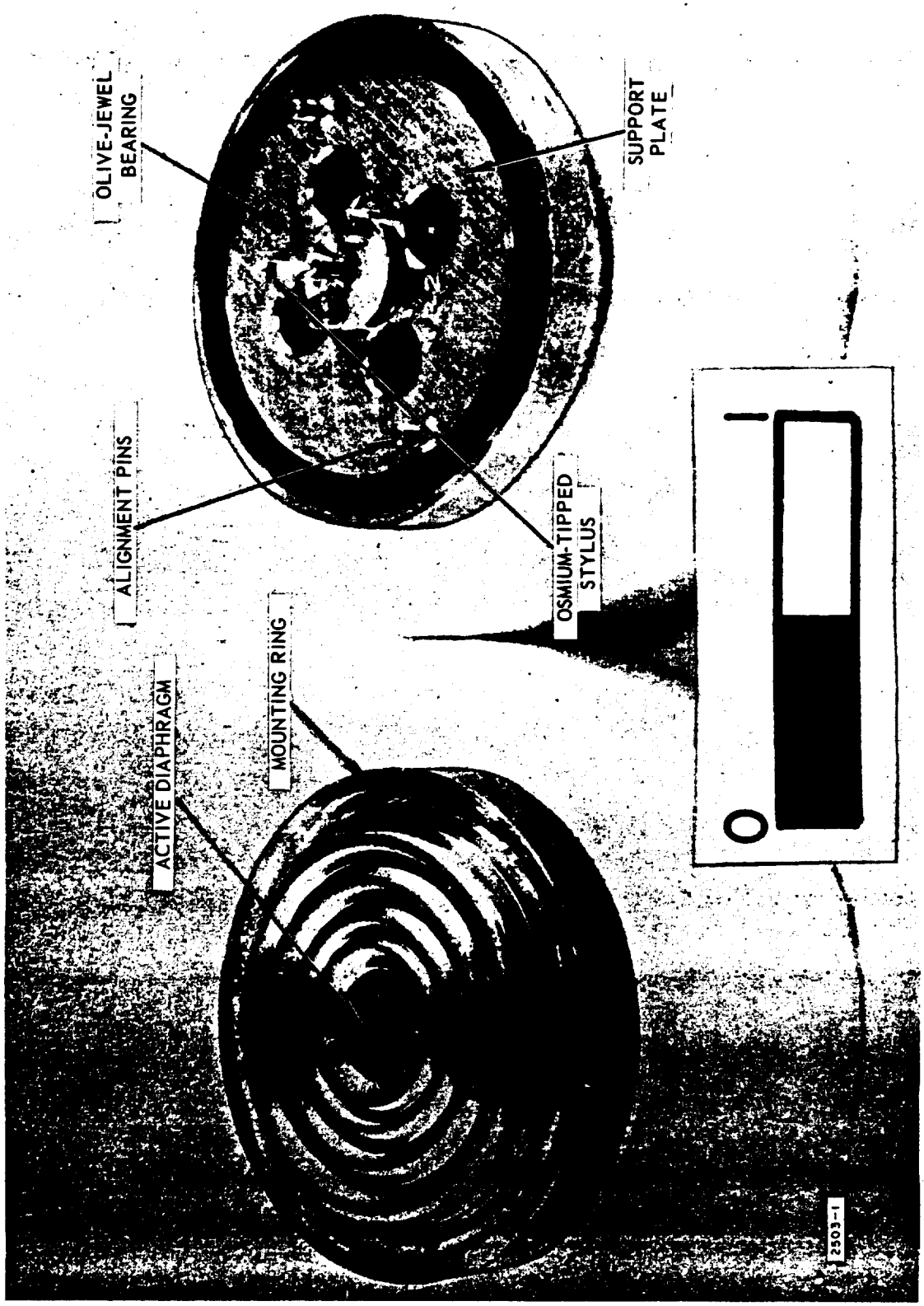

Figure B-1. Pressure Sensor.

Table B-1. Sensor Statistics.

Sensor Ranges (psi)	Sensor Natural Frequency (cps)	Sensor Characteristics		
		Deflection of Rated Pressure (mils)	Hysteresis (%)	Linearity (Terminal-Based)
0-1	820	15.30	0.70	1.60
0-2	1085	19.60	0.87	1.68
0-5	1570	20.20	0.00	1.60
0-10	1895	26.80	0.67	2.69
0-25	2726	23.90	0.20	0.70
0-50	2995	24.20	0.30	2.40
0-100	3615	28.60	0.35	0.87
0-200	4351	31.35	0.73	3.57
0-400	5105	23.17	0.86	3.75
0-600	5955	20.82	0.62	2.16
0-1000	6990	20.10	0.59	0.45
0-10 (Negative)	1915	25.70	0.20	0.70
0-0.50	430	18.15	0.55	1.70
0-0.125	250	17.40	0.60	4.90
0-0.030	250	18.20	1.10	4.20

The method of using a negator spring as both the drive motor and recorder was devised and patented by BRL. The negator spring motor has the inherent characteristic of providing a constant torque output during its entire running cycle. It consists basically of a supply or output drum, a recording drum, a storage drum, and a balanced frictional governor. The storage drum with the spring freely installed on it is mounted for free rotation about its fixed axis. With the outer end of the flat spring extended to pass over the recording drum and anchored to the output drum, the spring is reverse wound onto the output drum. Release of the output drum (the larger of the drums) at any degree of windup allows the material to revert to its natural prestressed curvature by returning to the smaller storage drum. Speed control of the spring to within 10% is provided by the governor through a gear coupling to the output drum. Speeds of 0.5 to 3 ips can be obtained by adjusting the governor. Springs are fabricated of stainless steel in 5/16-in. widths and in lengths of 30 to 60 in. The recording surface of the spring is vapor honed with a fine grit, preparing it for the scratch recording.

Arming, initiation, and shutoff are provided for in the gage system by associated gearing and switches. Two methods, either a solenoid with a balanced armature or an explosive piston actuator, are used for initiating the gage; both systems being triggered by a relay closure. The solenoid or the actuator releases a spring-loaded trigger arm that rapidly serves to bring the motor up to a constant speed. The startup time for the solenoid system is 18.8 msec, while the startup time for the explosive actuator system is 9.4 msec. A startup time of 4.4 msec can be achieved by using an explosive actuator as the sole means of initiation and by bringing the motor up to speed rapidly.

Three traces are recorded on the surface of the spring as it passes over the recording drum. These are the active pressure trace, the 50-cps squarewave timing trace, and the fixed reference trace. Timing is applied by solenoid-operated scribes in series with a 50-cps electromechanical oscillator. It operates from 12 v supplied by a nickel-cadmium battery mounted in the base of the gage canister.

Mounting of the motor-recorder, sensor, timing scribes, and release mechanism is made to a face plate 4 3/4 in. in diameter x 1/2 in. thick. A flange of matching dimensions is welded to a 3-1/2-in.-diameter x 4-in.-long aluminum canister. The timing oscillator,

with the initiation relay, battery, and condenser, is mounted on a removable section at the base of the canister. Electrical connections between the removable halves of the gage are achieved by matching sections of a Cannon connector. The initiation cable enters the gage through a micro-dot cable grip at the base of the gage. O-rings at the top and at the base of the gage provide pressure seals when installed in the canister. The gage is mounted flush with the ground surface. Figures B-2 to B-4 illustrate the gage.

The deflection time traces recorded on the negator spring are converted to real points with the aid of a specially equipped reading microscope. Telecomputing digital readout heads, mounted on the reading equipment for x and y measurements, furnish input to Telecordex accumulators whose output is recorded by an automatic typewriter and a paper-tape punch system.

These data, together with the calibration data, are fed into an automatic computer for obtaining final pressure-time information. An automatic plotter plots the final information.

The gage system described herein has not been completely certified as to accuracy under severe shock and vibration environments. Field data are being gathered as various field programs occur. Accuracies of $\approx 5\%$ can be achieved when the duration of the expected phenomena is greater than 15 msec.

B-3 GAGE POSITION

The original program plan provided for locating the BRL gages directly underneath the piezoelectric gage positions and for flush mounting with the ground. However, the available pressure sensors necessitated locating the gages at stations commensurate with the expected over-pressure. The pressure range of available sensors required three gage positions beyond the 40-ft gage circle. A gage line was established approximately half way between gage positions 3-7-11 and 4-8-12. Gage stations 13, 14, and 15 were established on this line at distances of 50, 60, and 70 ft from the test fixture.

B-4 TEST RESULTS

The results of the blast measurements are presented in Tables B-2 through B-5. Comparison of the test results from the BRL gages to the test results from the piezoelectric gage will show slightly higher values for the BRL gages in most cases.

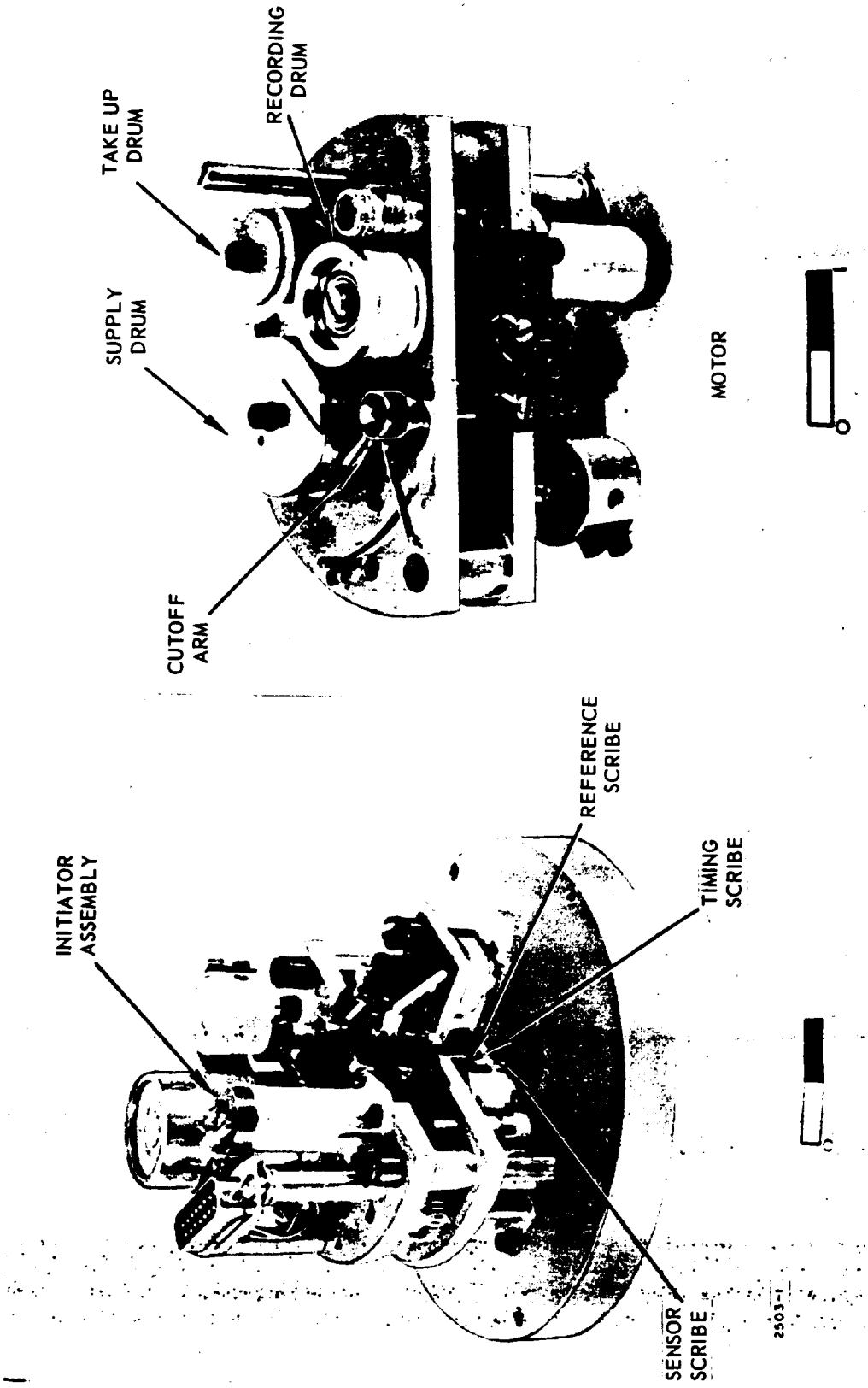

Figure B-2. Recording Assembly, PNS Gage.

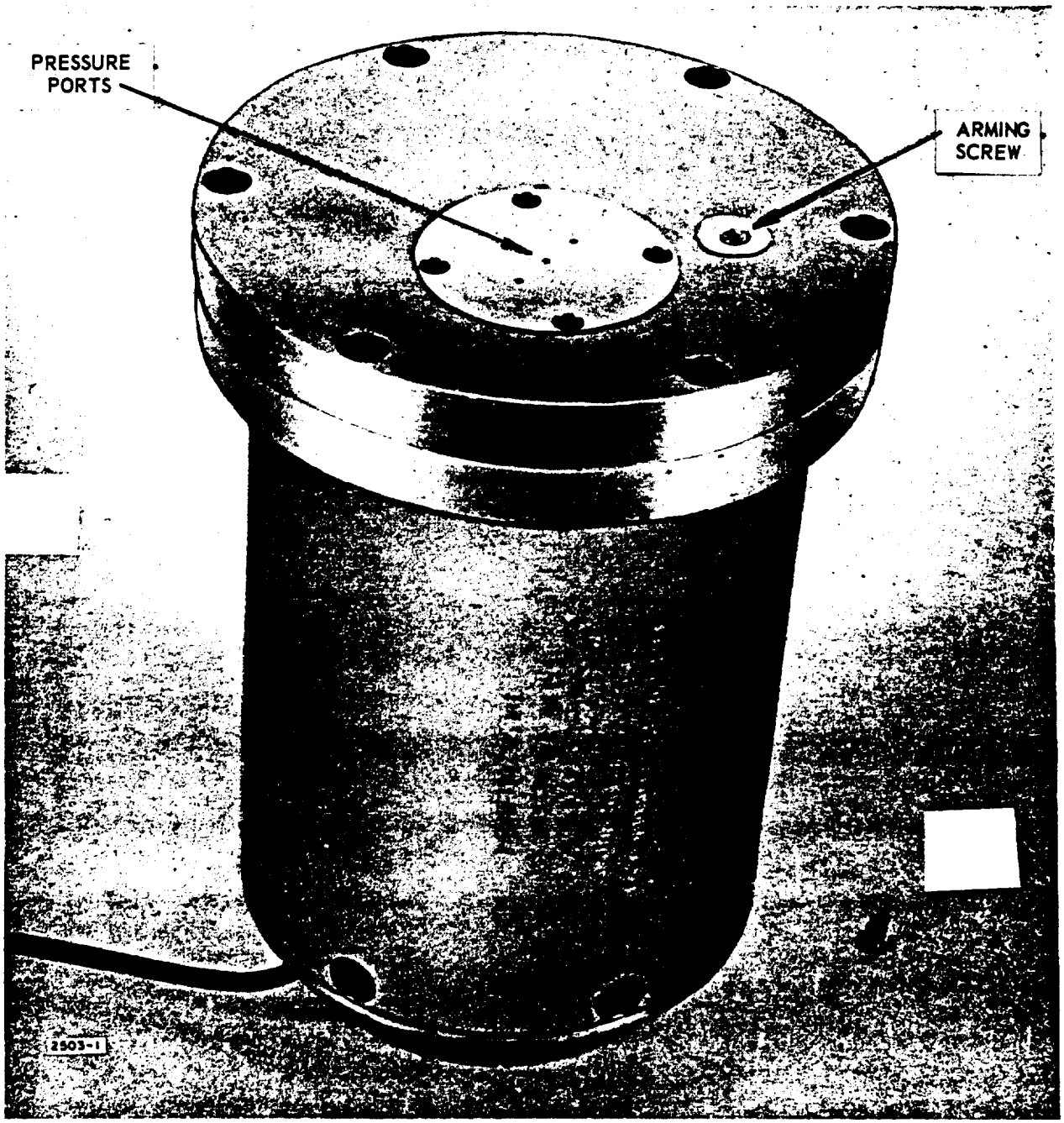

Figure B-4. Assembled PNS Gage.

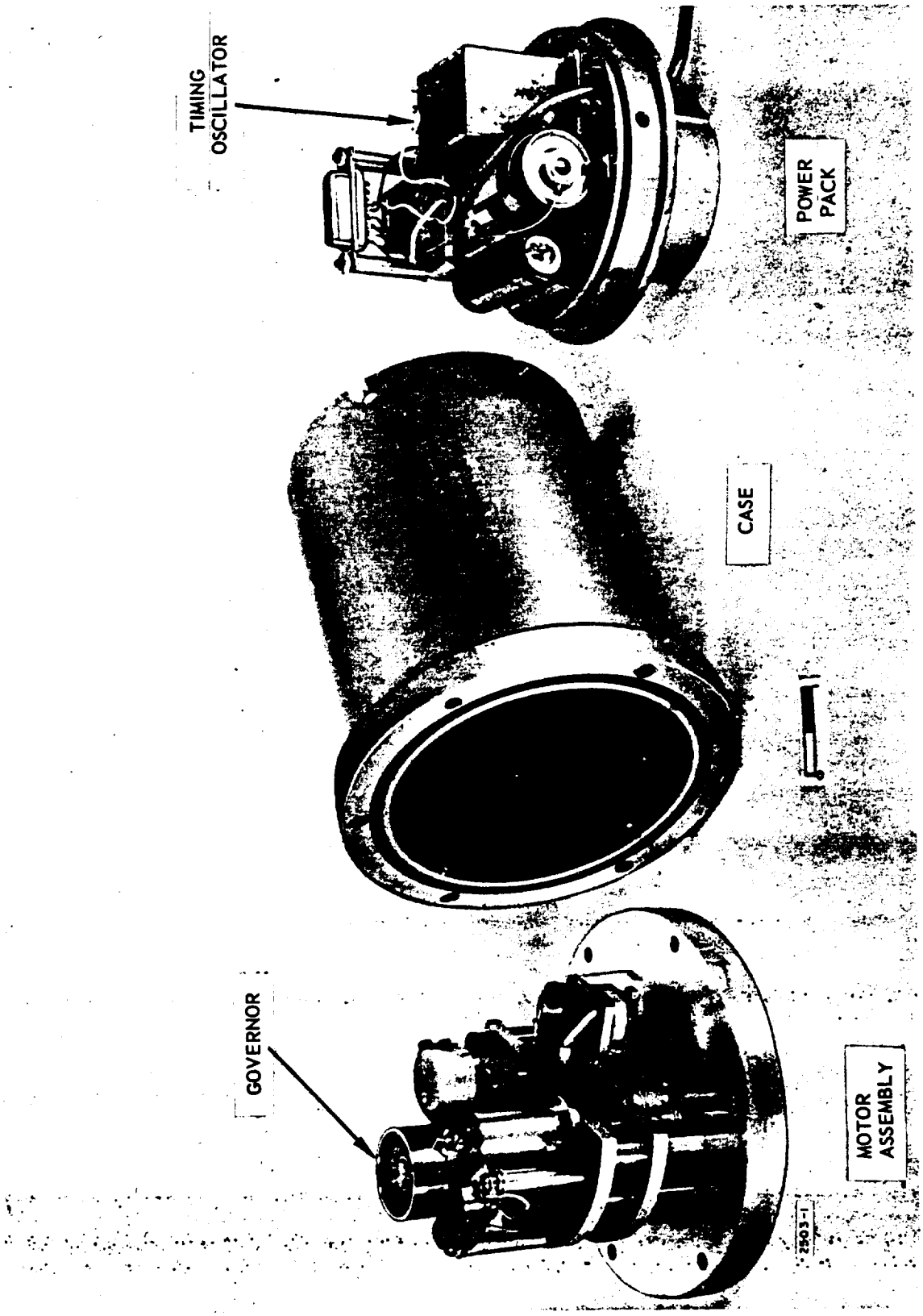

Figure B-3. Exploded View of PNS Gage.

Table B-2. N_2O_4/A-50 Test Results - MR = 3:1.

Contact Area (ft^2)	Distance from Event (ft)	Gage No.	Peak Overpressure (psi)	Positive Impulse (psi-msec)	Positive Pulse Duration (msec)
51.01	40	10	14.0	46.0	10.0
	40	11	14.0	46.0	10.0
	40	12	16.0	46.6	9.8
	50	13	9.4	35.0	14.0
	60	14	8.5	37.5	15.0
	70	15	6.5	27.7	15.0
25.44	40	10	6.8	35.0	14.5
	40	11	*	*	*
	40	12	6.2	30.9	13.7
	50	13	5.7	28.5	19.2
	60	14	3.6	22.8	20.0
	70	15	3.2	19.9	20.3
12.64	40	10	1.0	6.5	14.4
	40	11	2.0	15.0	36.0
	40	12	2.0	10.7	16.4
	50	13	1.5	*	4.8
	60	14	1.1	5.3	23.0
	70	15	0.9	6.3	22.0

* No data

Table B-3. N_2O_4/A-50 Test Results - MR = 2:1.

Contact Area (ft^2)	Distance from Event (ft)	Gage No.	Peak Overpressure (psi)	Positive Impulse (psi-msec)	Positive Pulse Duration (msec)
45.23	40	10	14.4	61.4	14.0
	40	11	15.0	93.2	19.0
	40	12	12.2	80.4	18.0
	50	13	10.0	49.5	17.5
	60	14	8.3	46.0	15.0
	70	15	6.5	35.5	19.5
22.90	40	10	8.0	50.0	17.0
	40	11	7.0	39.1	16.5
	40	12	6.8	22.3	12.0
	50	13	6.6	31.3	17.5
	60	14	4.5	26.0	18.5
	70	15	3.7	21.8	19.5
11.39	40	10	2.1	15.3	16.7
	40	11	1.7	14.7	19.8
	40	12	1.7	11.9	13.6
	50	13	1.0	10.8	32.1
	60	14	0.7	12.1	31.4
	70	*	*	*	*

* No data

Table B-4. N_2O_4/A-50 Test Results - MR = 1:1.

Contact Area (ft^2)	Distance from Event (ft)	Gage No.	Peak Overpressure (psi)	Positive Impulse (psi-msec)	Positive Pulse Duration (msec)
35.90	40	10	14.0	65.0	21.0
	40	11	14.7	54.0	16.5
	40	12	14.0	56.0	15.0
	50	13	10.0	56.0	20.0
	60	14	7.6	41.7	17.1
	70	15	7.8	32.3	20.0
17.96	25	6	10.0	44.9	13.0
	25	7	10.2	50.3	16.0
	25	8	11.0	55.3	13.5
	40	12	6.1	36.7	21.4
	50	13	5.7	29.9	15.0
	60	14	4.1	24.2	17.2
8.88	40	10	*	*	*
	40	11	*	*	*
	40	12	2.1	11.1	15.5
	50	13	*	*	*
	60	14	1.5	9.0	17.6
	70	15	0.8	7.3	19.4

* No data

Table B-5. LOX-RP-1 Test Results.

Oxidizer/Fuel Ratio	Contact Area (ft^2)	Distance from Event (ft)	Gage No.	Peak Overpressure (psi)	Positive Impulse (psi-msec)	Positive Pulse Duration (msec)
3.5:1	57.85	40	10	14.5	50.0	10.0
		40	11	11.5	44.0	10.5
		50	13	9.6	46.0	13.5
		60	14	7.2	40.0	13.5
	32.06	40	10	8.0	44.4	11.9
		40	11	9.0	44.3	11.7
		40	12	8.7	27.7	11.2
		50	13	7.2	32.2	14.4
		60	14	4.8	25.9	15.1
		70	15	4.5	31.7	22.0
2.5:1	59.38	40	10	17.5	68.0	10.0
		40	11	*	*	*
		40	12	17.0	56.4	11.0
		50	13	16.0	51.9	17.0
		60	14	4.2	24.1	10.3
		70	15	*	*	*
1.5:1	25.35	10	3	31.0	50.0	4.0
		25	7	16.0	40.0	7.5
		40	11	6.8	41.0	15.5
		40	12	6.0	30.7	12.8
	12.67	10	3	36.0	101.0	8.7
		25	7	16.0	39.9	5.0
		40	11	6.0	15.4	7.6
		40	12	5.5	30.6	11.5

* No data